SANDIA REPORT SAND81-2422 • TTC-0270 • Unlimited Release • UC-71
Printed March 1982

Prototype Spent Fuel Canister Design, Analysis, and Test

William B. Leisher, Richard G. Eakes

Thomas A. Duffey, Consultant

Prepared by
Sandia National Laboratories
Albuquerque, New Mexico 87185 and Livermore, California 94550
for the United States Department of Energy
under Contract DE-AC04-76DP00789

SF2900Q(8-81)

Issued by Sandia National Laboratories, operated for the United States Department of Energy by Sandia Corporation.

NOTICE: This report was prepared as an account of work sponsored by an agency of the United States Government. Neither the United States Government nor any agency thereof, nor any of their employees, nor any of their contractors, subcontractors, or their employees, makes any warranty, express or implied, or assumes any legal liability or responsibility for the accuracy, completeness, or usefulness of any information, apparatus, product, or process disclosed, or represents that its use would not infringe privately owned rights. Reference herein to any specific commercial product, process, or service by trade name, trademark, manufacturer, or otherwise, does not necessarily constitute or imply its endorsement, recommendation, or favoring by the United States Government, any agency thereof or any of their contractors or subcontractors. The views and opinions expressed herein do not necessarily state or reflect those of the United States Government, any agency thereof or any of their contractors or subcontractors.

Printed in the United States of America
Available from
National Technical Information Service
U.S. Department of Commerce
5285 Port Royal Road
Springfield, VA 22161

NTIS price codes
Printed copy: A04
Microfiche copy: A01

SAND81-2422
TTC-0270
Unlimited Release
Printed March 1982

Distribution
Category UC-71

Prototype Spent Fuel Canister Design, Analysis, and Test

William B. Leisher, Richard G. Eakes
Transportation Systems Technology and Analysis Division 4552
Sandia National Laboratories
Albuquerque, NM 87185

Thomas A. Duffey, Consultant
Albuquerque, NM 87185

Abstract

Sandia National Laboratories was asked by the US Energy Research and Development Administration (now US Department of Energy) to design the spent fuel shipping cask system for the Clinch River Breeder Reactor Plant (CRBRP). As a part of this task, a canister which holds liquid sodium and the spent fuel assembly was designed, analyzed, and tested. The canister body survived the regulatory Type-B 9.1-m (30-ft) drop test with no apparent leakage. However, the commercially available metal seal used in this design leaked after the tests.

This report describes the design approach, analysis, and prototype canister testing. Recommended work for completing the design, when funding is available, is included.

Contents

Summary 9
1 Introduction 11
1.1 Background 11
1.2 Work Accomplished 11
2 Canister Design 11
2.1 Design Constraints 11
2.2 Design Approach 11
2.2.1 Mechanical Seals 12
2.2.2 Seal Welded Closures 12
3 Analytical Effort 15
3.1 Investigation of Wall Stresses 16
3.1.1 Bare Canister Impact 16
3.1.2 Impact Using Crushable Attenuating Material 19
3.2 Investigation of Plastic Buckling 23
3.2.1 Model of the Problem 23
3.2.2 Determination of Amount of End Deformation 24
3.2.3 Buckling Results 24
3.3 Static Internal Pressure Capacity 27
3.3.1 Bursting of Cylindrical Portion 27
3.3.2 Bolt Thread Failure 28
3.3.3 Static Pressure Results 29
3.4 Conclusions 29
4 Prototype 9.1-m (30-ft) Drop Tests 29
4.1 Canister Assembly and Leaktest 29
4.2 Instrumentation 31
4.3 Photographic Coverage 31
4.4 Test Site 31
5 Test Results 34
5.1 0-Degree (End-On) Test 34
5.2 45-Degree Test 34
5.3 90-Degree (Side-On) Test 34
5.4 End-On Impact Energy Balance 34
5.4.1 Energy Absorption Modes 34
5.4.2 Mode 1: Plastic Hoop-Straining of the Canister Wall 59
5.4.3 Mode 2: Axial Plastic Crush-Up (Shortening) of the Canister 62
5.4.4 Mode 3: Rigid Body Rebound 62
5.4.5 Kinetic Energy Available at Impact 62
5.4.6 Overall Energy Balance and Conclusions 63
6 Conclusions and Recommendations 63
6.1 Conclusions 63
6.2 Recommendations 63
7 References 64
APPENDIX. Mass Properties Report 65

Figures

1 Early Canister Design 13
2 Mechanical Seal, Bolted Canister 14
3 Seal Welded Canister 15
4 Weld Joint Details 15
5 Model for Bare Canister Impact 16
6 Fluid Column as an Isolated System 17
7 Assumed Rigid-Plastic Stress-Strain Model for Canister Wall 19
8 Model Including Crushable Attenuating Material 19
9 Typical Stress-Strain Curve 24
10 Finding the Critical Buckling Stress 24
11 Subassembly Mass Mock-Up 30
12 Accelerometer Installation 32
13 Typical Strain Gage Installation 33
14 Pretest, End-On 36
15 Posttest, End-On, During Rebound 37
16 Posttest, End-On 38
17 Strain Gage Data, End-On, Track No. 1 39
18 Strain Gage Data, End-On, Track No. 2 40
19 Strain Gage Data, End-On, Track No. 3 41
20 Strain Gage Data, End-On, Track No. 4 42
21 Strain Gage Data, End-On, Track No. 5 43
22 Strain Gage Data, End-On, Track No. 6 44
23 Strain Gage Data, End-On, Track No. 7 45
24 Strain Gage Data, End-On, Track No. 8 46
25 Strain Gage Data, End-On, Track No. 9 47
26 Strain Gage Data, End-On, Track No. 10 48
27 Accelerometer Data, End-On, Track No. 11 49
28 Accelerometer Data, End-On, Track No. 12 50
29 Pretest, 45-Degree Drop 51
30 45-Degree Test, at Impact 52
31 Posttest, 45-Degree Drop 53
32 Posttest, 45-Degree Drop, Head 54
33 Posttest, 45-Degree Drop, Close-up of Head Impact Point 54
34 Body Deformation, 45-Degree Drop 55
35 Prettest, 90-Degree Drop 56
36 Posttest, 90-Degree Drop 57
37 Posttest, 90-Degree Drop, Head 58
38 Body Deformation, 90-Degree Drop 59
39 Residual Hoop Strain. 61
40 Stress-Strain Data for 304 Stainless at 21°C (70°F) (Quasi-static) 61
41 Construction of Cumulative Energy Curve 62
42 Cumulative Energy Density 62

Tables

1 Sandia Drawing Numbers for Completed Canister Designs 12
2 Results of Calculations 21
3 Impact Limiting Materials Considered 22
4 Stress-Strain Data, 304 Stainless at 204°C (400°F) and 2.96 x 10^{-4} s^{-1} 25
5 Stress-Strain Data, 304 Stainless at 315°C (600°F) and 2.96 x 10^{-4} s^{-1} 25
6 Stress-Strain Data, 304 Stainless at 21°C (70°F) and 2.96 x 10^{-5} s^{-1} 26
7 Stress-Strain Data, 304 Stainless at 21°C (70°F) and 6.95 x 10^{-1} s^{-1} 26
8 Plastic Buckling Results 26
9 Plastic Buckling Results With Various Mitigators 27
10 Mass Properties of Filled Canister–Mock-Up Assembly 29
11 Strain Gage Locations 31
12 Photometric Setup Sheet (Typical For All Tests) 31
13 0-Degree End-On Test Results 34
14 Pretest and Posttest Diametrial Measurements (End-On Drop) Measurements Made by SNL Division 1485-3 35
15 45-Degree Test Results 51
16 90-Degree (Side-On) Test Results 55
17 Energy Absorbed in Hoop Deformation Mode 60

Summary

The US Energy Research and Development Administration (now the US Department of Energy) assigned the task of designing the Clinch River Breeder Reactor Plant (CRBRP) spent fuel shipping cask system to Sandia National Laboratories.

The design work started with the innermost level of confinement, a leaktight, metal canister containing a coolant and the spent fuel assembly. At the CRBRP-specified 7-kW thermal output per assembly liquid sodium coolant is required to hold the cladding temperature below its required limit of 677°C (1250°F).

The approach used was to design the canister so that it could survive the regulatory 9.1-m (30-ft) drop test without the protection of a cask and so that it would be leaktight after the drop.

Several promising mechanical designs were suggested to and rejected by CRBRP. Prototypes of an acceptable canister concept which uses a mechanical metal seal and a bolted closure were built for testing. A seal-welded design was also completed and built. Both types are constructed of annealed AISI 304 stainless steel to provide compatibility with sodium and, because the annealed metal is relatively soft, to provide significant energy absorption during impact.

Simplified structural analyses made on the prototype design for the end-on (0-degree) impact included hoop stresses induced by the presence of the internal coolant as well as the possibility of axial plastic buckling. The effects of impact limiters such as foamed aluminum were included.

Ambient temperature 9.1-m (30-ft) drop tests were conducted at three impact orientations, 0 degrees (end-on), 45 degrees, and 90 degrees (side-on). No body leakage was noted after any test although the mechanical seals leaked. The seal-welded prototypes were not tested.

Due to budgetary restraints, only a limited amount of posttest analysis was made. An energy balance for the end-on drop showed that approximately 68% of the initial energy was absorbed by body plastic deformation. Much analytical work on the test data remains to be done.

Recommendations made include completing test data analysis, refining the mathematical model, selecting a different mechanical seal, and testing modified, sodium-filled canisters at actual operating temperature if funding becomes available.

Prototype Spent Fuel Canister Design, Analysis, and Test

1 Introduction

1.1 Background

Sandia National Laboratories was asked by the US Energy Research and Development Administration (now the US Department of Energy) to design the spent fuel shipping cask system for the Clinch River Breeder Reactor Plant (CRBRP). To simplify handling and to help meet expected regulatory multilevel containment requirements, it was decided to place each fuel assembly in a separate, sealed canister with sufficient liquid sodium to provide the necessary conductivity for heat rejection. These canisters serve as the first level of containment and are the only portion of the cask system exposed to liquid sodium. The canister would also be used when shipping other reactor components such as blanket assemblies, primary and secondary control assemblies, and radial shields.

1.2 Work Accomplished

This report describes the work accomplished through September 30, 1980 (Fiscal 1980) in making the conceptual design for the canister. It includes an analytical assessment, a mechanical design, and limited prototype test results. Also included are recommendations for additional work necessary to complete the design if funding becomes available.

Note that dual units are used throughout the text. Some tables and figures, however, have only British units because the measurements were made in these units.

2 Canister Design

2.1 Design Constraints

According to information furnished by the CRBRP, the spent fuel assemblies have envelope dimensions of 0.14 m (5.48 in.) in diameter by 4.32 m (170 in.) long. Mass is 201 kg (443 lb), and maximum expected bow is 25 mm (1 in.). Maximum heat output was given as 7 kW and maximum allowable cladding temperature is 677°C (1250°F). Canister in-cask operating temperature can range from sub-zero for an empty cask shipped in midwinter to an estimated possible 550°C (1010°F) in a cask fully loaded with seven 7-kW assemblies. Peak temperature has not yet been determined.

It was considered desirable to have a loaded canister, perhaps with an energy absorbing impact limiter, capable of surviving the regulatory 9.1-m (30-ft) drop test without exceeding allowable leakage. This concept has two advantages: (1) It reduces development costs by eliminating the need for a cask during testing. (2) It is ultraconservative because it ignores the protection provided by the cask body during the drop test.

Allowable leak rate test sensitivities for radioactive material shipping containers are set forth in the proposed 10CFR71-1979[1] as a function of the isotopes present in the contents. Because it has not yet been determined what portion of the contents could escape through a leak, it was assumed for design purposes that the canister would be required to have no leakage. U.S. Nuclear Regulatory Commission (NRC) Regulatory Guide 7.4[2] accepts the leak test procedures and definitions given in American National Standards Institute (ANSI) standard N14.5-1977.[3] This standard defines a minimum leak test boundary as an air leak rate of 1×10^{-8} Pa m^3/s (1×10^{-7} atm cc/s). For practical purposes then, a leak rate of 1×10^{-8} Pa m^3/s (1×10^{-7} atm cc/s) or less, based on dry air at 25°C with an upstream pressure of 1 atm and a downstream pressure of 0.01 atm or lower, is considered leaktight.

Since the canister is to be loaded in the CRBRP Fuel Handling Cell (FHC), provisions had to be included to permit remote handling, closure, and seal testing.

2.2 Design Approach

The philosophy adopted to satisfy the previously mentioned constraints was as follows: First, select a body material which can tolerate the temperature range and liquid sodium and that can absorb a significant amount of energy during deformation. Second,

utilize the services of designers familiar with restrictions imposed by remote handling requirements. Third, subject full scale canisters at both ambient and elevated temperatures to the 9.1-m (30-ft) drop test to verify that they can indeed meet regulatory requirements without the protection of the cask.

A common material which meets the needs is fully annealed AISI 304 stainless steel. Round, seamless, mechanical tubing of 177.8-mm (7.00-in.) outside diameter with a 6.3-mm (0.25-in.) wall thickness was selected for the body material.

Several different mechanical designs were made. All of these concepts are not described in this report, but Table 1 lists all of the pertinent Sandia drawing numbers.

Figure 1 shows an early concept using a quarter turn locking cap with screws to load the metal seal ring and a thin welded plate for the fixed end. This concept, although promising, was rejected by CRBRP as being too complex.

The canister body design required modification because the analyses presented in Section 3.0 indicated the possibility of closed-end rupture during impact. Two stress-reducing options were examined: impact limiters and a thicker-walled closure end. It was decided to replace the last 380 mm (15 in.) of body tube and the welded end plate with a tapered wall, closed-end, forged or machined section. Both the lid and closure ends are welded to the body tube, and the welds are heat treated, radiographed, and helium leak tested. This modified design, shown in Figure 2, was used for the prototype tests described in Section 4.0.

Several features are used to permit ease of remote operation. The lid incorporates a cavity designed to mate with the CRBRP fuel grapple for handling the lid and assembled canister as well as the fuel. The lid hold-down studs are pointed to provide automatic alignment with the seal ring and the lid nuts. These floating nuts are captive in the lid and have a tapered upper end for guiding wrench application.

A seal test feature was not included in this early design. However, it will be added to later versions and will consist of a secondary seal surrounding the main seal. The cavity formed between the two seals is then used for the leak test. An access passage from the outside to the cavity provides a connecting point for the leak detector.

Table 1. Sandia Drawing Numbers for Completed Canister Designs

Part No.	Title
T57588	Canister Assembly
T57583	Canister Body
T57584	Closure, Canister
T57585	Stud, Closure
T57586	Nut, Captive
T57587	"K" Seal
T39847	Fuel Shipping Canister
T39843	Body, Canister
T39844	Closure Canister
T39845	Seal Plate, Closure
T39846	Bolt, Remote Hand
T39848	Retainer, Seal
T48872	Fuel Shipping Canister with Graylock Seal
T57588	Canister Assembly
T57583	Canister Body
T57584	Closure, Canister
T57585	Stud, Closure
T57586	Nut, Captive
T57587	"K" Seal
T61021	"K" Seal
T61022	Ring, Spacer
T61024	Canister Body, Thread & Weld
T61023	Closure, Canister, Thread & Weld

2.2.1 Mechanical Seals

The combination of high operating temperatures and liquid sodium eliminates many common seal materials, such as elastomers, copper, and silver. Remaining material candidates are stainless steels and annealed nickel. Since the canister head material is annealed AISI 304 stainless steel, it will probably be necessary to harden the mating surfaces, perhaps by using a flame-sprayed, hard facing material. The mechanical seal selected for the prototype was a commercially available, proprietary design. This type seal leaked after the regulatory 9.1-m (30-ft) drop test (this testing is described in Section 4) and will not be used in future versions.

2.2.2 Seal Welded Closure

A second type of closure was designed to use a quarter-turn locking plug as the lid (Figure 3). Sealing is accomplished by welding a joint as shown in Figure 4. The weld is machined away when the canister is

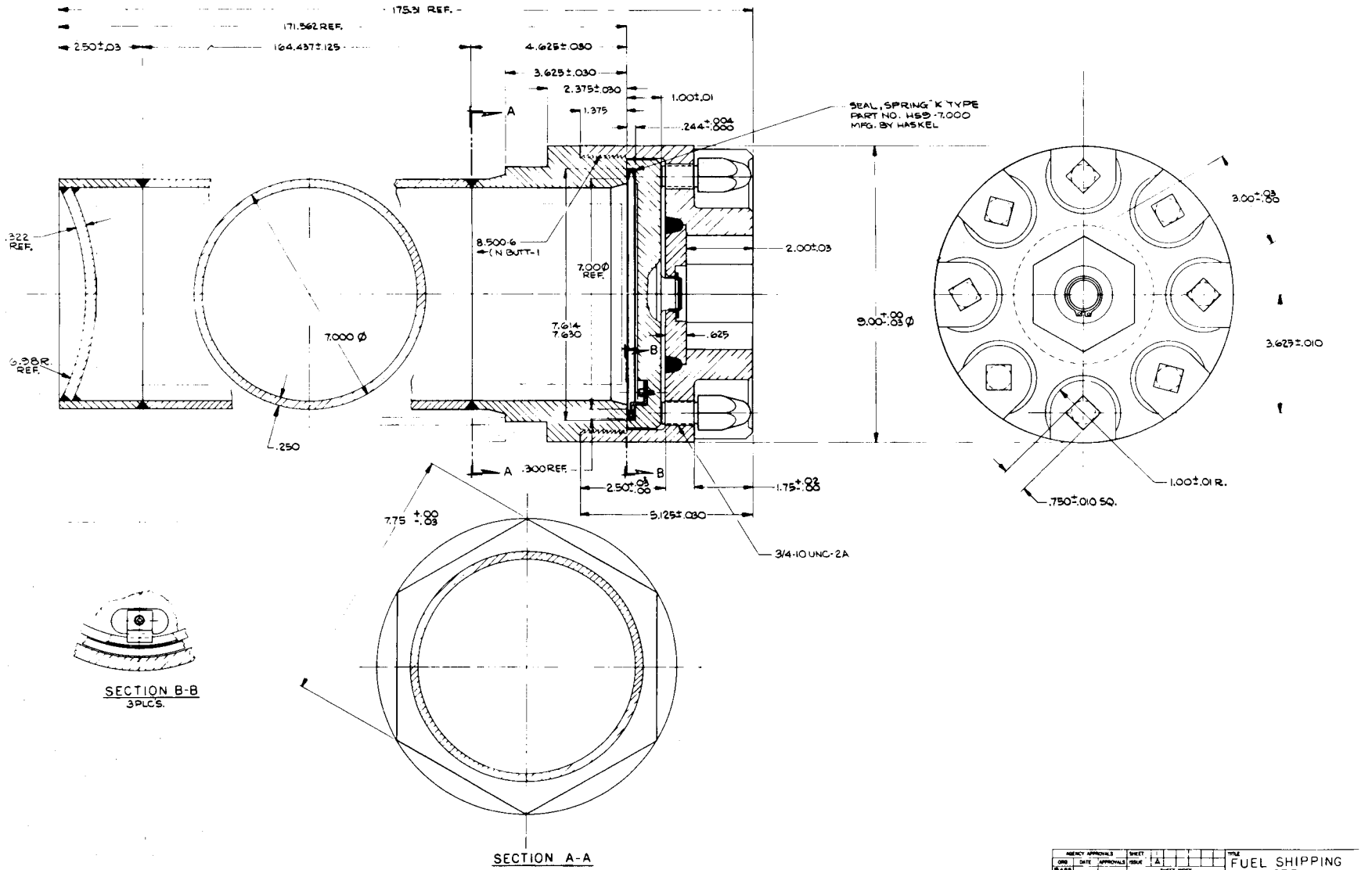

Figure 1. Early Canister Design

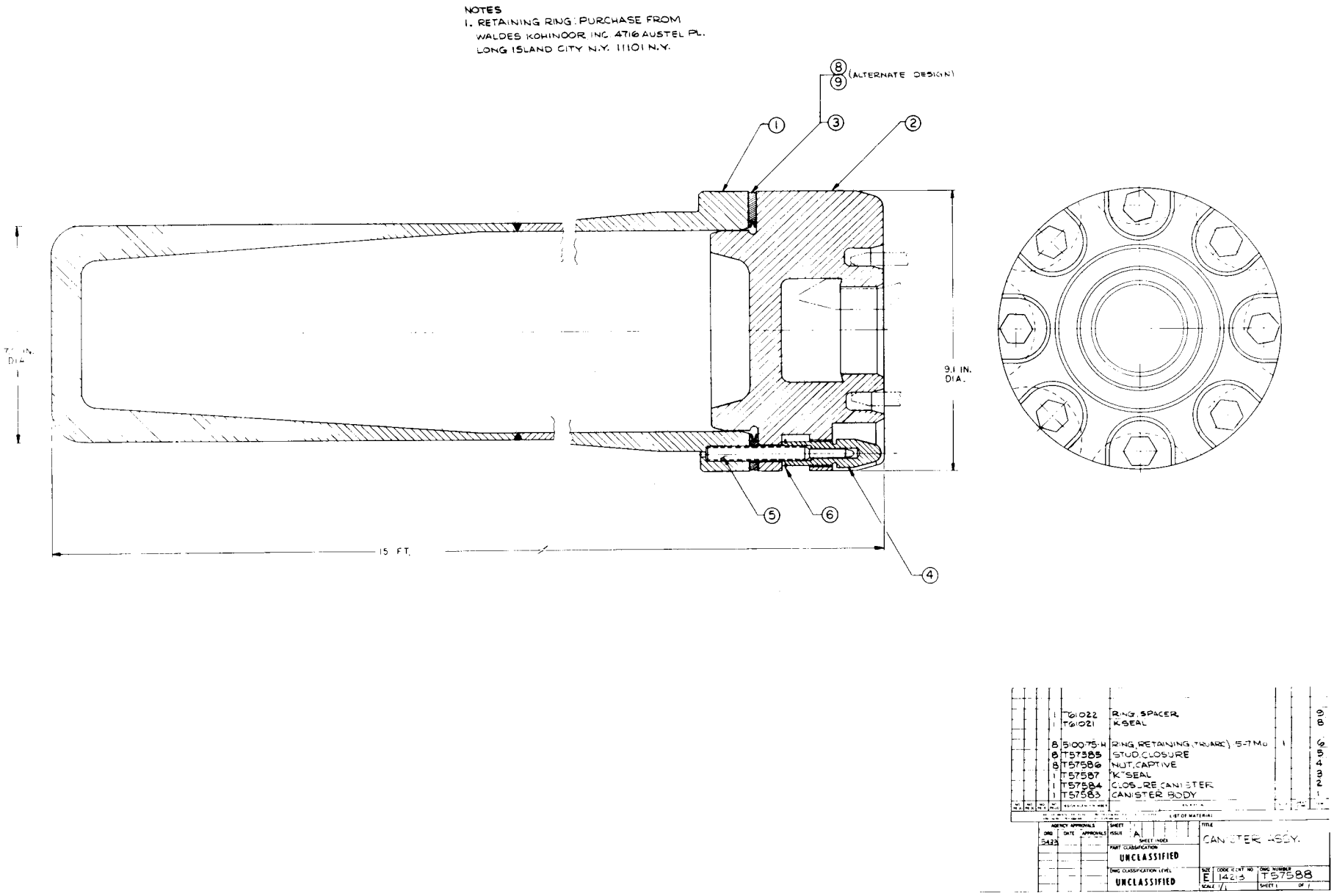

Figure 2. Mechanical Seal, Bolted Canister

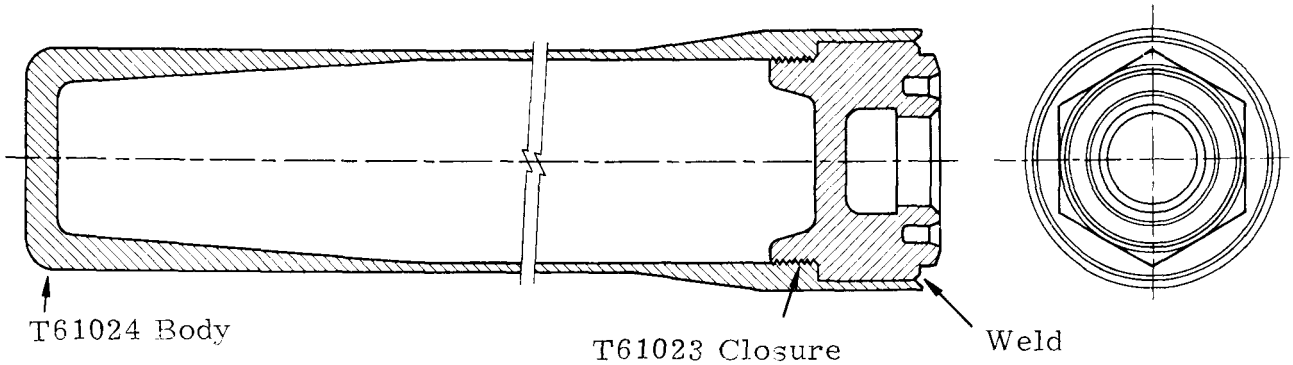

Figure 3. Seal Welded Canister

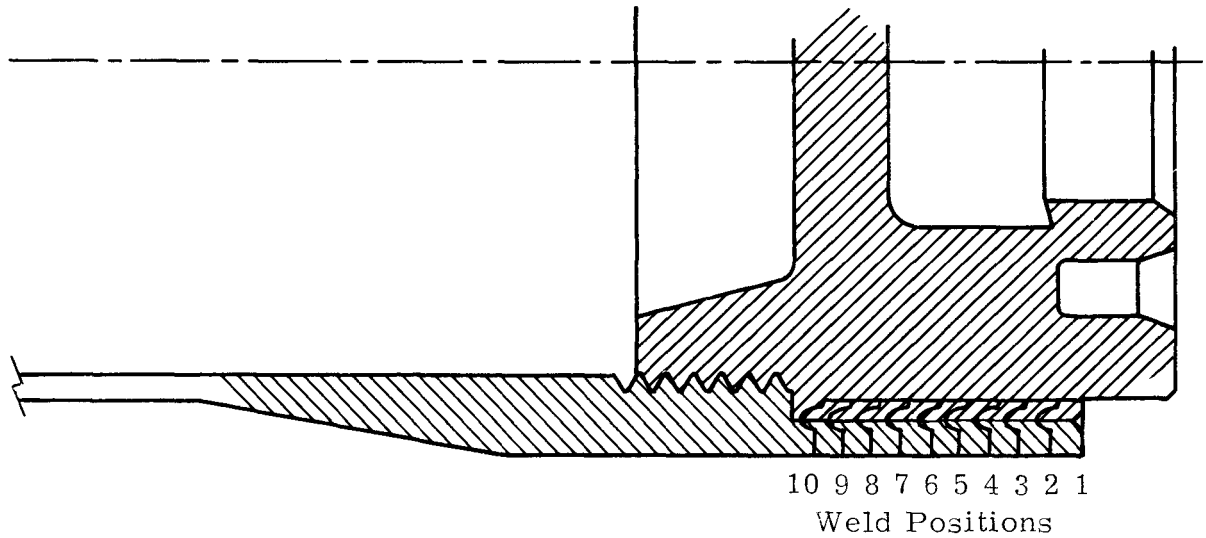

Figure 4. Weld Joint Details

opened. Sufficient material is provided for 10 weld-machine cycles before the closure must be rebuilt or replaced. Again, seal test provisions were not included in this design, but were to be added later. The seal welding concept was also rejected by CRBRP.

3 Analytical Effort

A series of approximate analyses are presented in this section for evaluation of the preliminary canister design outlined in Section 2. Conclusions based on these analyses indicate the necessity for certain design modifications, also described in Section 2.2.

It is important to note that the purpose of performing the various analyses presented herein was to evaluate, indicate weaknesses in, and suggest modifications to the preliminary design of the CRBRP canister. Ultimately, a final design will evolve which will be subjected to a variety of regulatory tests and analyses, as prescribed by 10CFR71.[1]

Required final-design analyses, to appear in a subsequent Safety Analysis Report, will be performed for the load cases indicated in both the "normal" and "hypothetical accident conditions" sections of 10CFR71.[1] These calculations will be performed utilizing the design criteria for structural analysis indicated in NRC Regulatory Guide 7.6[4] based upon the load combinations indicated in NRC Regulatory Guide 7.8.[5]

A number of the regulatory requirements, such as the 1-m puncture test, are not deemed to be as serious a threat as other requirements, such as the 30-ft drop. Hence, preliminary analysis efforts reported here were directed to those loadings which were believed to indicate the major aspects of the design.

Material presented in this section includes development of design guidelines regarding canister wall thickness, the influence of adding impact energy absorbing material, and the influence of the internal fluid on the end impact response of the canister

(Section 3.1). Next, end crush-up of the canister is investigated by means of plastic buckling calculations (Section 3.2). Results of these preliminary analytical efforts are presented in Section 3.3.

Note that in the above analyses, only the situation of normal, symmetric impact is considered. The case of angle impact is believed to be best handled by experiment once a canister is designed to withstand end impact. Results of such an experimental program are presented in Section 5.

3.1 Investigation of Wall Stresses

The canister is modeled as a reasonably thin-walled, long cylinder, closed at both ends, and subjected to a normal, symmetrical impact on one end. The canister is assumed to contain a hexagonal inner tube of fuel, surrounded by an ideal, inviscid, compressible fluid (heat transfer medium). The impact is assumed to occur on a target consisting of a rigid half space.

Two impact situations are considered: one in which the bare canister directly impacts the half space, and one in which crushable, energy absorbing material is incorporated in the design.

In the first case, the end impact causes a sudden change in the velocity of the end cap. Due to the resulting plastic deformation of the end cap, no rebound of the cap is assumed; that is, the impact is modeled as perfectly plastic. As a result of this sudden change in the velocity of the end cap, pressure waves are radiated into the adjacent fluid that is located between the inner hexagonal fuel assembly and the inner wall of the canister. These pressure waves serve to decelerate the ideal fluid. This deceleration then causes a reduction of the pressure radiated into the canister. It is this pressure-time history which, when applied to the wall of the canister, causes a significant dynamic radial impulsive pressure loading of the modeled long cylinder.

In the second impact case considered—the case in which a crushable, energy absorbing material is utilized—the end cap changes velocity at a relatively slow rate, depending primarily upon the total canister mass and force-deflection behavior of the crushable material. As a result, the pressure at the fluid-solid interface inside the canister during the impact process is reduced, causing a less severe pressure-time history loading to be imparted to the canister wall.

First the case of impact of the bare canister is considered, followed by an analysis of the canister impact problem including the crushable, impact energy absorbing material.

3.1.1 Bare Canister Impact

The modeled configuration for bare canister impact is as shown in Figure 5. For simplicity, it is assumed that plane waves propagate upward through the compressible fluid medium within the shell; that is, two-dimensional effects such as rarefactions and reflections off the concentric inner (hexagonal fuel cylinder) and outer (inside diameter of canister) boundaries are ignored.

This plane wave assumption is deemed reasonable near the impact end of the cylinder, becoming progressively poorer (but increasingly conservative) at increased distances from the impact end. Since attention here is focused primarily at the impact end, the assumption is considered totally justified.

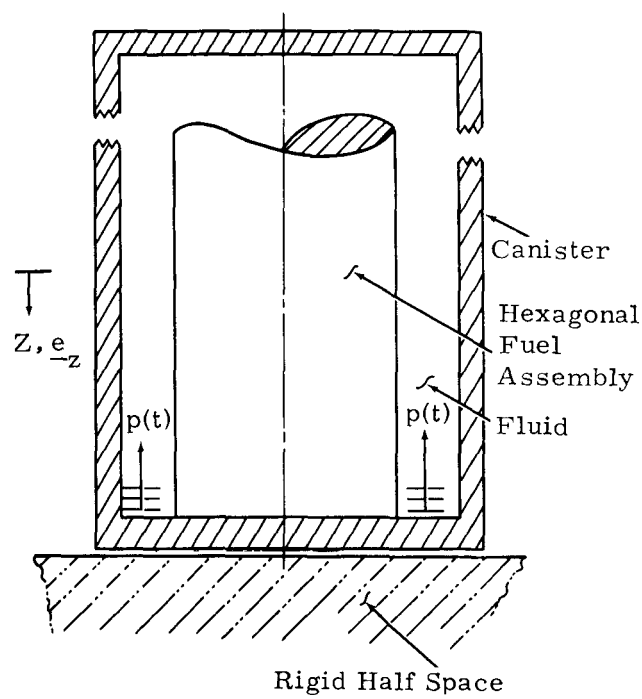

Figure 5. Model for Bare Canister Impact

Pressure-Time Determination. At the time of impact, the end hits the unyielding target. The canister end, initially traveling at impact velocity, $v_o\underline{e}_z$ (see Figure 5), is suddenly stopped. The relative speed of the fluid and solid (impacting end cap) is then v_o, resulting in a fluid-solid interaction and resultant generation of pressure waves as the end cap (solid) attempts to decelerate the fluid. These pressure waves, assumed planar, propagate upward into the

canister interior and interact with the canister wall. The pressure for plane waves is given by

$$p(t) = \rho_f c_f v \,, \tag{1}$$

where

ρ_f = Mass density of internal fluid
c_f = Sonic velocity of internal fluid
v = Relative velocity of the end cap and the fluid (away from the interface).

To develop the specific pressure-time history of the plane wave, consider the fluid column as an isolated system, as shown in Figure 6. Since the fluid is taken as inviscid, no shear stresses act on the lateral boundaries of the fluid column. Interactions with the upper end cap will occur later (approximately 3 ms following impact) and will be of low magnitude due to attenuation, dispersion, and two-dimensional losses by rarefactions through lateral boundaries.

Assuming the end cap is essentially at rest following impact, the equation of motion of the fluid column is

$$\underline{F} = m\underline{a}_{cm} \,, \tag{2}$$

where F, the total force acting on the system,

$$\underline{F} = F = -A\rho c \frac{dz}{dt} \underline{e}_z \,, \tag{3}$$

where

A = contact area of fluid

$\frac{dz}{dt}$ = velocity of the fluid center of mass

and $\underline{a}_{cm} = \frac{d^2z}{dt^2} \underline{e}_z$ is the acceleration of the fluid center of mass.

The resulting differential equation of fluid system motion is given by

$$\frac{d^2z}{dt^2} + \frac{c}{L}\frac{dz}{dt} = 0 \tag{4}$$

subjected to the initial conditions

$z(o) = 0$
$\dot{z}(o) = v_o$.

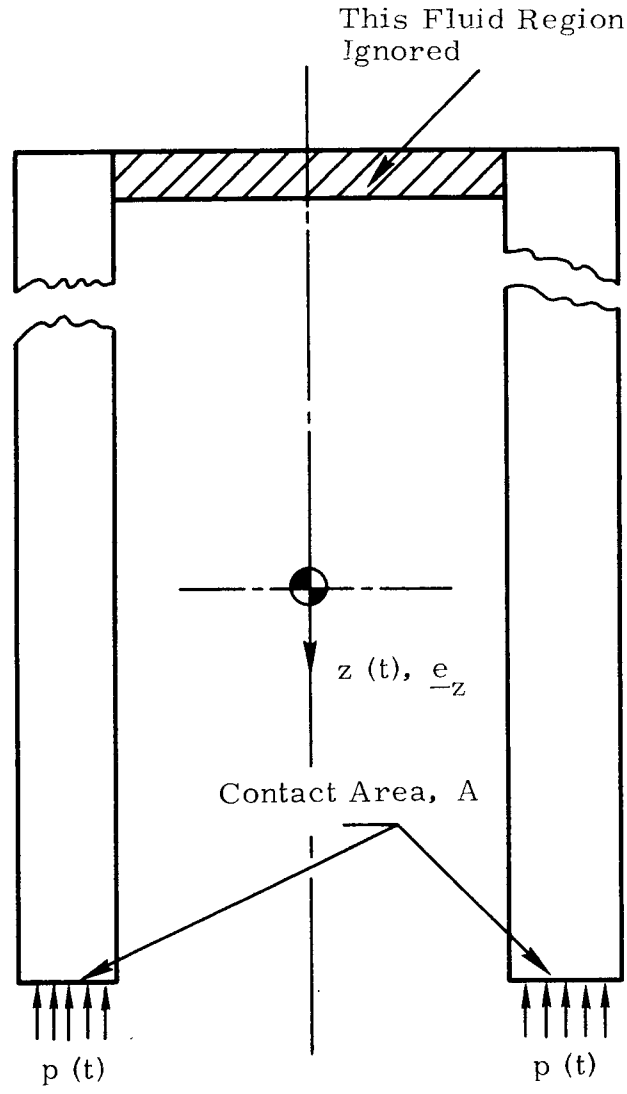

Figure 6. Fluid Column as an Isolated System

Here L denotes the length of the canister.

The solution for vertical velocity of the fluid center of mass (i.e., free field velocity) is then directly determined by standard methods to be

$$v(t) = \frac{dz}{dt}(t) = v_o e^{-\frac{c}{L}t} \,. \tag{5}$$

The resulting pressure at the fluid-solid interface is found from Eqs (1) and (5) to be

$$p(t) = \rho c v_o e^{-\frac{c}{L}t} \,. \tag{6}$$

This is the driving pressure that interacts with the shell. Note that reflection effects due to the propagation of this pulse do not have to be considered as the pulse is side-on to the canister wall. Next the structural response due to this pulse is considered.

Structural Response of Canister. Consider for simplicity a fluid-filled cylinder of unit length representing the canister wall in the vicinity of the impacting end where the pressure-time function is the most severe. Thus, as the shell begins to move out as a result of the above pressure pulse, a rarefaction is reradiated back into the shell as a result of the interaction of the shell wall, its motion, and the contained, ideal compressible fluid.

At this point, a number of methods of analysis could be attempted, including a proper accounting of the fluid-shell interaction at the shell wall. The approach here considers highly simplified structural calculations.

Method One:

In this case, neglect fluid-shell interaction with the canister wall (conservative) and consider static shell response only (unconservative).

By a work-energy method, the impact velocity of the canister is given by

$$v_o = \sqrt{2g\delta}\,, \tag{7}$$

where

δ = Height of drop, and
g = Gravitational constant .

Consider the hoop stress in the canister wall, σ, to be given by the static equilibrium equation for a long cylindrical shell,

$$\sigma = p\,\frac{a}{h}\,, \tag{8}$$

where

a = Mean radius of cylinder
h = Cylinder thickness.

Combining Eqs (6)-(8), the hoop stress is given by

$$\sigma(t) = \frac{a\rho_f c_f}{h}\sqrt{2g\delta}\; e^{-\frac{c}{L}t}\,. \tag{9}$$

Thus the maximum stress is directly proportional to the radius, the fluid density, its sonic velocity, and the square root of drop height. Further, maximum stress is inversely proportional to canister thickness.

Eq (9) should be treated with caution and viewed as overly conservative. Further, it suggests that the canister material ought to have a high ultimate tensile strength, and totally discounts ductility as an important physical property. However, Eq (9) does give an indication of the role played by the various parameters. Clearly, by varying the internal fluid to one of lower density and sonic velocity, hoop stress is greatly reduced.

Note that the influence of the additional axial loading on the canister wall due to impact is not included in Eq (9).

Method Two:

Now consider the dynamic effects of the pressure pulse in Eq (6), i.e.,

$$p(t) = \rho_f c v_o e^{-\frac{c}{L}t}\,. \tag{10}$$

The total impulse, I, imparted to the cylindrical vessel near the impacting end per unit vessel surface area is given by the time integral of Eq (10),

$$I = \int_0^\infty p\,(t)dt = \rho_f v_o L\,, \tag{11}$$

where again

ρ_f = Fluid density
v_o = Impact velocity
L = Canister length.

Again, in the interest of simplicity and conservatism, neglect the fluid-shell interaction and assume the material behavior is rigidly-perfectly plastic, as shown in Figure 7. Then the maximum strain is given by[6]

$$\epsilon_{max} = \frac{I^2}{2\rho_s h^2 \sigma_y}\,, \tag{12}$$

where

ρ_s = Shell density
h = Shell thickness
σ_y = Yield stress of shell material.

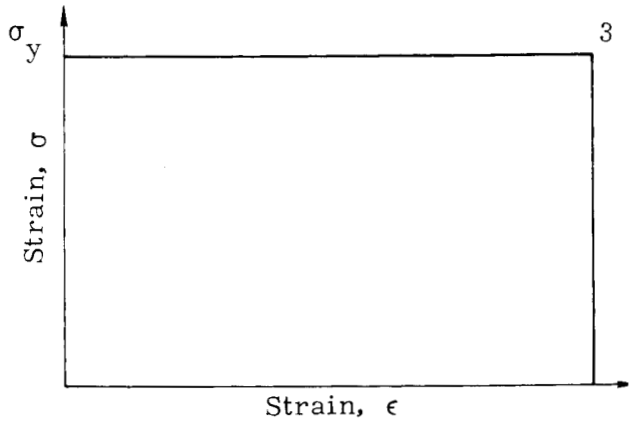

Figure 7. Assumed Rigid-Plastic Stress-Strain Model for Canister Wall

The maximum plastic strain thus calculated for a given problem can be written in terms of parameters introduced earlier as

$$\epsilon_{max} = \frac{\rho_f^2 L^2 g \delta}{\rho_s h^2 \sigma_y} . \tag{13}$$

Eq (12) is based upon a balance of initial kinetic energy imparted to the shell (by the impulsive pressure) with plastic energy absorption through shell deformation. Eq (12) is based upon a total impulse,

$$I = \int p(t)dt \quad , \tag{14}$$

applied in a time duration short compared to the response time of the shell. Since the actual application time is long, Eq (12) and hence (13) appear overly conservative in the present problem. However, Eq (13) illustrates the dependence of the maximum plastic strain on the physical parameters of the problem.

3.1.2 Impact Using Crushable Attenuating Material

Consider again the situation of end impact, but now introduce an impact limiter mounted on the impact end. The situation is now as shown in Figure 8.

For many mitigator or crushable materials, the crush force remains nearly constant over a large range in deflection until the point of "lockup" occurs, after which the load-deflection curve suddenly becomes extremely steep. Based upon this nearly rigid-perfectly plastic constitutive behavior of the crushable material, the rigid-body canister deceleration is constant

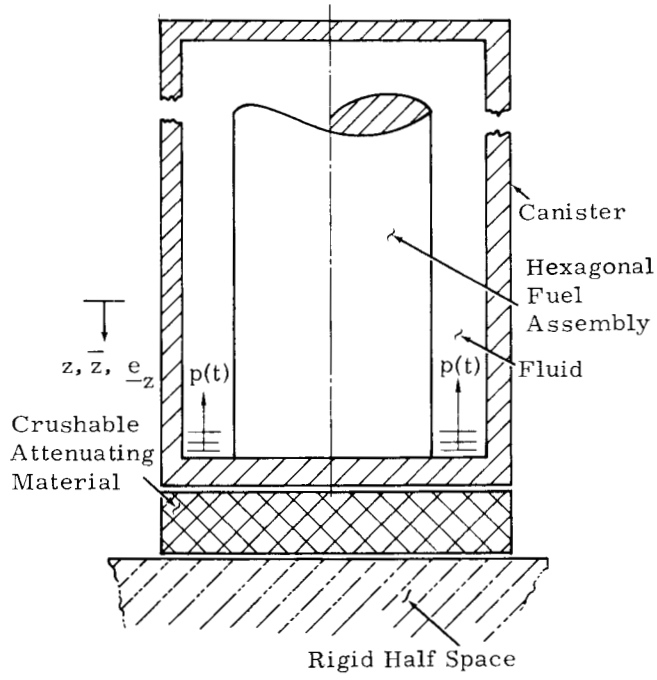

Figure 8. Model Including Crushable Attenuating Material

(at least to lockup), and the velocity-time of the front canister surface can be determined. Then, making a plane wave assumption, the pressure-time pulse radiated into the inner annular core of fluid (and subsequently acting on the canister wall) can be determined.

Based upon Newton's Second Law,

$$\underline{F} = m\underline{a} , \tag{15}$$

the equation of motion of the front canister surface (behind the impact limiter) is

$$-F_o = M \frac{d^2z}{dt^2} \tag{16}$$

subjected to the impact conditions

$$\begin{aligned} z(o) &= 0 \\ \dot{z}(o) &= v_o , \end{aligned} \tag{17}$$

where

F_o = Total crush force
M = Total canister mass
v_o = Impact velocity.

The resulting velocity-time history from Eqs (16) and (17) is

$$\dot{z}(t) = v_o = -\frac{F_o}{M}t \text{ for } 0 < t < \frac{v_o M}{F}, \tag{18}$$

where it is assumed that a perfectly plastic collision occurs. The upper time limit after Eq (18) corresponds to the time at which the canister comes to rest. It is also assumed in Eq (18) that sufficient energy absorbing material is present so that the canister motion is fully arrested before the point of lockup of the crushable material is reached. It should be mentioned in passing that the combined problem of partial impact energy absorption followed by lockup can be solved by similar methods.

Again, assuming one-dimensional wave propagation from the end-cap–fluid interface, the pressure pulse radiated vertically into the fluid is given by

$$p(t) = \rho_f c_f (v_f - v_c), \tag{19}$$

where

v_f = Free field vertical fluid velocity
v_c = Velocity of canister end cap.

(Recall that in the previous analysis v_c was taken as zero at the instant of impact.) Eq (19) can be written as

$$p(t) = \rho c\left[\frac{d\bar{z}}{dt} - \left(v_o - \frac{F}{M}\right)t\right] \quad o < t < \frac{v_o M}{F}, \tag{20}$$

where $\bar{z}$ denotes vertical displacement of the center of mass of the fluid. Now isolating the fluid volume and writing Newton's Second Law for its center of mass, the equation for fluid motion is

$$-\rho_f c_f\left[\frac{d\bar{z}}{dt} - \left(v_o - \frac{F}{M}t\right)\right]A = \rho_f AL\frac{d^2\bar{z}}{dt^2}, \tag{21}$$

where

A = Fluid-solid contact area, and
L = Canister length

with the initial conditions $\dot{\bar{z}}(0) = v_o$, and $\bar{z}(0) = 0$. The solution of Eq (21) is found, using standard techniques, to be

$$\frac{d\bar{z}}{dt} = v_o - \frac{FL}{Mc}\left(e^{-\frac{c}{L}t} + \frac{c}{L}t - 1\right) \tag{22}$$

with the restrictions

$$o < t < \frac{v_o M}{F} \tag{23}$$

and

$$\frac{d\bar{z}}{dt} > 0 \quad . \tag{24}$$

The first restriction simply means that the differential equation takes on a new form once the end cap has completely stopped; the second restriction means that when the fluid mass stops, motion upward (rebound) is not considered. Actually, cavitation would occur at this point in time, changing the response equations.

The pressure-time history is then uniquely determined by substituting Eq (22) into Eq (20), resulting in

$$p(t) = \frac{\rho_f FL}{M}\left[1 - e^{-\frac{c}{L}t}\right], \tag{25}$$

where again,

L = Total canister length
M = Total canister mass (container, fuel, fluid)
F = Total crush force of mitigator
ρ_f = Fluid density
c_f = Fluid sonic velocity.

A comparison of Eqs (25) and (6) reveals that bare impact results in a peaked, exponentially decaying pressure whereas Eq (25) increases from zero, becoming asymptotic to the value ($\rho_f FL/M$). Looking only at peak values, the comparison is as follows:

Without Impact Limiter	With Impact Limiter	
$p_{peak} = \rho_f c_f \sqrt{2g\delta}$	$p_{peak} = \frac{\rho_f FL}{M}$	(26)

Summary of Calculations

Consider the following geometry, material, and loading parameters, corresponding to a 9.1-m (30-ft) drop on a rigid half space with a sodium-filled canister with stainless steel wall (preliminary design configuration).

L = 4.47-m (176-in.) total canister length
M = 484-kg (1067-lbm) total canister mass
ρ_f = 918-kg/m^3 (8.59 x 10^{-5} lb$_f$-sec^2/in.^{4}) liquid sodium density

c_f = 2.52 x 10^3 m/sec (9.94 x 10^4in./sec) sodium sonic velocity

a = 8.57-cm (3.375-in.) average radius of canister wall

h = 0.635-cm (0.25-in.) thickness of canister wall

δ = 9.1-m (30-ft) drop height

Using the above values, as well as a number of different impact limiter materials, predictions utilizing the theories developed above are presented in Table 2. Note that the impact limiter material properties are based upon static and dynamic test results from References 7 and 8. In fact, the impact limiter materials considered in Table 2 are all those from References 7 and 8 of an inorganic nature. The materials are described in more detail in Table 3.

Table 2. Results of Calculations

Impact Limiter Utilized	Crush Stress	Specific Energy Absorption	Peak Radiated Fluid Pressure	Peak Hoop Stress in Canister Wall	Required Length of Impact Limiter*	Comment
None	--	--	31.04 MPa (4501 psi)	419 MPa (60767 psi)	0	Hoop stress high, especially when taking axial stres into account
Aluminum Honeycomb 109 kg/m³ (6.8 PCF)	4.04 MPa (585 psi)	26500 J/kg (8866 ft-lb/lb)	0.848 MPa (123 psi)	11.48 MPa (1665 psi)	0.701 m (27.6 in.)	Limiter too long
High Density Foamed Aluminum 389 kg/m³ (24.3 PCF)	16.5 MPa (2390 psi)	33082 J/kg (11068 ft-lb/lb)	3.46 MPa (502 psi)	46.86 MPa (6795 psi)	0.157 m (6.19 in.)	Length of limiter and hoop stress reasonable
Low Density Foamed Aluminum 160 kg/m³ (10.0 PCF)	2.23 MPa (324 psi)	10503 J/kg (3514 ft-lb/lb)	0.470 MPa (68.1 psi)	6.36 MPa (922 psi)	1.204 m (47.4 in.)	Impact limiter too long
Spiralgrid 600 590 kg/m³ (36.8 PCF)	40.75 MPa (5909 psi)	39712 J/kg (13286 ft-lb/lb)	8.56 MPa (1242 psi)	115.9 MPa (16817 psi)	0.086 m (3.40 in.)	Length of limiter and hoop stress reasonable
Fiberfrax 639 kg/m³ (39.9 PCF)	8.52 MPa (1235 psi)	5894 J/kg (1972 ft-lb/lb)	1.793 MPa (260.0 psi)	24.24 MPa (3515 psi)	0.536 m (21.1 in.)	Impact limiter too long
Marinite 634 kg/m³ (39.6 PCF)	17.97 MPa (2607 psi)	8806 J/kg (2946 ft-lb/lb)	3.78 MPa (548 psi)	51.17 MPa (7420 psi)	0.361 m (14.2 in.)	Impact limiter too long

*To prevent "lockup" or bottoming out of canister

Table 2 is arranged as follows:

Impact Limiter Utilized—See Table 3 for description of each material.

Crush Stress—The average crush stress of the material. Reference 8 indicates that, at the low loading rates considered here, dynamic effects of loading are unimportant; that is, static properties can be utilized. Further, most materials have a reasonably flat (i.e., rigid-perfectly plastic) load-deflection relationship to the point of lockup. Crush stress is used to compute F in Eq (26) based upon a 248.3-cm^2 (38.5-sq in.) impact area.

Specific Energy Absorption—The energy absorbed by the material per unit mass of material.

Peak Radiated Fluid Pressure—The peak pressure generated during the impact process. (See Eq (26).

Peak Hoop Stress in Canister Wall—See Eq (9) and (26).

Required Length of Impact Limiter—The minimum length of a 0.178-m (7.0-in.) diameter cylinder of distended material to prevent lockup. This minimum length is determined by solving for the volume (and hence length) of material necessary to just absorb the impact kinetic energy of the impacting canister system. Specific energy absorption and density, both of which are indicated in other columns of Table 2, are utilized. A 9.1-m (30-ft) drop is assumed.

Table 3. Impact Limiting Materials Considered*

Material	Description
Aluminum Honeycomb	5052 aluminum with 0.48 cm (3/16 in.) cell size, 0.0063 cm (0.0025 in.) foil thickness, compressed parallel to the cell axis.
High Density Foamed Aluminum	Nominally 384 kg/m^3 (24 lb/ft^3) foamed aluminum, compressed parallel to rise direction.
Low Density Foamed Aluminum	Nominally 160 kg/m^3 (10 lb/ft^3) foamed aluminum, compressed parallel to rise direction.
Spiralgrid 6000	Nominally 41 MPa (6000 psi) spirally wound steel honeycomb, compressed parallel to cell direction.
Fiberfrax	Nominally 641 kg/m^3 (40 lb/ft^3) ceramic (alumina, silica) insulation, compressed perpendicular to rolling direction.
Marinite	Nominally 577 kg/m^3 (36 lb/ft^3) asbestos base insulation, compressed perpendicular to rolling direction.

*Information based upon References 7 and 8.

Inspection of Table 2 reveals that, in the absence of any mitigating material, the peak hoop stress is nominally 419 MPa (60,700 psi). As a class, all impact limiting materials serve to significantly reduce radiated pressure and resultant canister wall hoop stress. However, a number of impact limiter materials are not suitable because the length (i.e., volume) required to absorb the kinetic energy of the canister at impact is excessive and would significantly increase the cost of the enclosing cask.

Of all materials considered, the two remaining possibilities are the High Density Foamed Aluminum and the Spiralgrid. In the case of the foamed aluminum, the peak hoop stress is reduced by more than a factor of eight from the impact situation with no limiter, although 15.7 cm (6.2 in.) of material would be required. The Spiralgrid requires only 8.6 cm (3.4 in.) of limiter length, but the resulting pressure in the fluid and corresponding peak hoop stress are not as beneficial as with the foamed aluminum, representing a factor of 3.6 decrease over the case of no impact limiter.

3.2 Investigation of Plastic Buckling

3.2.1 Model of the Problem

Due to symmetric, end-on canister impact, it is anticipated that a certain degree of crush-up of the cylindrical portion of the canister due to plastic buckling may occur. Such symmetric, accordion-type buckling deformations are of particular concern to the canister design for the following reason: A fuel assembly is contained within the canister. This fuel assembly has a significant axial clearance from the canister ends. Should the canister crush to the point at which "bottoming out" occurs, significant axial loading of the end cap would result, possibly causing seal failure. It is thus important to determine canister shortening.

The problem of symmetric axial impact of cylindrical shells and resultant plastic buckling has been a subject receiving considerable attention by a number of investigators.[9-13]

It is known[9-11] that plastic shells may buckle either in the nonaxisymmetric diamond-shaped wave pattern characteristic of elastic buckling or in an axisymmetric mode. Only the latter, axisymmetric, buckling mode is considered here due to the fact that the canister is a relatively thick-walled shell.

It is found in References 10-12 that the critical buckling stress is practically independent of length of the cylinder. Thus the more simplified formula for a semi-infinite shell is utilized here. The critical axial stress for buckling with simply supported ends is given by [10 11]

$$\sigma_{crit} = \frac{2Eh}{a} \frac{1}{\{3[(5-4\nu)\lambda - (1-2\nu)^2]\}^{1/2}}, \qquad (27)$$

where

- E = Young's modulus
- h = Canister thickness
- a = Mean canister radius
- ν = Poisson's Ratio
- λ = E/E_t
- E_t = Local tangent modulus at the buckling stress.

It should be mentioned that the tangent modulus is a nonlinear function of stress (or strain). The above theory is obviously very sensitive upon the degree of strain hardening. Thus, evaluation of Eq (27) requires accurate tangent modulus information ($d\sigma/d\epsilon$) at the conditions of impact (i.e., correct temperature and strain rate). Note further that for $\lambda = 1$, the result reduces to the case of elastic buckling.

An additional comment is in order. It is reported in Reference 12 that the difference between the load for first bifurcation and the theoretical maximum load can be expected to be small. This fact will be useful in determining total crush displacement.

The method of determination of the critrical buckling stress using Eq (27) is not completely straightforward (except when λ = constant) and warrants further discussion. The difficulty lies in the fact that the slope ($d\sigma/d\epsilon$) of the strain hardening portion of a typical stress strain curve is not a constant, but rather a function of stress itself. (In the elastic range, $\lambda = 1$, a constant.) The procedure for finding the critical buckling stress is done by incrementing the applied stress from zero on up until Eq (27) is satisfied, at which point buckling occurs. The problem can be divided into two phases:

Phase 1: Check for Elastic Buckling. This phase covers the range in stress, $0 \leq \sigma \leq \sigma_y$, where σ_y is the yield stress of the material. Since in this phase, λ = constant = 1, simply calculate σ_{crit} directly from Eq (27) from geometrical and material parameters of the problem. If $\sigma_{crit} < \sigma_y$, elastic buckling occurs. (This is not likely in the present problem due to the relative thickness of the canister.) Proceed no further. If $\sigma_{crit} > \sigma_y$, plastic buckling must be investigated.

Phase 2: Plastic Buckling. In this case, $\lambda = f(\sigma)$. Determine the slope $d\sigma/d\epsilon$ as a function of σ from the stress-strain curve of the material (e.g., see Figure 9). Starting at σ_y, increment σ and evaluate the right side of Eq (27) for the correct value of λ. Plot, as shown in Figure 10, the value of σ_i used and the value of σ calculated from the right side of Eq (27) versus increment number. The intersection of these two curves gives σ_{crit}.

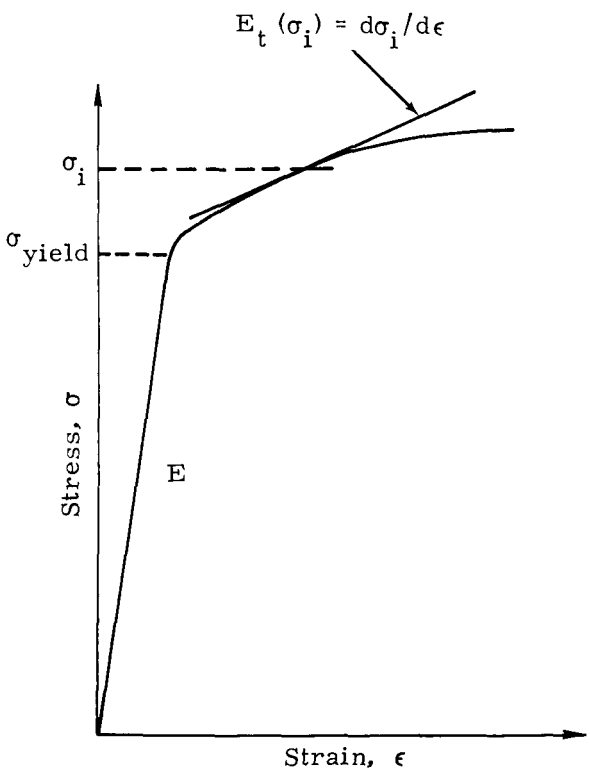

Figure 9. Typical Stress-Strain Curve

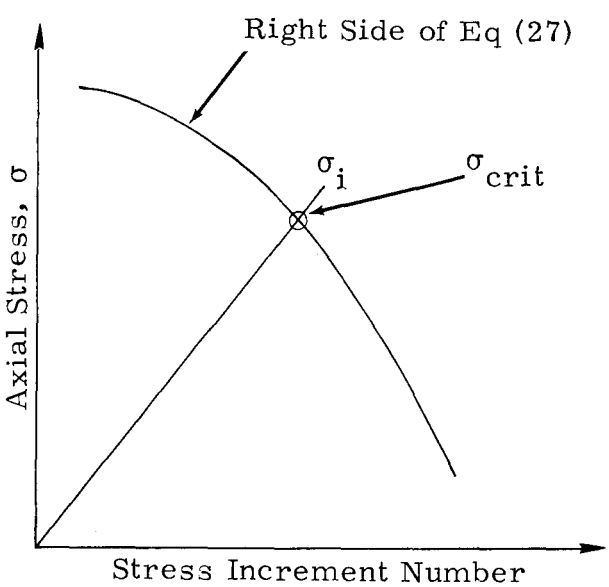

Figure 10. Finding the Critical Buckling Stress

3.2.2 Determination of Amount of End Deformation

As reported in Reference 11, the difference between the load for first bifurcation and the theoretical maximum load can be expected to be very small. For simplicity, assume that the bifurcation load remains constant as the shell deforms; i.e., assume a rigid-perfectly plastic resistance to crushing.

Since the initial kinetic state at impact is known, the amount of crush-up may be readily calculated. It is assumed here that any additional resistance to crush-up due to the presence of the internal fluid as well as the fuel assembly can be ignored. Equating the impact kinetic energy with the critical plastic buckling force results in the following relationship for the end shortening, δ:

$$\delta = \frac{Mv_o^2}{4\pi a h \sigma_{cr}}, \tag{28}$$

where

M	=	Mass of canister only (i.e., fluid and fuel rod masses are neglected)
v_o	=	Impact velocity ($\sqrt{2gh}$)
a	=	Mean canister radius
h	=	Canister thickness
σ_{cr}	=	Critical plastic buckling stress.

3.2.3 Buckling Results

Experimental stress-strain information was supplied by H. Rack, Sandia National Laboratory, Division 5832, for annealed, 304 stainless steel subjected to uniaxial tension. Test conditions for the four sets of data supplied are as follows:

Data Set	Strain Rate(s^{-1})	Temperature
1	2.96×10^{-4}	204°C (400°F)
2	2.96×10^{-4}	315°C (600°F)
3	2.96×10^{-5}	21°C (70°F)
4	6.95×10^{-1}	21°C (70°F)

Raw data for the above four data sets (stress in MPa, strain in m/m) is presented in Tables 4 through 7, respectively.

Table 4. Stress-Strain Data for 304 Stainless at 204°C (400°F) and 2.96 x 10^{-4} s^{-1}

Stress (MPa)	Strain (m/m)
0.897E+02	0.599E−03
0.953E+02	0.700E−03
0.101E+03	0.800E−03
0.107E+03	0.120E−02
0.112E+03	0.130E−02
0.118E+03	0.170E−02
0.123E+03	0.220E−02
0.126E+03	0.260E−02
0.129E+03	0.250E−02
0.135E+03	0.340E−02
0.140E+03	0.410E−02
0.147E+03	0.540E−02
0.160E+03	0.780E−02
0.174E+03	0.122E−01
0.197E+03	0.226E−01
0.226E+03	0.384E−01
0.254E+03	0.544E−01
0.279E+03	0.705E−01
0.319E+03	0.103E+00
0.361E+03	0.136E+00
0.391E+03	0.170E+00
0.413E+03	0.204E+00
0.429E+03	0.238E+00
0.440E+03	0.273E+00
0.444E+03	0.300E+00
0.445E+03	0.314E+00
0.441E+03	0.321E+00
0.431E+03	0.329E+00
0.411E+03	0.337E+00
0.385E+03	0.346E+00
0.347E+03	0.356E+00
0.308E+03	0.364E+00
0.288E+03	0.367E+00

As discussed in the previous section, first the possibility of elastic buckling was checked and found not to occur. Next, stress-strain points for each of the four data sets were finite differenced to determine the local tangent modulus

$$E_t = \frac{d\sigma}{d\epsilon}$$

as a function of stress. Both sides of Eq (27) were then evaluated at each stress increment using the appropriate elastic modulus (function of temperature). The

Table 5. Stress-Strain Data for 304 Stainless at 315°C (600°F) and 2.96 x 10^{-4} s^{-1}

Stress (MPa)	Strain (m/m)
0.297E+03	0.170E−02
0.320E+03	0.260E−02
0.332E+03	0.440E−02
0.357E+03	0.127E−01
0.374E+03	0.209E−01
0.423E+03	0.545E−01
0.459E+03	0.887E−01
0.482E+03	0.123E+00
0.499E+03	0.158E+00
0.501E+03	0.171E+00
0.501E+03	0.178E+00
0.496E+03	0.185E+00
0.480E+03	0.194E+00
0.448E+03	0.205E+00
0.392E+03	0.216E+00
0.376E+03	0.218E+00

plastic buckling stress was then determined graphically. Finally, the corresponding end deformation, δ, was then calculated using Eq (28). Results are presented in Table 8 for the case of no mitigating material.

An inspection of Table 8 reveals the following: Data sets 1 through 3, nominally at quasi-static strain rates, give the influence of canister wall temperature on buckling stress, whereas data sets 3 and 4 give an indication of the influence of strain rate. It can be seen that, at least for plastic buckling, the critical buckling stress is little influenced by rate of straining or significant temperature variation.

Corresponding end shortening, in the vicinity of 1 cm (0.4 in.) in all cases, is also indicated in Table 8. Note finally that calculations presented in Table 8 are based upon the elastic modulus at the corresponding test temperature, as given in Reference 14.

Bifurcation will, of course, not be initiated unless the critical buckling stress is reached during the impact process. The stress generated at impact is given early in time (before two-dimensional effects become important) by the plane wave equation

$$\sigma = \rho c v \ , \tag{29}$$

where

σ = Axial compressive stress at point of impact
c = Bar velocity in the canister
v = Impact velocity.

Table 6. Stress-Strain Data for 304 Stainless at 21°C (70°F) and 2.96 x 10^{-5} s^{-1}

Stress (MPa)	Strain (m/m)
0.133E+03	0.150E−02
0.170E+03	0.220E−02
0.194E+03	0.280E−02
0.209E+03	0.340E−02
0.222E+03	0.400E−02
0.232E+03	0.470E−02
0.250E+03	0.650E−02
0.268E+03	0.890E−02
0.281E+03	0.123E−01
0.301E+03	0.230E−01
0.326E+03	0.408E−01
0.365E+03	0.763E−01
0.396E+03	0.112E+00
0.422E+03	0.147E+00
0.445E+03	0.183E+00
0.464E+03	0.218E+00
0.483E+03	0.254E+00
0.499E+03	0.290E+00
0.513E+03	0.325E+00
0.526E+03	0.361E+00
0.537E+03	0.396E+00
0.547E+03	0.432E+00
0.555E+03	0.467E+00
0.562E+03	0.503E+00
0.583E+03	0.574E+00
0.585E+03	0.610E+00
0.581E+03	0.645E+00
0.540E+03	0.663E+00
0.483E+03	0.672E+00
0.439E+03	0.675E+00
0.415E+03	0.676E+00
0.396E+03	0.677E+00

Since the critical buckling stresses are calculated based upon material properties at various temperatures, over which the elastic modulus, E, varies, the stress generated due to a 9.1-m (30-ft) drop must be calculated for each case to determine whether bifurcation will actually occur.

Table 7. Stress-Strain Data for 304 Stainless at 21°C (70°F) and 6.95 x 10^{-1} s^{-1}

Stress (MPa)	Strain (m/m)
0.115E+03	0.600E−03
0.159E+03	0.100E−02
0.196E+03	0.150E−02
0.214E+03	0.200E−02
0.229E+03	0.270E−02
0.237E+03	0.330E−02
0.247E+03	0.450E−02
0.255E+03	0.600E−02
0.323E+03	0.477E−01
0.397E+03	0.131E+00
0.443E+03	0.214E+00
0.482E+03	0.298E+00
0.515E+03	0.381E+00
0.543E+03	0.464E+00
0.561E+03	0.548E+00
0.579E+03	0.631E+00
0.590E+03	0.714E+00
0.595E+03	0.756E+00
0.597E+03	0.798E+00
0.598E+03	0.819E+00
0.595E+03	0.839E+00
0.570E+03	0.860E+00
0.513E+03	0.877E+00
0.359E+03	0.896E+00

Table 8. Plastic Buckling Results

Data Set	E*	Critical Buckling Stress, σ_{crit}	End Deformation, δ
1	1.83x10^5 MPa (26.6x10^6 psi)	410.3 MPa (59,500 psi)	1.02 cm (0.40 in.)
2	1.75x10^5 MPa (25.4x10^6 psi	460.6 MPa (66,800 psi)	0.91 cm (0.36 in.)
3	1.95x10^5 MPa (28.3x10^6 psi)	431.0 MPa (62,500 psi)	0.97 cm (0.38 in.)
4	1.95x10^5 MPa (28.3x10^6 psi)	410.3 MPa (59,500 psi)	1.02 cm (0.40 in.)

*See Reference 9.

Using

ρ = 4.50 kg/m^3 (.281 lbm/ft^3)

v = 13.38 m/s (527 in./s) (9.1-m (30-ft) drop, neglecting air drag)

E = 1.95 x 10^5 MPa at 21°C (28.3 x 10^6 psi at 70°F)
1.83 x 10^5 MPa at 204°C (26.6 x 10^6 psi at 400°F)
1.75 x 10^5 MPa at 316°C (25.4 x 10^6 psi at 600°F),

the peak impact stress for each data set is as follows:

Data Set 1: σ = 506.2 MPa (73400 psi),
Data Set 2: σ = 492.4 MPa (71400 psi),
Data Set 3: σ = 521.4 MPa (75600 psi),
Data Set 4: σ = 521.4 MPa (75600 psi).

Comparison of this peak generated impact stress with the corresponding impact stress listed in Table 8 reveals that bare canister impact (that is, non-mitigating material) results, in all cases, in loading sufficient to initiate bifurcation.

In the case of mitigating, impact energy absorbing material located at the ends of the canister (see Reference 15) the force transmitted to the canister wall is dependent upon mitigator type. Using the six mitigating materials considered in Table 2, the transmitted axial canister wall stress for each mitigating material is presented in Table 9. Note that, in all cases, the axial stress in the canister is below all bifurcation values determined for the four sets of stainless material properties. Hence, the canister will not crush up (buckle) when sufficient mitigating material is present to prevent mitigator lockup. Inclusion of adequate mitigator volume therefore appears to "save" about 1/2 in. of canister length.

3.3 Static Internal Pressure Capacity

The purpose of this section is to determine the maximum static internal pressure which can be withstood by the spent fuel shipping canister. The shipping canister can be envisioned as a long, tapered circular cylinder, closed on one end. On the other end is a specially bolted (studded) closure.

There are two potential failure modes of the canister assembly: bursting of the cylindrical portion (thinnest region in Item 1 of Figure 2) and failure of bolts/threads in the closure region. These are analyzed individually in the following sections.

3.3.1 Bursting of Cylindrical Portion

Modeling the canister body as a long cylindrical shell, the burst pressure is given by[15]

$$P_{burst} = 2\sigma_{ULT}\frac{(b-a)}{(b+a)}, \tag{30}$$

where

σ_{ULT} is the ultimate tensile stress of the material,
a = inner radius
b = outer radius.

For

a = 8.26 cm (3.25 in.)
b = 8.89 cm (3.50 in.)
σ_{ULT} = 403.4 MPa (58,500 psi) (304 stainless steel, 70°F),

the burst pressure is

$$P_{burst} = 29.88 \text{ MPa (4333 psi)}. \tag{31}$$

Table 9. Plastic Buckling Results With Various Mitigators

Impact Limiter Material	Canister Wall Axial Stress	Comment
Aluminum Honeycomb	27.2 MPa (3948 psi)	No buckling occurs
High Density Foamed Aluminum	111.2 MPa (16130 psi)	No buckling occurs
Low Density Foamed Aluminum	15.1 MPa (2186 psi)	No buckling occurs
Spiralgrid 6000	275.0 MPa (39880 psi)	No buckling occurs
Fiberfrax	57.5 MPa (8335 psi)	No buckling occurs
Marinite	121.3 MPa (17594 psi)	No buckling occurs

3.3.2 Bolt Thread Failure

Bolts (studs) are constructed of 15-5 PH stainless steel, either in the 1025°F or 1075°F (579°C) temper. Assume conservatively that it is in the 1075°F (579°C) temper.

Failure in the vicinity of the bolts (for the case of the bolted closure design) could occur in one of three modes:

Mode 1: Tensile Bolt Failure—For the possibility of tensile bolt failure, the eight 1/2-in. bolts each has a "stress" area (area of minor diameter) of 1.03 cm² (0.16 in.²). The eight bolts must carry the total force on the end closure due to the internal pressure. Equating the pressure-induced force on the closure to the total opposing bolt force results in

$$P_i A_P = N A_B \sigma_{ULT} , \tag{32}$$

where P_i is internal pressure, A_P is projected end closure area, N is number of bolts, A_B is bolt stress area, and σ_{ULT} is ultimate tensile stress of the 15-5 PH stainless bolt material. Solving for internal pressure results in

$$P_i = N \frac{A_B}{A_P} \sigma_{ULT} \tag{33}$$

For

$N = 8$
$\sigma_{ULT} = 1000$ MPa (145,000 psi)
$A_B = 1.03$ cm² (0.16 in.²)
$A_P = 214$ cm² (33.1 in.²)

Then

$$(P_i)_{max} = 38.7 \text{ MPa (5607 psi)} \tag{34}$$

Mode 2: Bolt Thread Shear Failure—Now consider the possibility of the bolt threads shearing off. This could occur either in the blind hole location (Item 5 of Figure 2) or at the captive nut (Item 6 of Figure 2). Since the engagement length at the captive nut is considerably less (estimated as 1.9 cm (.75 in.)), this situation governs. Again the total end closure pressure-induced force is equated with the bolt resistive force (this time in shear):

$$P_i A_P = N A_s \sigma_{ULT\,SHEAR} \tag{35}$$

where A_s is the shear area available and $\sigma_{ULT\,SHEAR}$ is the ultimate shear stress of the bolt material. Assuming $\sigma_{ULT\,SHEAR} = 1/2\ \sigma_{ULT} = 500$ MPa (72,500 psi), $A_s = \pi D_\mu L_e$ where D_μ = minor diameter, and L_e is engagement length, then the maximum internal pressure becomes:

$$P_i = \frac{N \pi D_\mu L_e \sigma_{ULT}}{2 A_P} . \tag{36}$$

For

$N = 8$
$D_\mu = 1.15$ cm (.453 in.)
$L_e \cong 1.9$ cm (.75 in.)
$\sigma_{ULT} = 100$ MPa (145,000 psi)
$A_P = 214$ cm² (33.1 in.²)

then,

$$P_i = 128.9 \text{ MPa (18693 psi)} . \tag{37}$$

Mode 3: Thread Failure in Blind Hole—For the blind hole, the softer stainless threads might shear out. Engagement length is estimated from Figure 2 as 1.0 in. Again, equilibrium requires

$$P_i A_P = N A_s \sigma_{ULT\,SHEAR} \tag{38}$$

where previous definitions apply now to the 304 stainless. The internal maximum pressure is now

$$P_i = \frac{N \pi D L_e}{A_P} \frac{\sigma_{ULT}}{2} \tag{39}$$

where D is major diameter of the tapped hole.

For

$N = 8$
$D = 1.27$ cm (0.5 in.)
$L_e \cong 2.54$ cm (1.0 in.)
$A_P = 214$ cm² (33.1 in.²)
$\sigma_{ULT} = 403$ MPa (58,500 psi)

then,

$$(P_i)_{max} = 76.5 \text{ MPa (11099 psi)} . \tag{40}$$

3.3.3 Static Pressure Results

The failure mode governing is obviously the minimum value of the pressures calculated above. Thus failure will occur by bursting at approximately 29.8 MPa (4333 psi).

3.4 Conclusions

1. As a result of impact from a 9.1-m (30-ft) drop on any unyielding target, hoop stresses generated in the preliminary canister design (with 0.635-cm (0.25-in.) wall) are expected to be in the neighborhood of 419 MPa (60,700 psi).
2. It is believed that this stress state, when superimposed with axial stresses in the canister wall, may well result in failure.
3. The addition of crushable, energy absorbing materials is one possible design modification for reducing canister wall stresses and is found to cushion the impact, reduce the peak pressure generated in the liquid sodium, and therefore reduce the peak hoop stress in the canister wall. The reduction in peak stress level is dependent upon the properties of the crushable material. Generally, the required length of impact limiter (which must be minimized) is inversely proportional to the peak stress in the canister wall. For two impact materials considered—High Density Foamed Aluminum and Spiralgrid 6000—the length of limiter material is reasonable and the peak loop stress is still substantially reduced from the "bare" impact situation. It is believed that 9.1-m (30-ft) impacts with these two materials would not lead to failure.
4. Other possible methods of reducing the high canister wall stress include increasing the wall thickness, particularly near the impacting end.
5. The possibility of axial buckling could be eliminated by either increasing wall thickness (particularly near the impacting end) or adding energy absorbing materials.
6. The most probable mode of failure is by bursting from excessive hoop stress.

4. Prototype 9.1-m (30-ft) Drop Tests

Prototype testing was restricted and abbreviated due to limited funding. Because it was felt that the seal welded canister could survive the drop without leaking, tests were conducted on two mechanically sealed canisters.

The first canister was used for 0- (end-on) and 45-degree impacts. The second canister was used only for the 90-degree (side-on) test.

A fuel assembly mass mock-up (Figure 11) was in the canisters for the tests.

Because it was desired to conduct these preliminary tests at ambient temperature, it was necessary to use a liquid with room temperature dynamic properties similar to those of 400°C liquid sodium. (Actual peak operating temperature is not yet known, but 400°C is felt to be a reasonable estimate.) As shown in Section 3, the liquid property of primary concern is the acoustic impedance (product of density and acoustic velocity). The liquid used was a 1:3.65 (volumetric) mixture of methanol and glycerine. This resulted in an acoustic impedance of 2.0×10^6 kg/m^{2}s (4.1×10^5 lb/ft^{2}s), essentially the same as that of 400°C (750°F) liquid sodium.

Combined mass properties of the canisters as tested are listed in Table 10. It is assumed that mock-up and canister are concentric and assembly is filled to 0.10 m (3.88 in.) from top flange with the methanol/glycerine mixture. Mass properties for the canister and mock-up are given in the Appendix.

Table 10. Mass Properties of Filled Canister–Mock-Up Assembly

Item	Description
Mass	454 kg (1000 lb)
CG Location	2.21 m (86.8 in.) above bottom
Moment of Inertia	808 kgm^2
About CG	(2.76×10^6 lb in.^{2}

4.1 Canister Assembly and Leaktest

After the canister was placed in a hole in the ground to permit easier access to the top, the mock-up was lowered into the canister and the methanol/glycerine mixture added until the top end of the mock-up was just covered. This allowed an ullage of about 1640 cc (100 in.^{3}).

The seal and seats were washed with methanol and inspected carefully. The seal and lid were placed in position and the hold-down nuts tightened to hand tightness. The nuts and studs were lubricated with a molybdenum disulfide grease to prevent galling on the first canister. A dry molybdenum disulfide spray was used for the second.

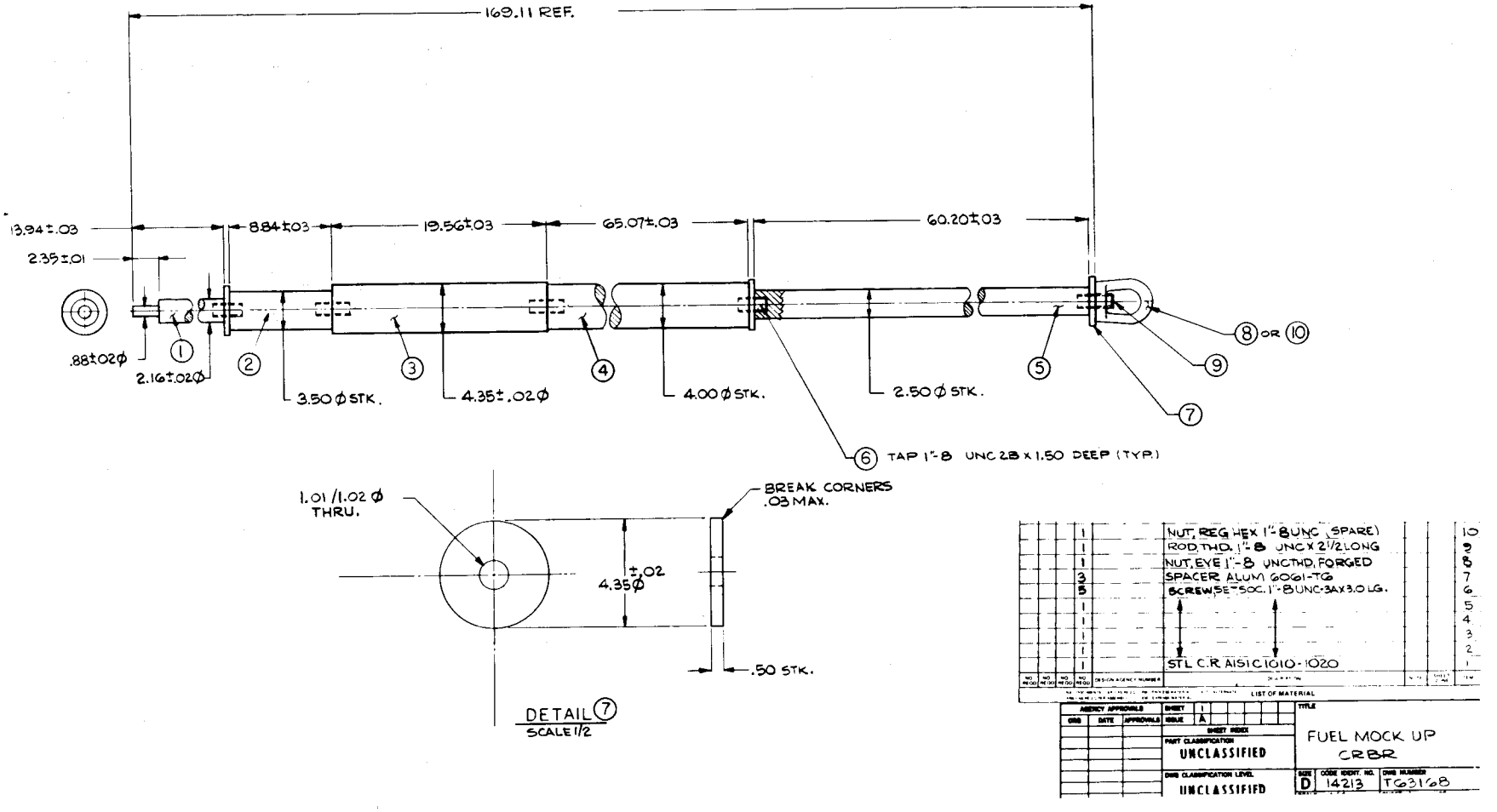

Figure 11. Subassembly Mass Mock-Up

The nuts were then torqued in 14 Nm (10 ft-lb) increments in a criss-cross pattern to the final value of 130 Nm (95 ft-lb).

The canister was pressurized to 140 kPa (20 psig) with helium through a fill port in the lid and checked with a Gow-Mac model 21 leak sniffer. (Sniffer sensitivity is approximately 1 x 10^{-6} Pa m^3/s, 1 x 10^{-5} atm cc/s.) If leaks were apparent, a pressure drop per unit time check was made so a leak rate could be calculated.

An attempt was made to measure the leak rate with a Veeco model MS170 helium mass spectrometer leak detector. It was found that the vapor pressure of the molybdenum disulfide grease was too high to permit proper leak detector operation.

4.2 Instrumentation

The canister for the first test (0 deg) was instrumented with two Endevco 2262-1000 accelerometers and five BLH FAB-12-12-S6 biaxial strain gages (Figures 12 and 13).

Both accelerometers were mounted on the lid with their sensitive axis in the axial direction. The biaxial strain gages were mounted to monitor axial (A) and hoop (H) strain at locations shown in Table 11: (Axial locations are measured from the closed end.)

Analog data were converted to FM, 216 kHz center frequency and recorded on a 14-channel FM/FM tape recorder. For playback the data were digitized at 50 kHz and filtered at 5 kHz.

Table 11. Strain Gage Locations

Name	Axial Location (m)	Calibrate Value (μm/m)
SA1, SH1	0.15	2000
SA2, SH2	0.30	2000
SA3, SH3	0.61	2000
SA4, SH4	1.83	2000
SA5, SH5	3.05	1000

No instrumentation was used for the second and third tests.

4.3 Photographic Coverage

High speed cameras were used to observe the drops and were placed as shown in Table 12. Film data were reduced to determine impact velocity, impact angle, and rebound height.

4.4 Test Site

The free drops were conducted at the SNL Old Cable Site Facility. This facility has an essentially "unyielding" hard target for such tests.

Table. 12. Photometric Setup Sheet (Typical For All Tests)

174-94

TEST NO. R-901891

REQUESTER Leishes | ORG. [redacted] | EXT. 1188 | DATE REQUESTED 6-3-80 | CLASSIFICATION Test CNL/CL Unit Data | TEST NAME C.K.B.R. Canister

REQUESTED BY [ ] Phone [ ] Memo [X] Other | TEST DATE 8-29-80 | TIME 11:30 | TEST LOCATION Old Cable Site | PREPARED BY C. Holland | DATE 8-29-80

CAMERA TYPE	FRAME RATE	TIMING RATE	LENS FOCAL LENGTH	SUBJECT DIST-ANCE	FILM USED	FOOT-AGE	LIGHTING	LAMP DIST-ANCE	f-STOP	CAMERA LOCATION	EVENT VELOCITY	EVENT DURA-TION
Nova	2000	1000 2	2"	100'	UND	100'	Good	—	3.5	E/GZ	30 MPH	Live
Milliken	400	100 2	1"	100'	UND	100'	Good	—	5.6	E/GZ	"	"
Nova	2000	1000 2	1"	100'	UND	100'	Good	—	3.5	S/GZ	"	"
Nova	2000	1000 2	10"	80'	UND	100'	Good	—	3.5	S/GZ	"	"
Nova	2000	1000 -	6"	80'	UND	100'	Good	—	3.5	S/GZ	"	"
Milliken	400	100 2	40MM	80'	UND	100'	Good	—	5.6	S/GZ	"	"
Milliken	400	100 2	10MM	80'	UND	100'	Good	—	5.6	S/GZ	"	"
T.V. Camera	30	—	6"	80'	NONE		Good	—	8	S/GZ	"	"

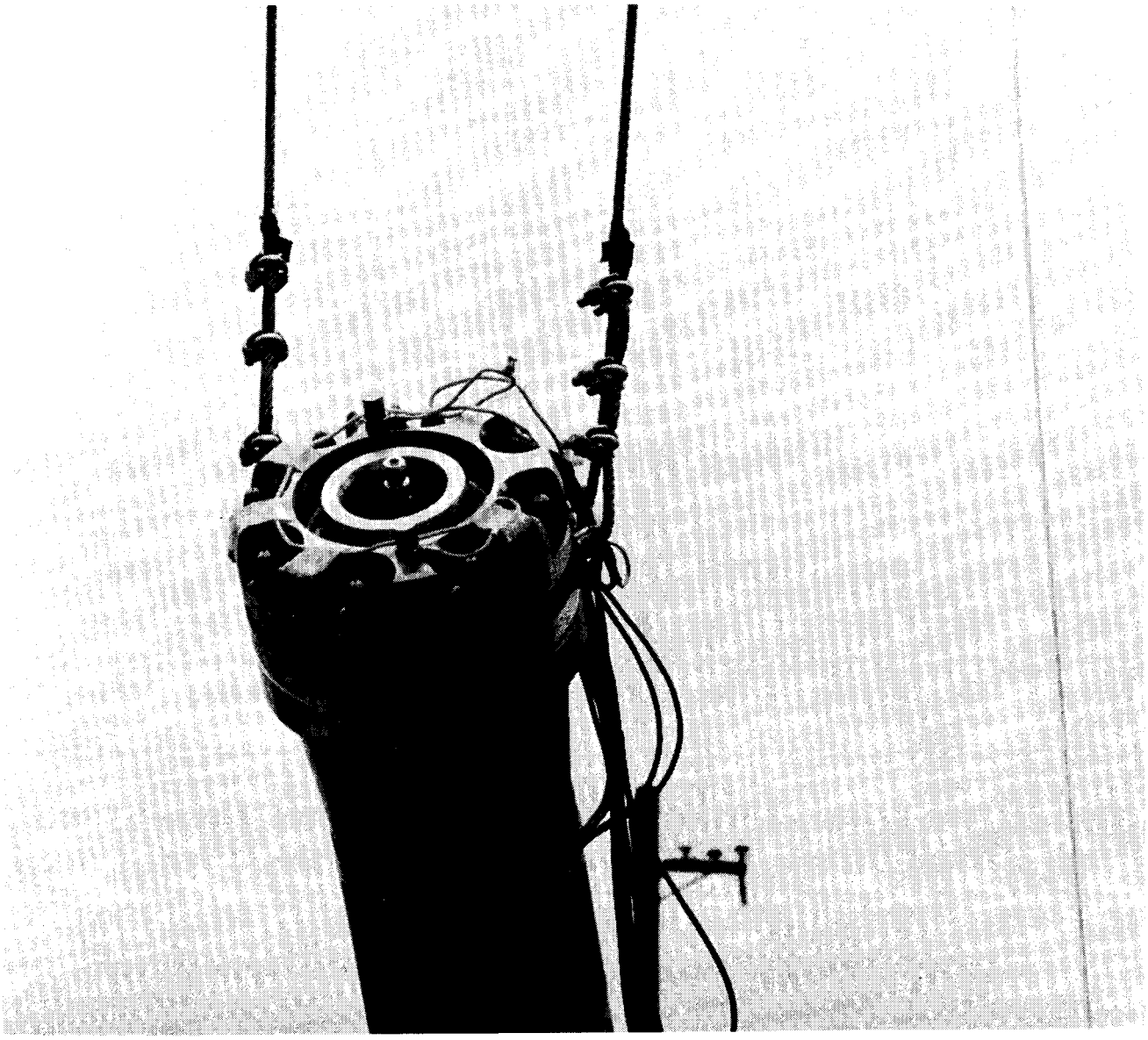

Figure 12. Accelerometer Installation

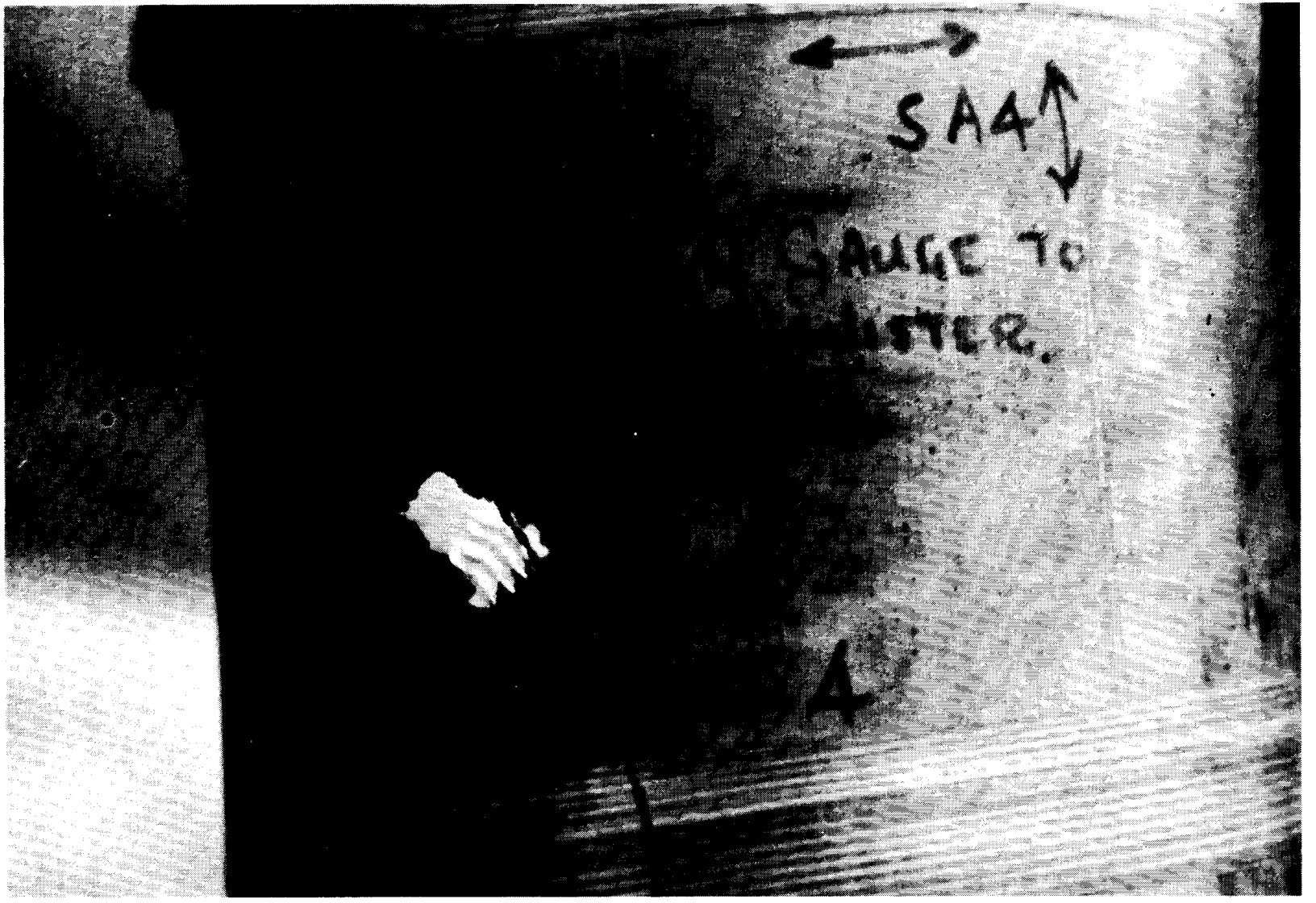

Figure 13. Typical Strain Gage Installation

5 Test Results

5.1 0-Degree (End-On) Test

Table 13 summarizes the results of the 0-degree test. Posttest photos and measurements of body deformation are shown in Figures 15 and 16 and in Table 14. No body leakage was noted; however, welds were not radiographed or helium leak-tested. Hold-down nut torque values at lid removal ranged from 54 to 102 Nm (40 to 75 ft-lb).

An energy balance (Section 5.4) showed that approximately 68% of the initial impact energy was absorbed by body plastic deformation.

Figures 17 through 28 show plots of strain and acceleration data. Usable data were obtained from all instrumentation except strain gages SA3 and SH3, which failed at impact. Failure cause could not be determined. The double cables visible in the photos were to keep the canister from falling over after impact.

Table 13. 0-Degree End-On Test Results

Item	Result
Pretest photo	Figure 14
Pretest Helium Leak Rate ($v\Delta p/\Delta t$)	2×10^{-3} atm cc/s
Impact Velocity	13.53 m/s (44.4 ft/s)
CG Rebound Height	0.69 m (27.3 in.)
Posttest Leak Rate	Fluid found around seal area but no indications on sniffer. Possibly, fluid sealed the leak or leak was only momentary.

5.2 45-Degree Test

The end-on test canister was reused for the 45-degree test. The lid was removed and replaced to permit cleaning the sealing surface. Table 15 summarizes the results. Pre- and posttest photos and measurements of body deformation (bow) are shown in Figures 29 through 34. No body leakage was noted; however, welds were not radiographed or helium leak-tested. The lid was not removed, and an energy balance was not made.

5.3 90-Degree (Side-On) Test

A new canister was used for the 90-degree test. Table 16 summarizes the results. Pre- and posttest photos and measurements of body deformation are shown in Figures 35 through 38. The fluid visible in Figure 36 was from an earlier spill. No body leakage was noted; however, welds were not radiographed or helium leak-tested. Due to budgetary constraints, no final posttest leak rate determination was made. No energy balance was made.

5.4 End-On Impact Energy Balance

The first fluid-filled canister was dropped in an end-on orientation onto an unyielding target at ambient temperature.

Following the first fluid-filled canister end drop, some plastic deformations occurred in a hoop bulging mode at points near the impact end of the canister (Table 13). Further, subsequent measurements of the posttest canister length indicated that some "shortening" or crush-up did occur. It is the purpose of this section to perform an energy balance to determine what percentage of the total drop energy is partitioned into plastic deformations of the canister as well as to determine the general partitioning of energy to other modes of energy extraction.

5.4.1 Energy Absorption Modes

The canister contained a mild steel pin, the purpose of which was to dynamically simulate the fuel assembly. The approach taken here is to ignore the steel pin since the pin, through its own plastic deformation, effectively stops itself and does not impart significant loading into the canister (except as compression of the end cap).

An assembly drawing of the canister with end cap (but with steel pin omitted) is shown in Figure 2. The canister is fluid filled as well.

Energy absorption modes considered are

Mode 1: Plastic hoop-straining of the canister wall.

Mode 2: Axial plastic crush-up (shortening) of the canister.

Mode 3: Rigid body rebound.

Table 14. Pretest and Posttest Diametrial Measurements* (End-On Drop) Made by SNL Division 1485-3

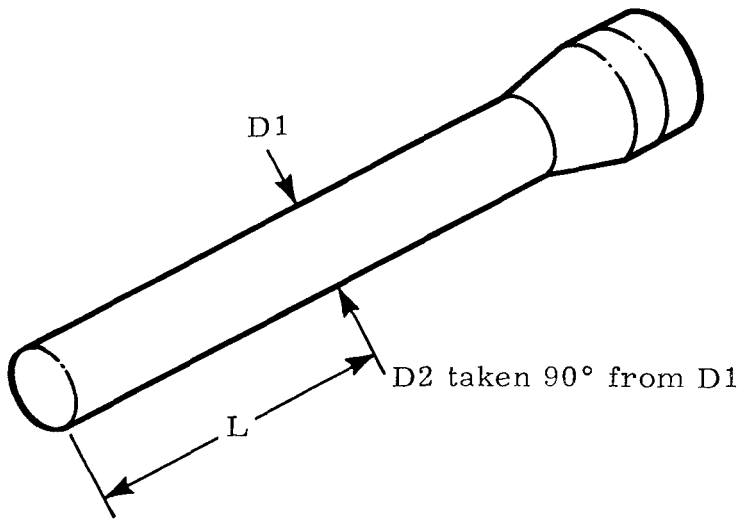

L (in.)	D1 Pre (in.)	D2 Pre (in.)	D1 Post (in.)	D2 Post (in.)	L (in.)	D1 Pre (in.)	D2 Pre (in.)	D1 Post (in.)	D2 Post (in.)
2	7.026	7.024	7.032	7.029	19.5			7.132	7.108
4	7.026	7.026	7.026	7.026	20	7.010	7.005	7.117	7.100
6	7.024	7.024	7.024	7.025	20.5	7.010	7.005	7.111	7.098
8	7.026	7.026	7.025	7.027	21	No further		7.107	7.100
10	7.024	7.025	7.025	7.028	21.5	pretest		7.103	7.100
12	7.027	7.027	7.039	7.042	22	measurements		7.098	7.101
12.5	†	†	7.052	7.052	24	made		7.090	7.095
13			7.066	7.061	36			7.057	7.054
13.5			7.071	7.069	48			7.027	7.033
14	7.013	7.018	7.069	7.068	60			7.022	7.016
14.5			Weld Zone		72			7.012	7.011
15			Weld Zone		84			7.014	7.007
15.5			Weld Zone		96			7.010	7.003
16	6.996	6.989	7.093	7.072	108			7.010	6.993
16.5			7.140	7.115	120			7.006	6.999
17			7.159	7.138	132			7.010	6.985
17.5			7.159	7.136	144			7.000	6.986
18	7.014	7.005	7.154	7.129	156			7.001	6.998
18.5			7.143	7.120	168			7.090	7.069
19			7.133	7.114					

*Measurements were made, and are therefore reported, in inches.
†Not all axial locations were measured before test.

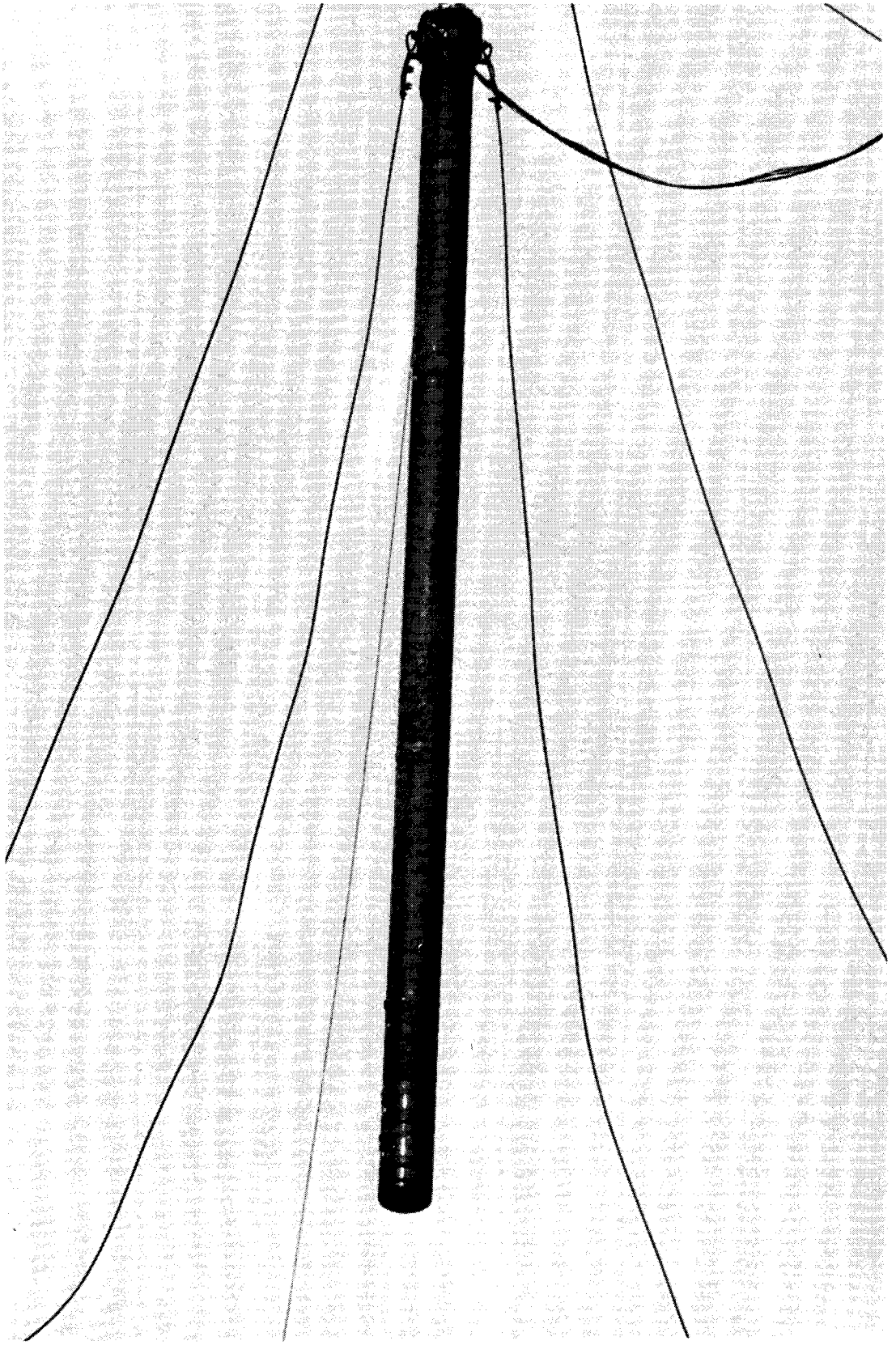

Figure 14. Pretest, End-On

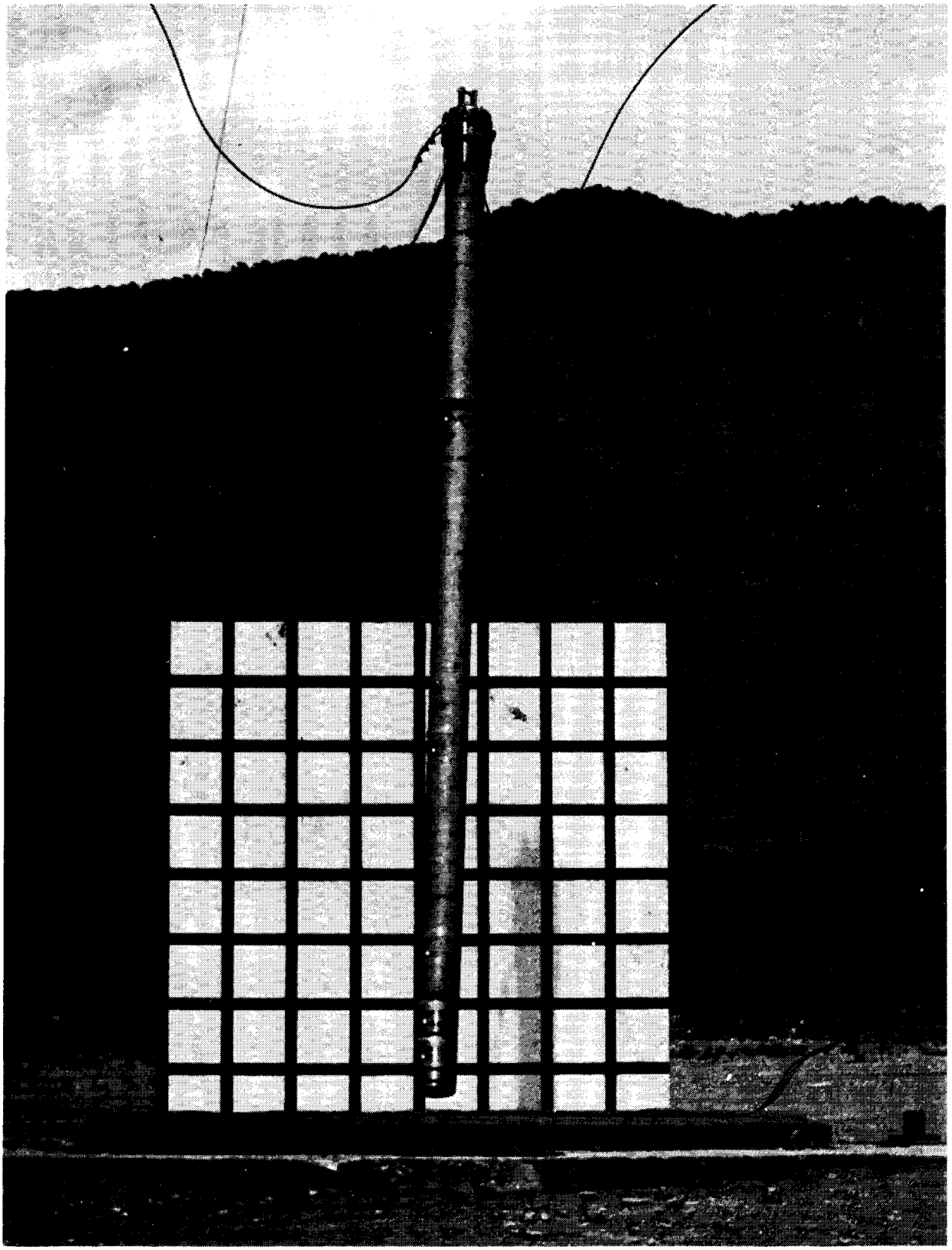

Figure 15. Posttest, End-On, During Rebound

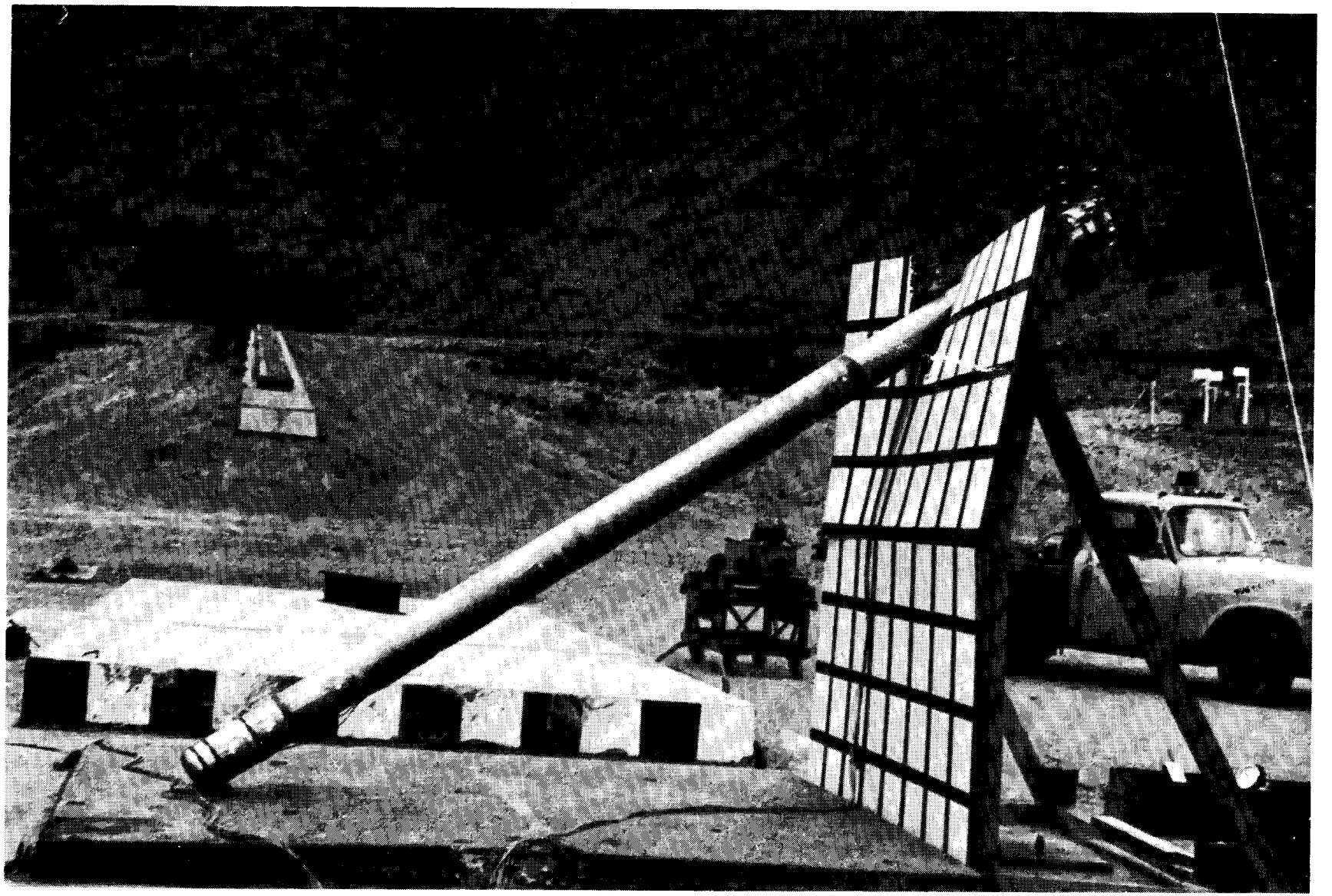

Figure 16. Posttest, End-On

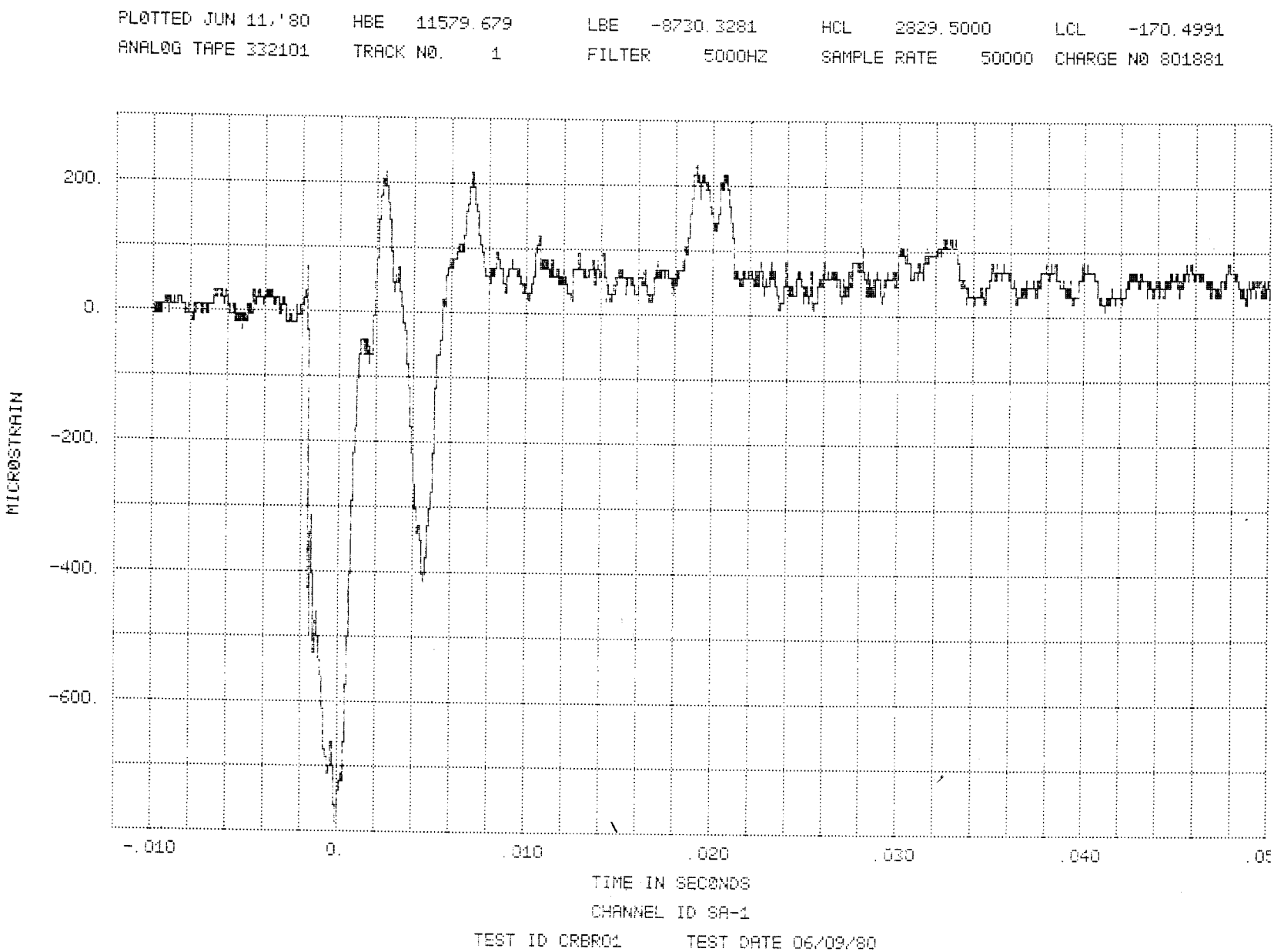

Figure 17. Strain Gage Data, End-On, Track No. 1

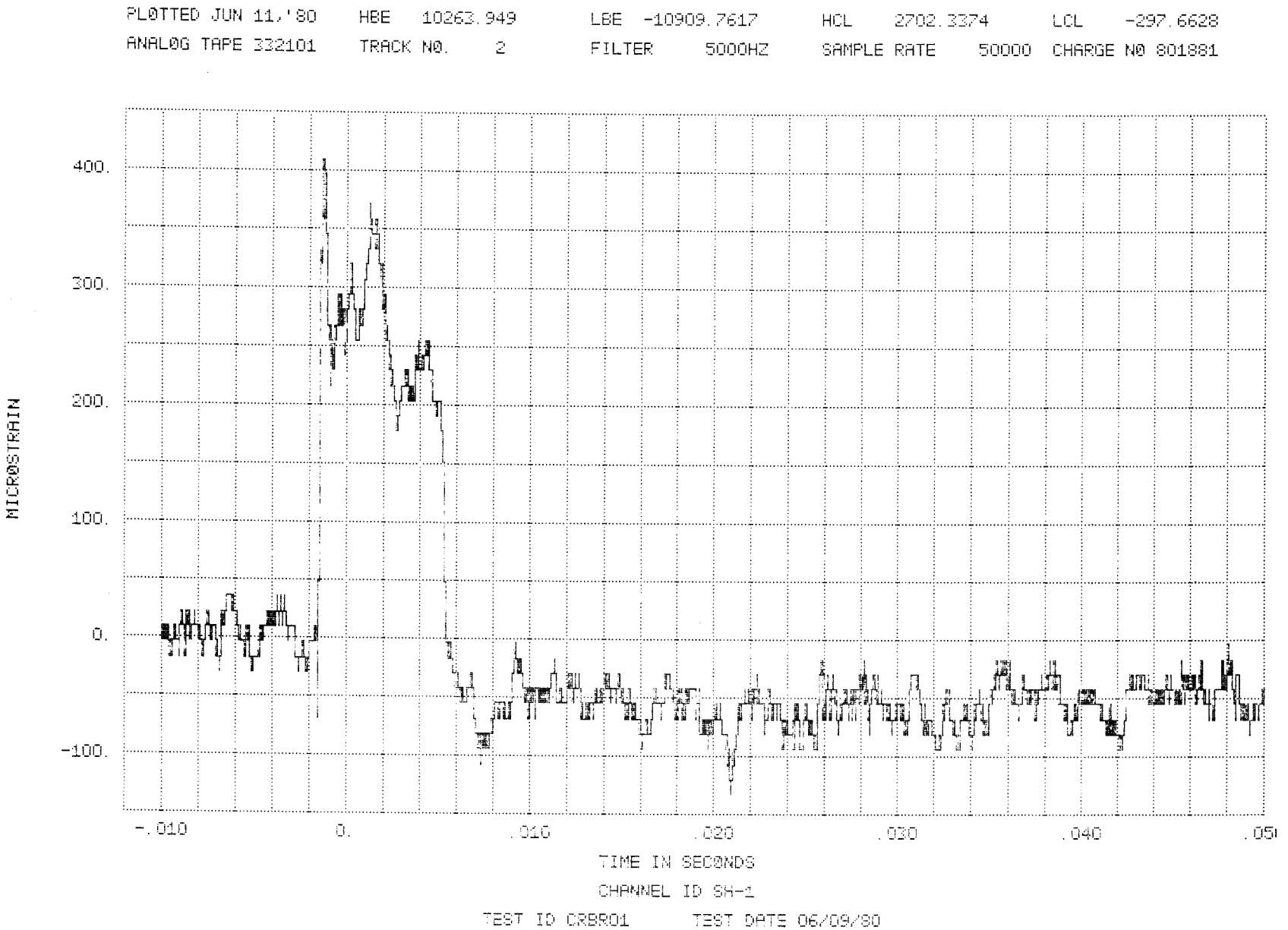

Figure 18. Strain Gage Data, End-On, Track No. 2

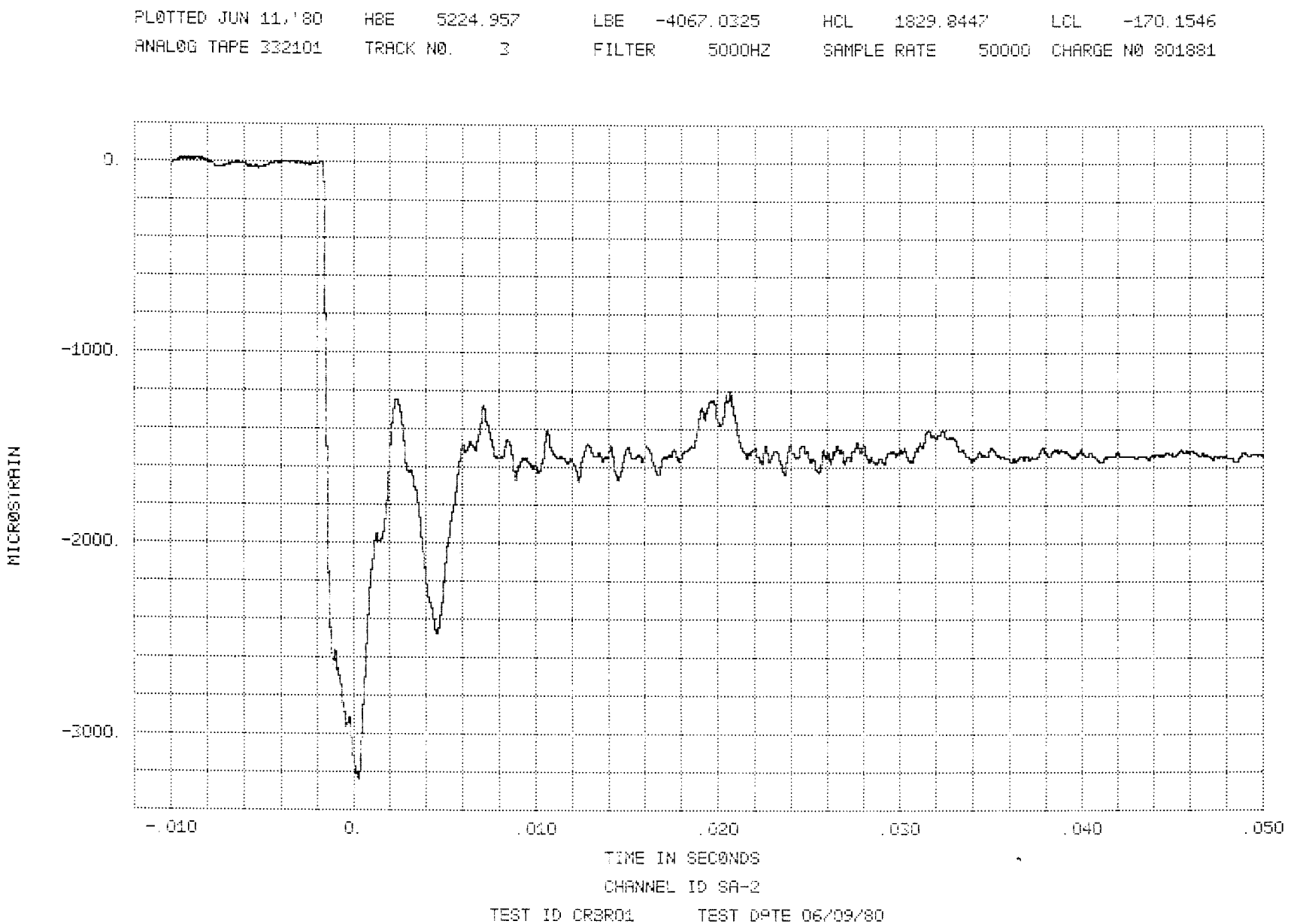

Figure 19. Strain Gage Data, End-On, Track No. 3

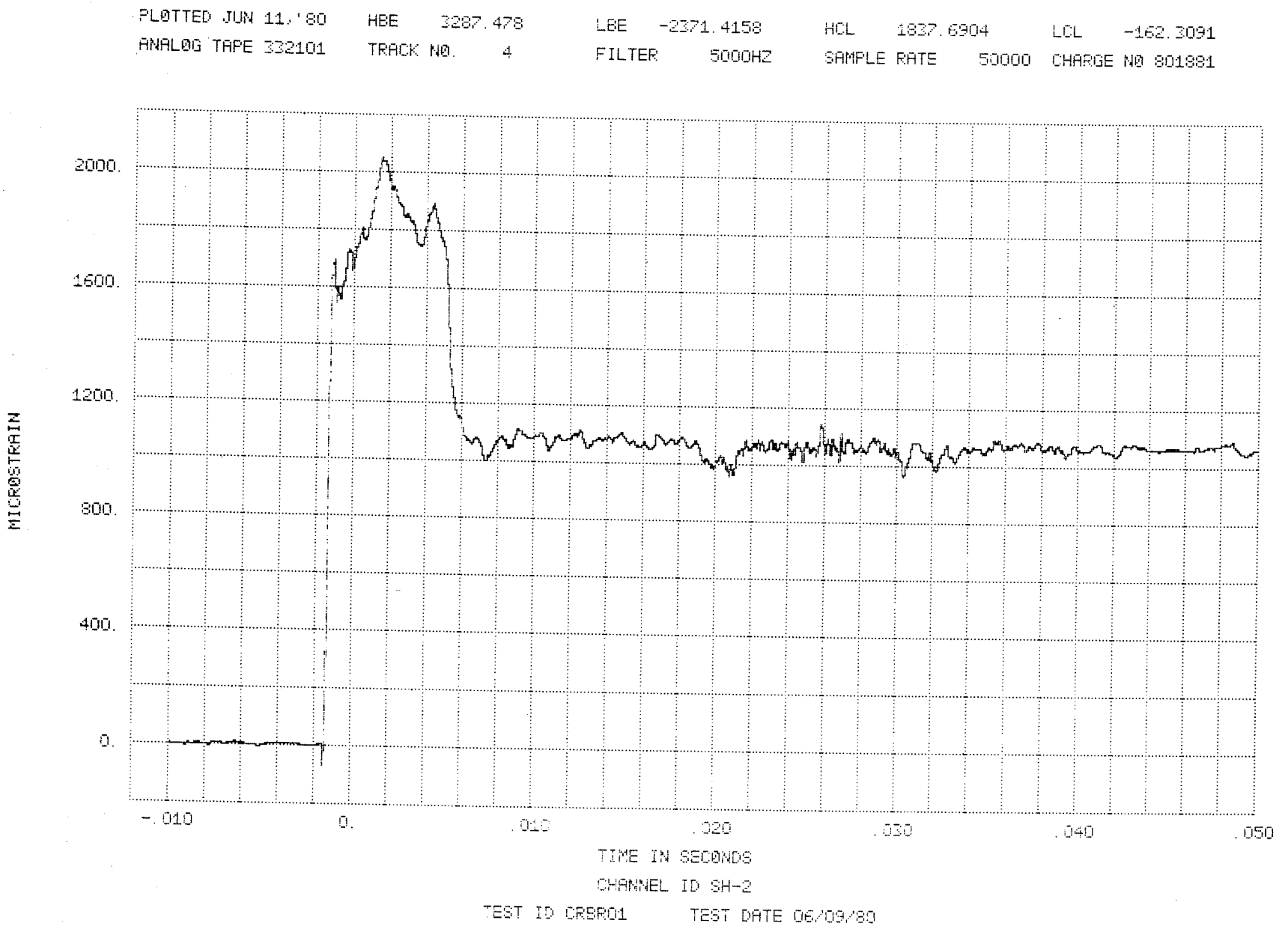

Figure 20. Strain Gage Data, End-On, Track No. 4

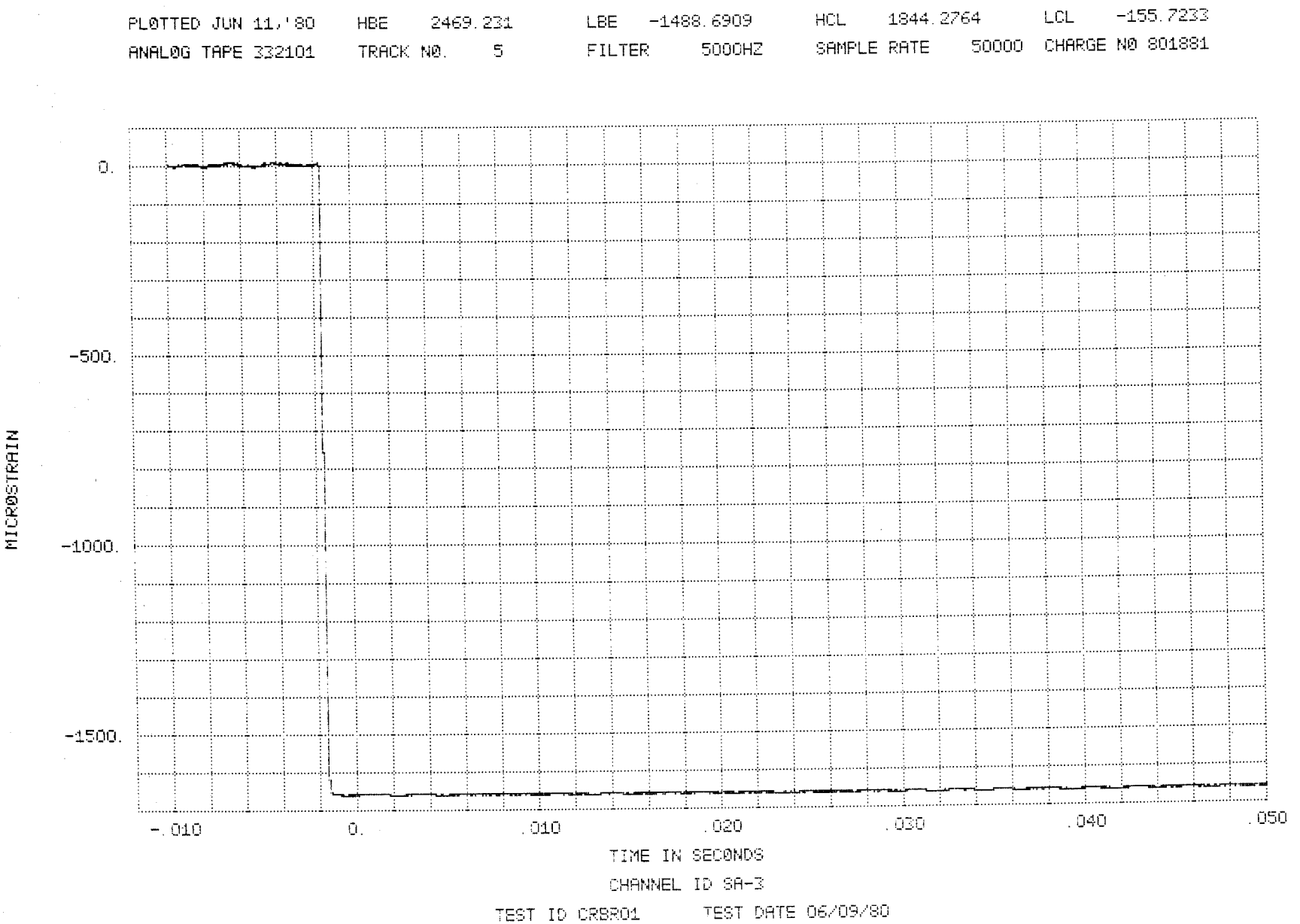

Figure 21. Strain Gage Data, End-On, Track No. 5

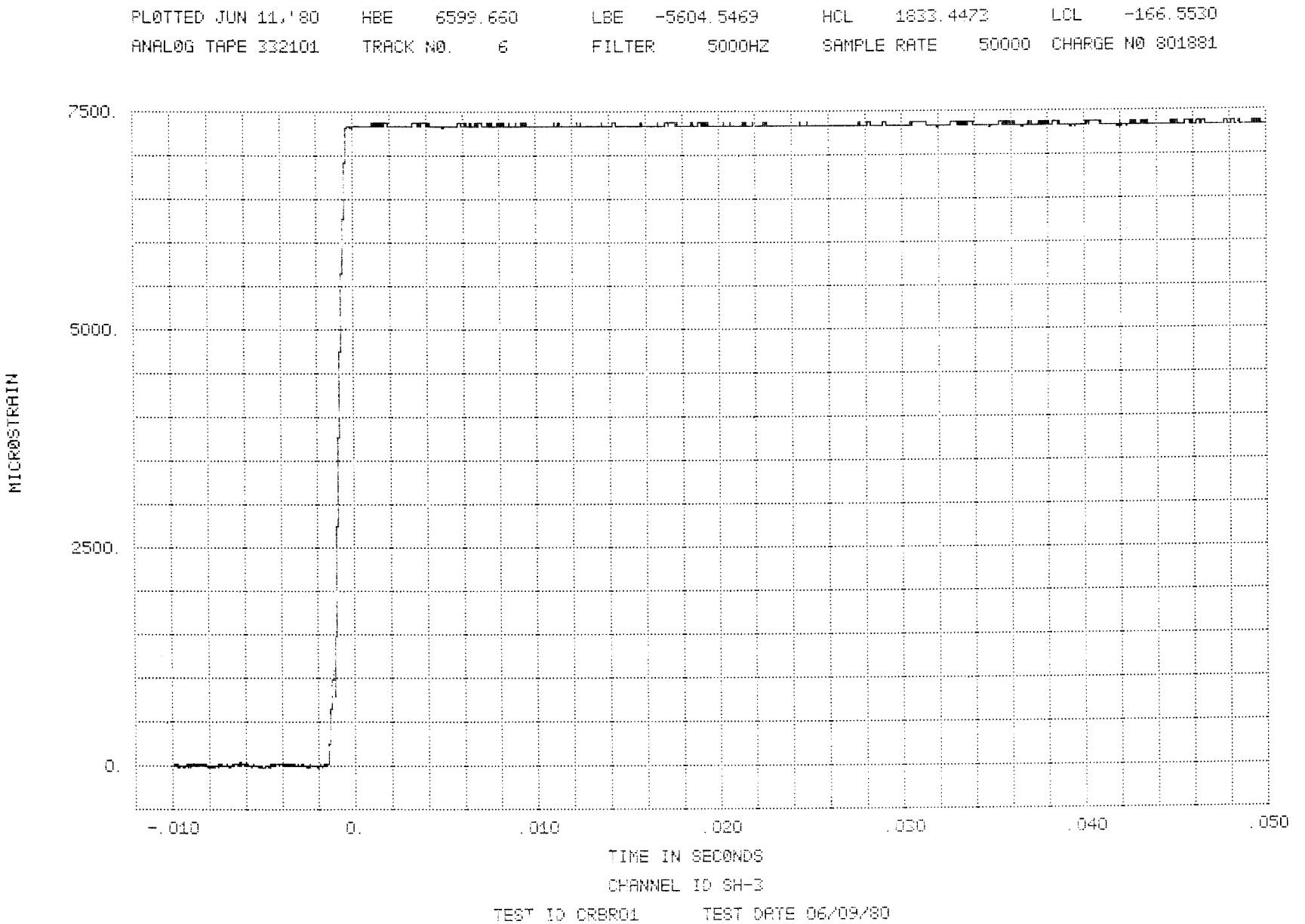

Figure 22. Strain Gage Data, End-On, Track No. 6

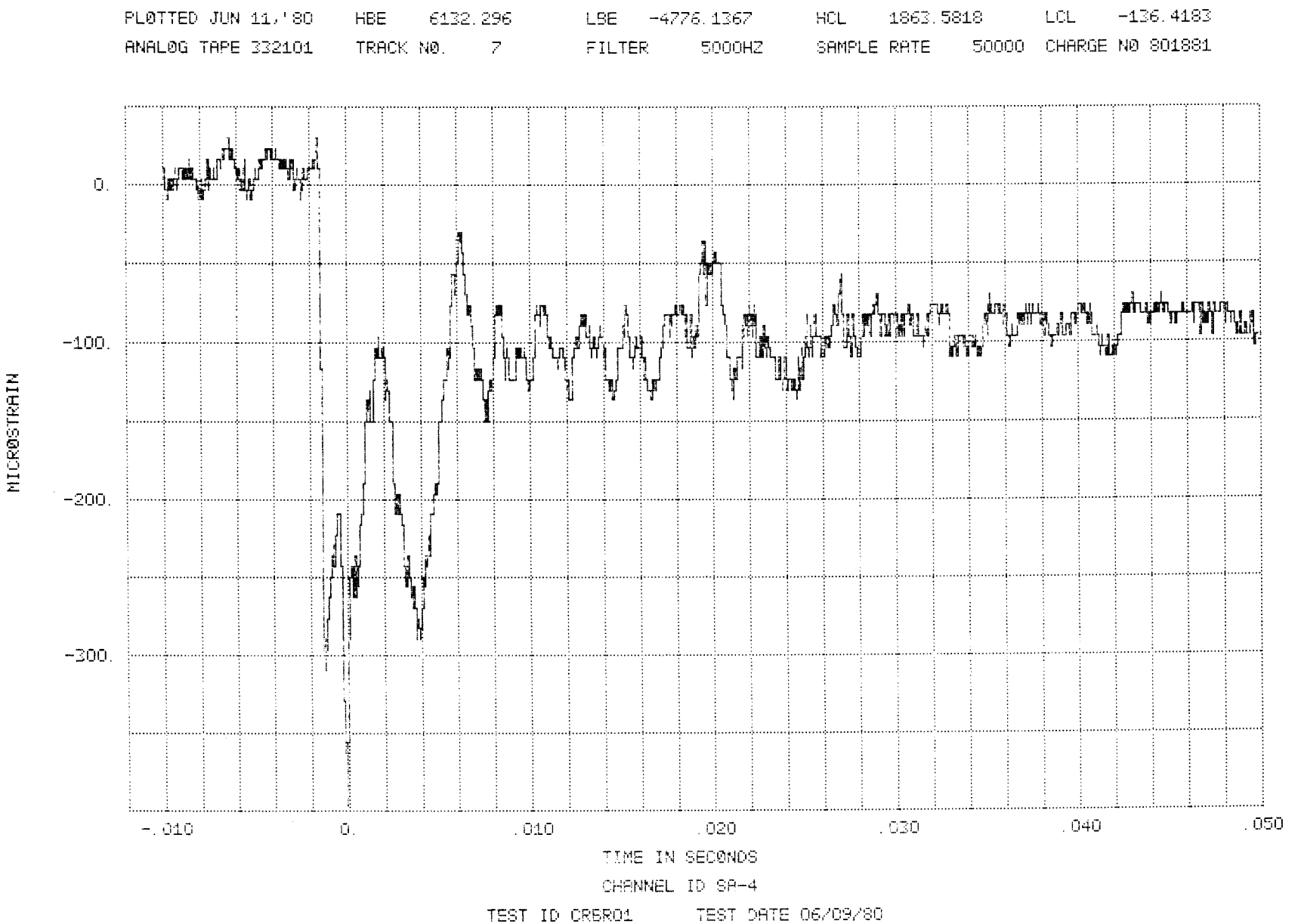

Figure 23. Strain Gage Data, End-On, Track No. 7

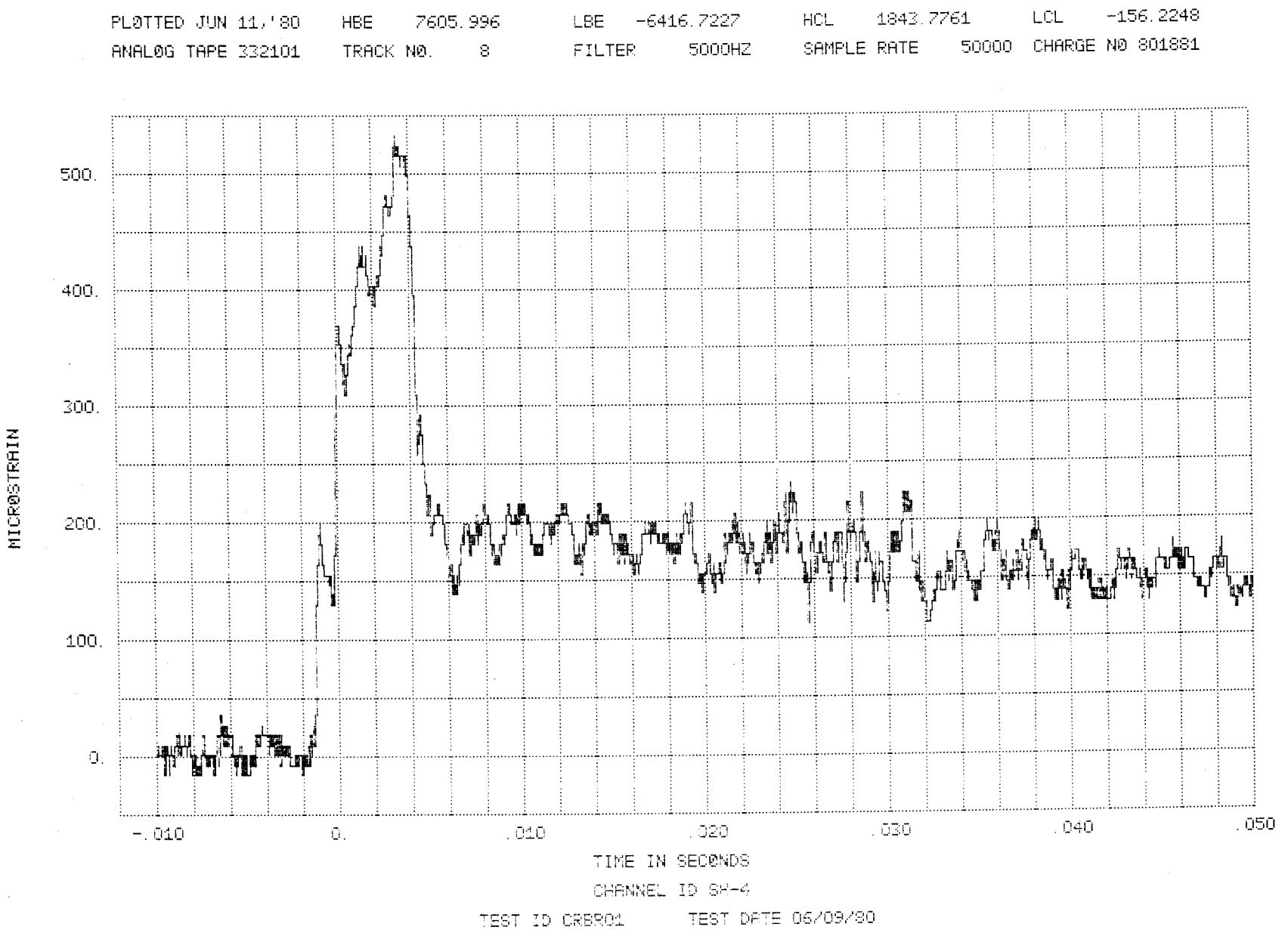

Figure 24. Strain Gage Data, End-On, Track No. 8

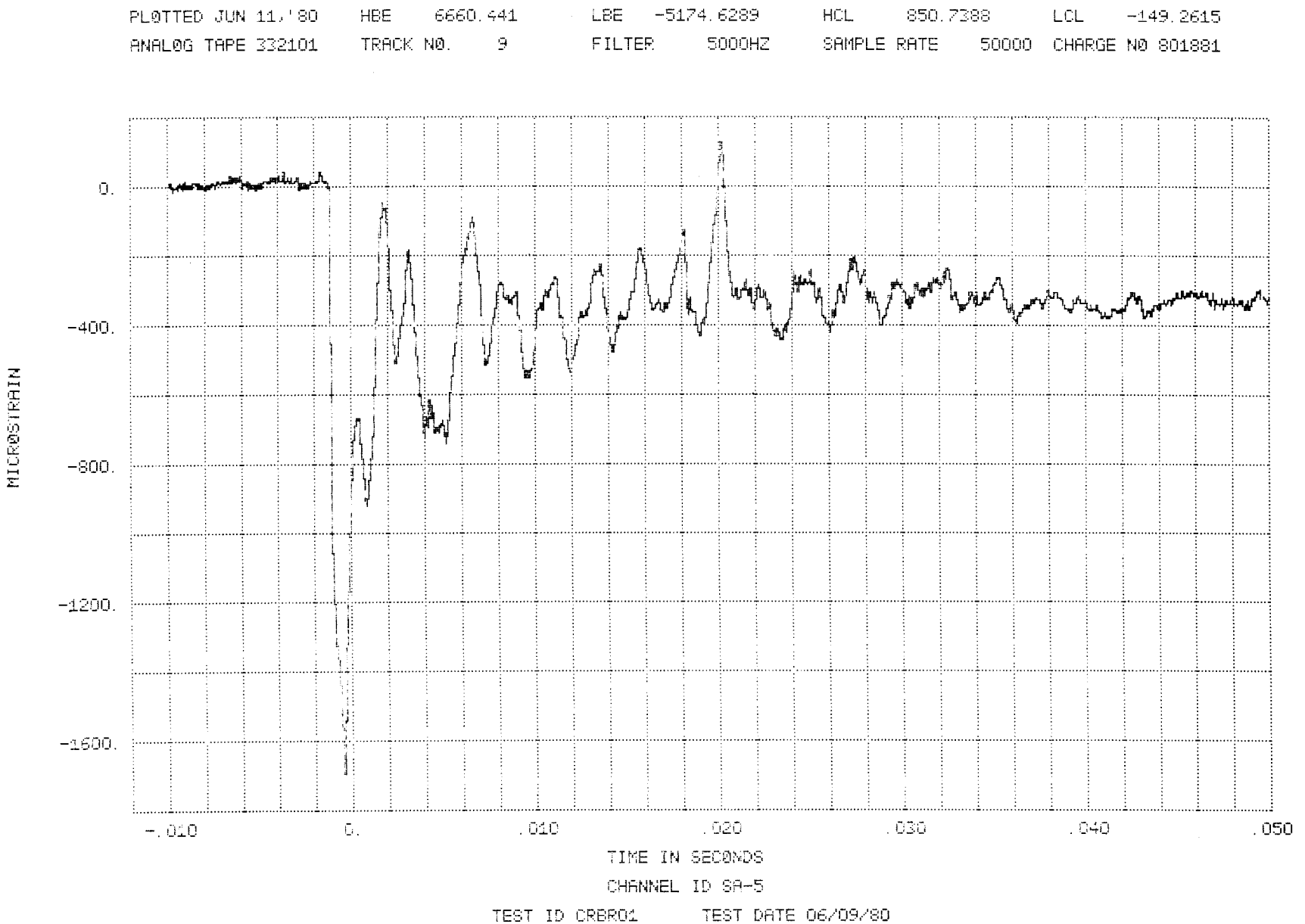

Figure 25. Strain Gage Data, End-On, Track No. 9

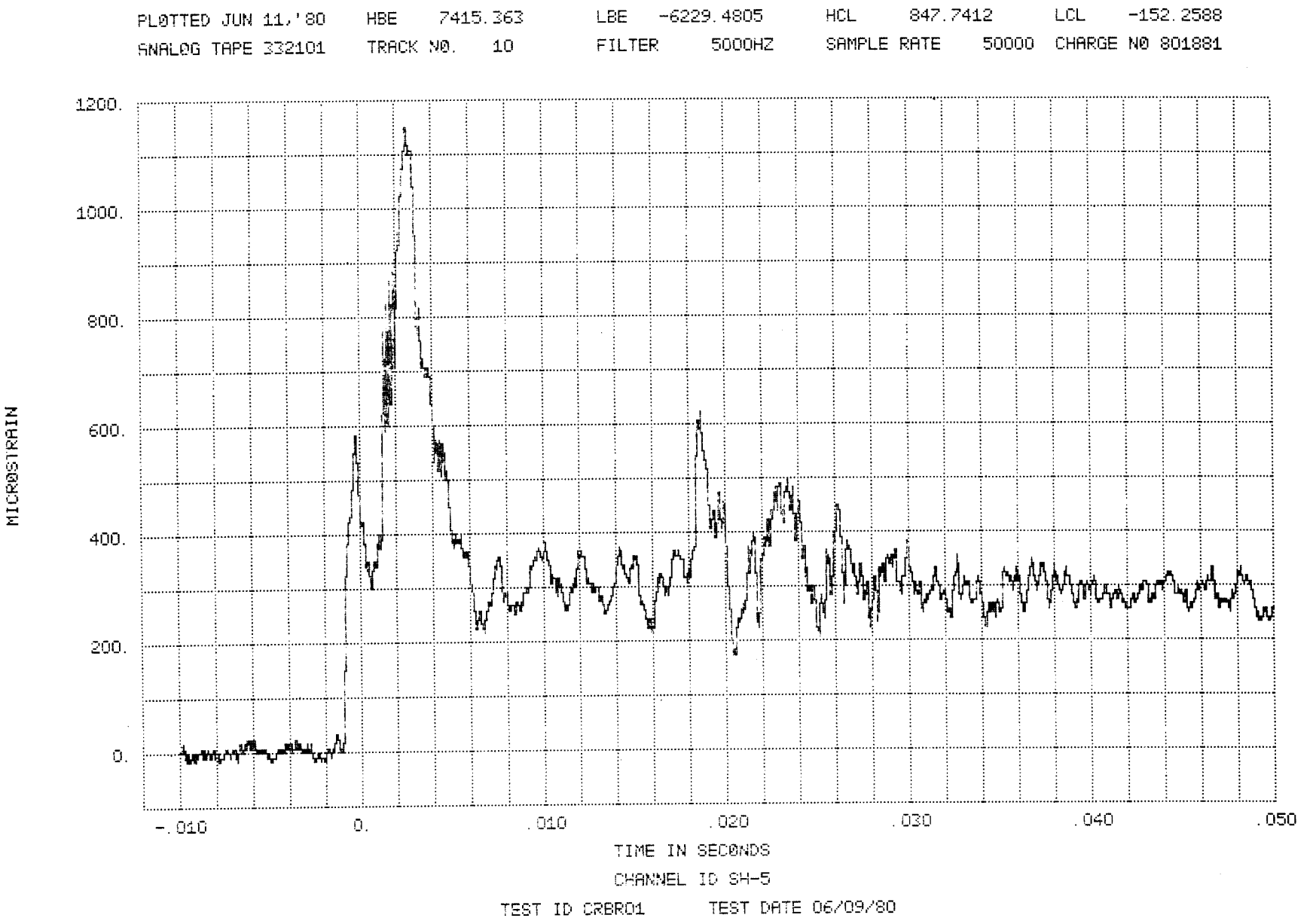

Figure 26. Strain Gage Data, End-On, Track No. 10

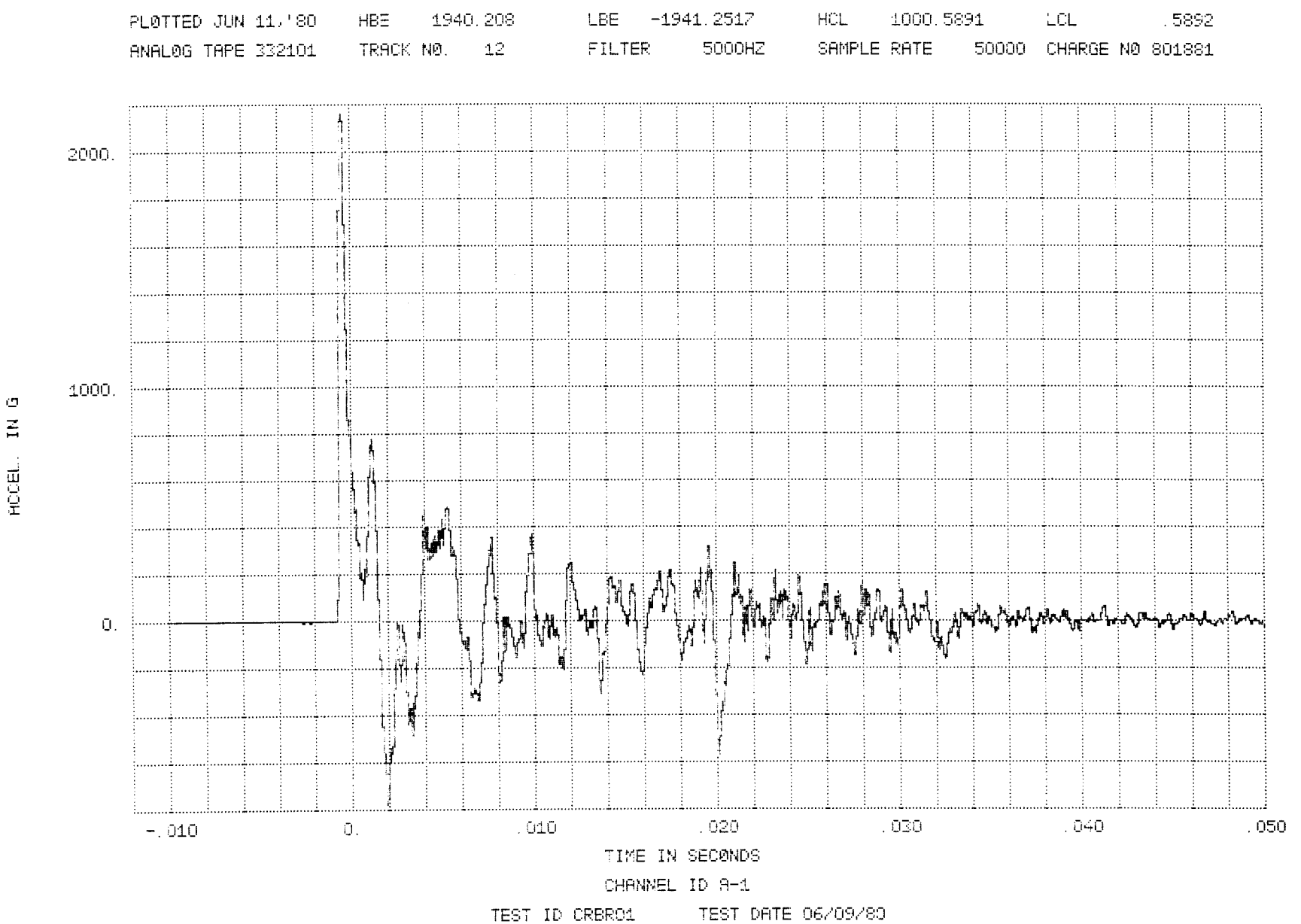

Figure 27. Accelerometer Data, End-On, Track No. 11

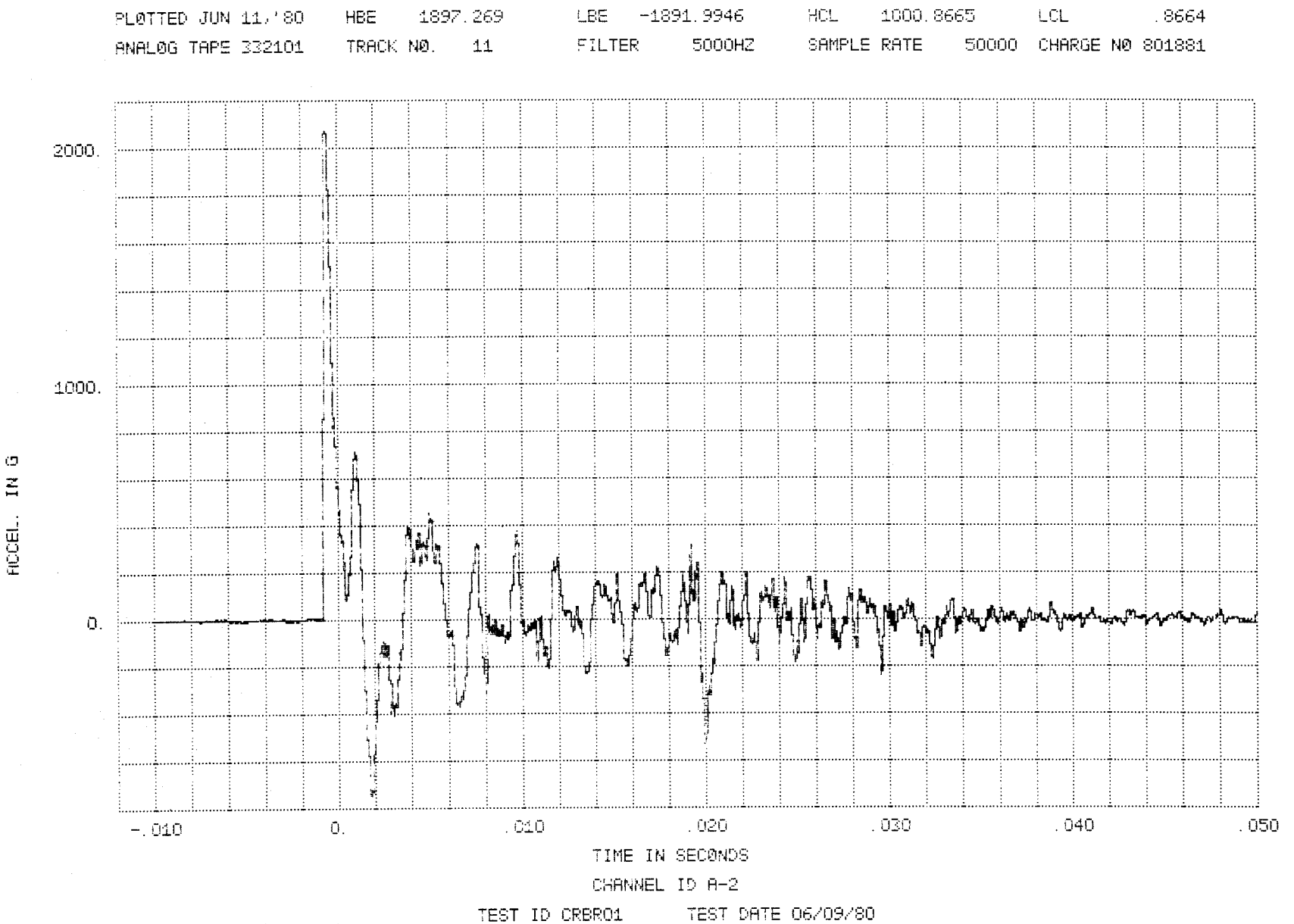

Figure 28. Accelerometer Data, End-On, Track No. 12

Table 15. 45-Degree Test Results

Item	Result
Pretest Photos	Figures 29 and 30
Pretest Helium Leak Rate ($v\Delta p/\Delta t$)	0.42 atm cc/s
Impact Angle (from vertical)	40 degrees
Impact Velocity	13.4 m/s (43.8 ft/s)
Head Slap-Down Velocity	20.7 m/s (68.0 ft/s)
CG Velocity at Head Slap-Down	7.6 m/s (25.0 ft/s)
Head Slap-Down Angle (from vertical)	95 degrees
CG Rebound Height 2nd impact	0.11 m (0.37 ft)
Posttest Leak Rate	Fluid flowed from seal

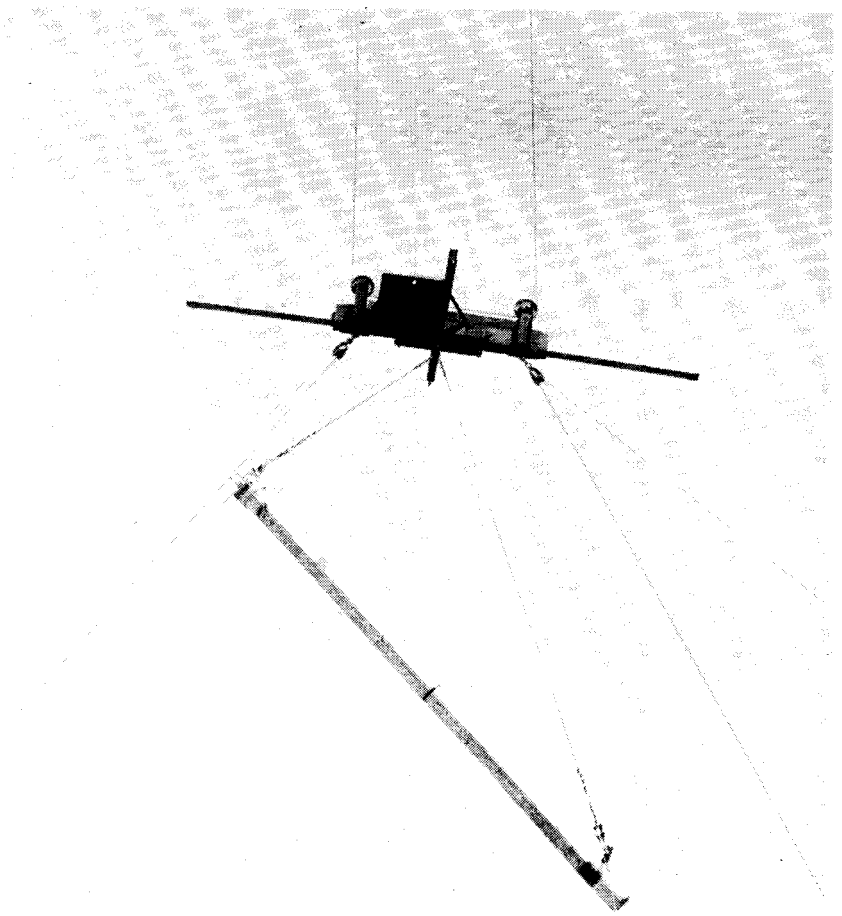

Figure 29. Pretest, 45-Degree Drop

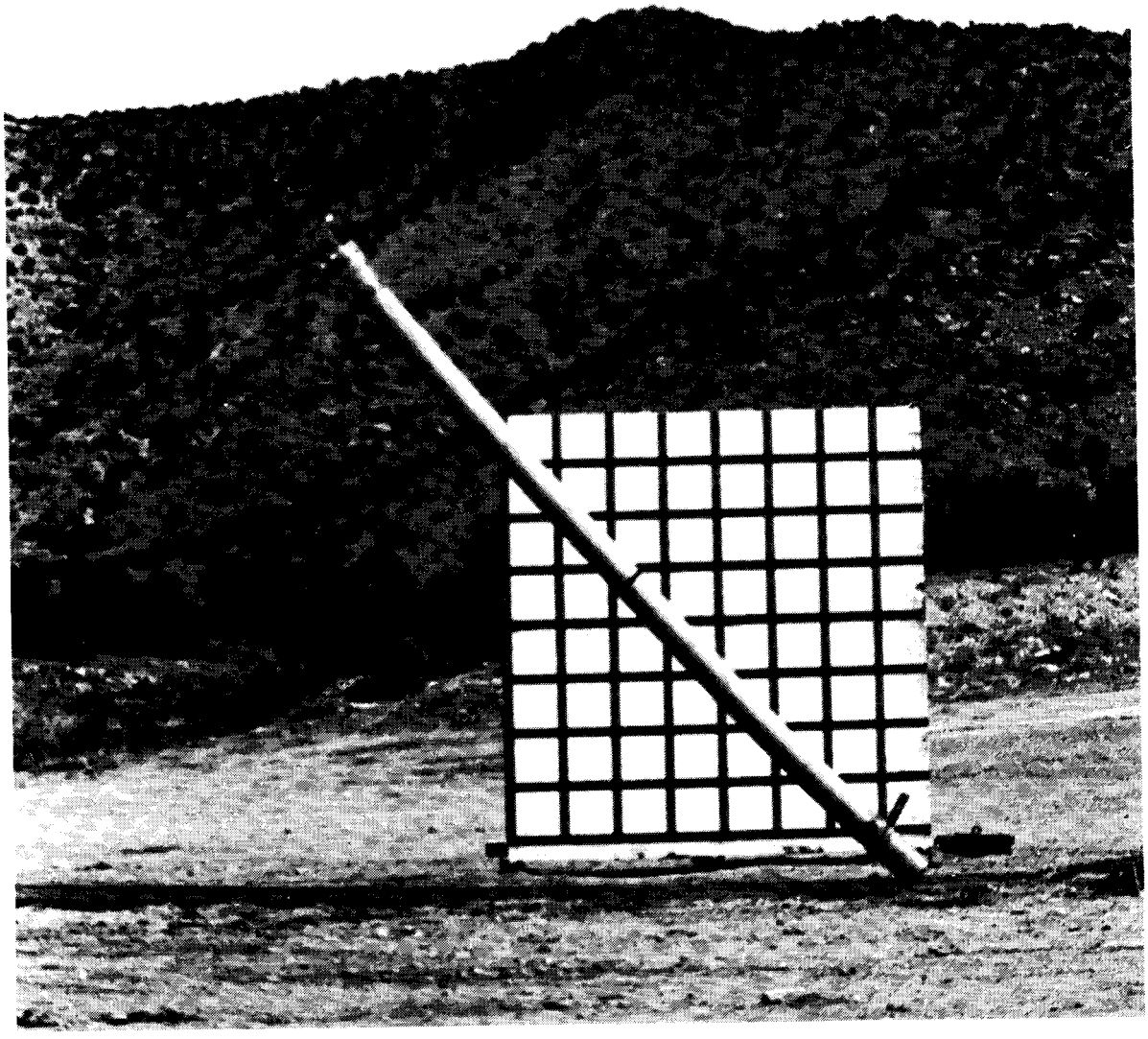

Figure 30. 45-Degree Test, at Impact

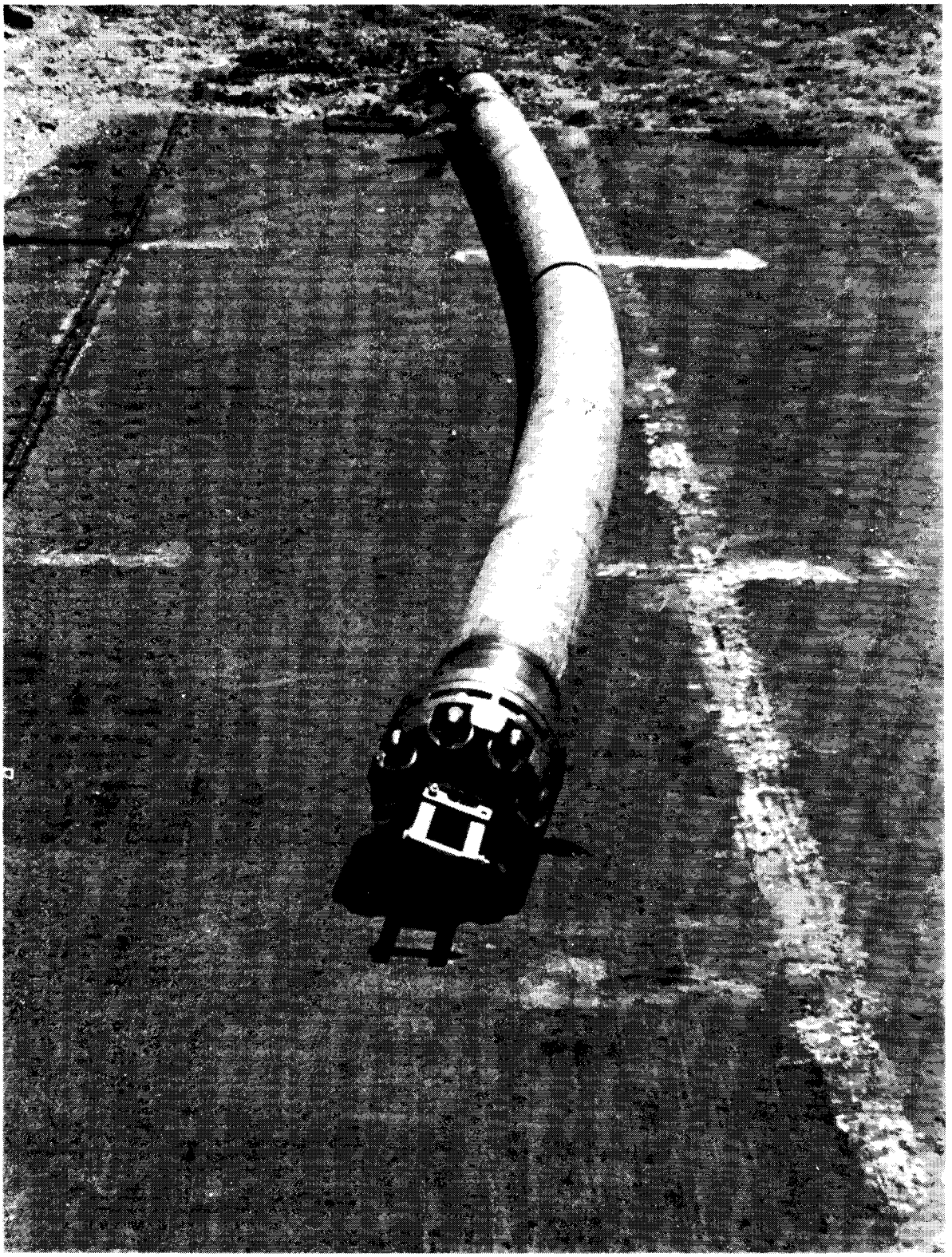

Figure 31. Posttest, 45-Degree Drop

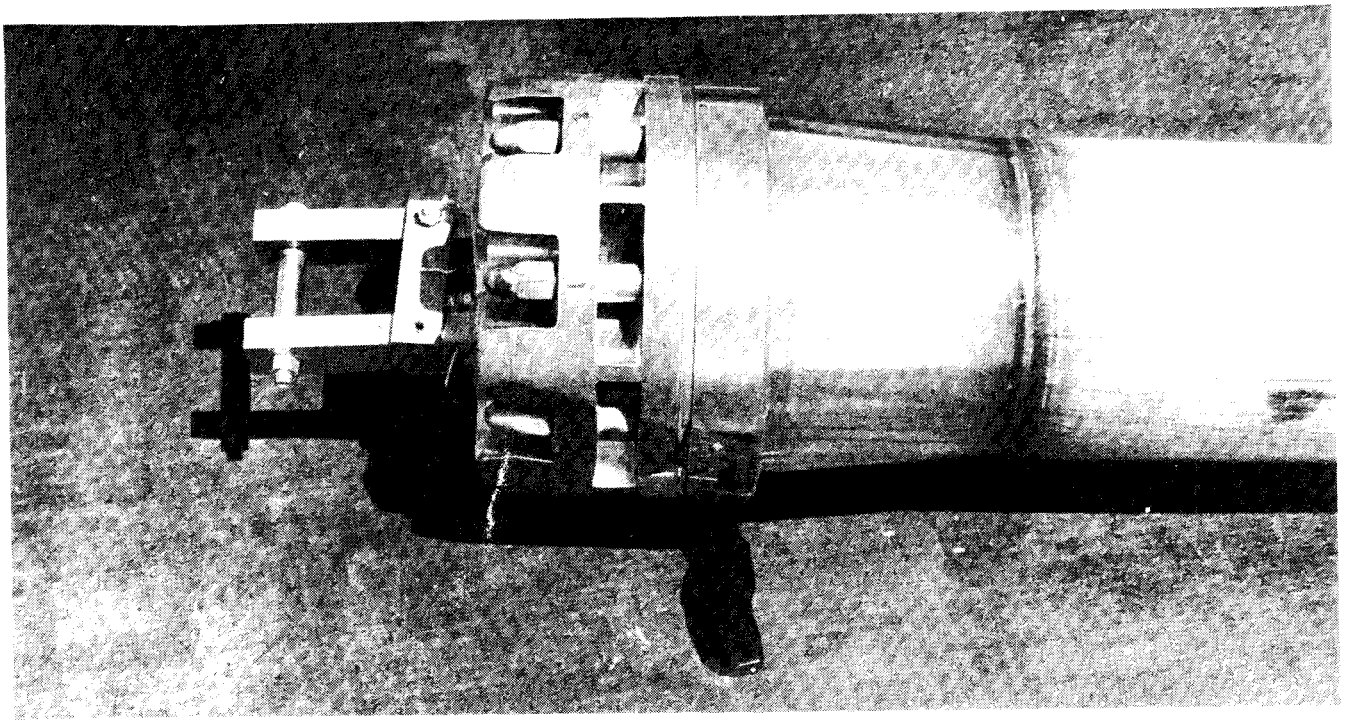

Figure 32. Posttest, 45-Degree Drop, Head

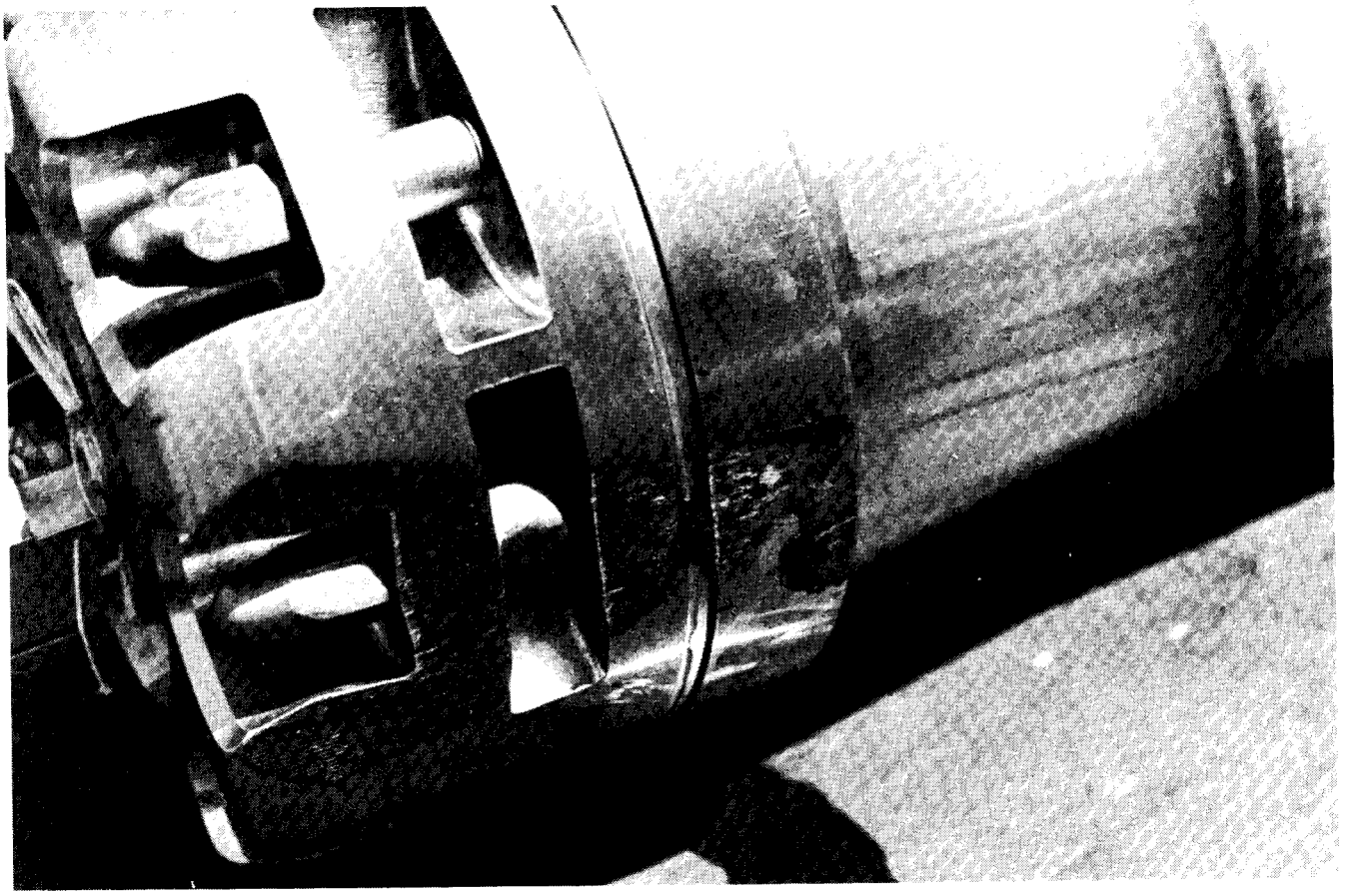

Figure 33. Posttest, 45-Degree Drop, Close-up of Head Impact Point

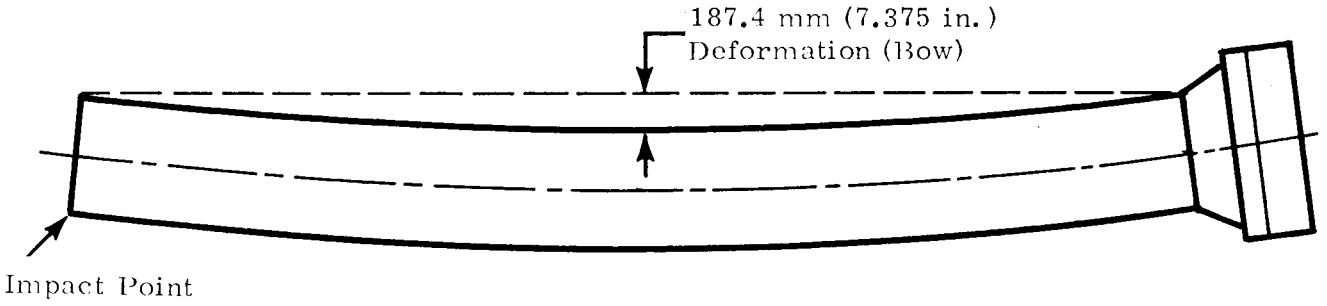

Figure 34. Body Deformation, 45-Degree Drop

Table 16. 90-Degree (Side-On) Test Results

Item	Result
Pretest Photos	Figure 35
Pretest Helium Leak Rate	$1x10^{-5}$ cc/s (No apparent leak by sniffer. Veeco inoperative.)
Impact Angle (from vertical)	89 degrees
Impact Velocity	13.0 m/s (42.7 ft/s)
CG Rebound Height	0.1 m (0.32 ft)
Posttest Leak Rate	Some fluid in seal area. Washed clean, no noticeable seepage. Too windy for sniffer.

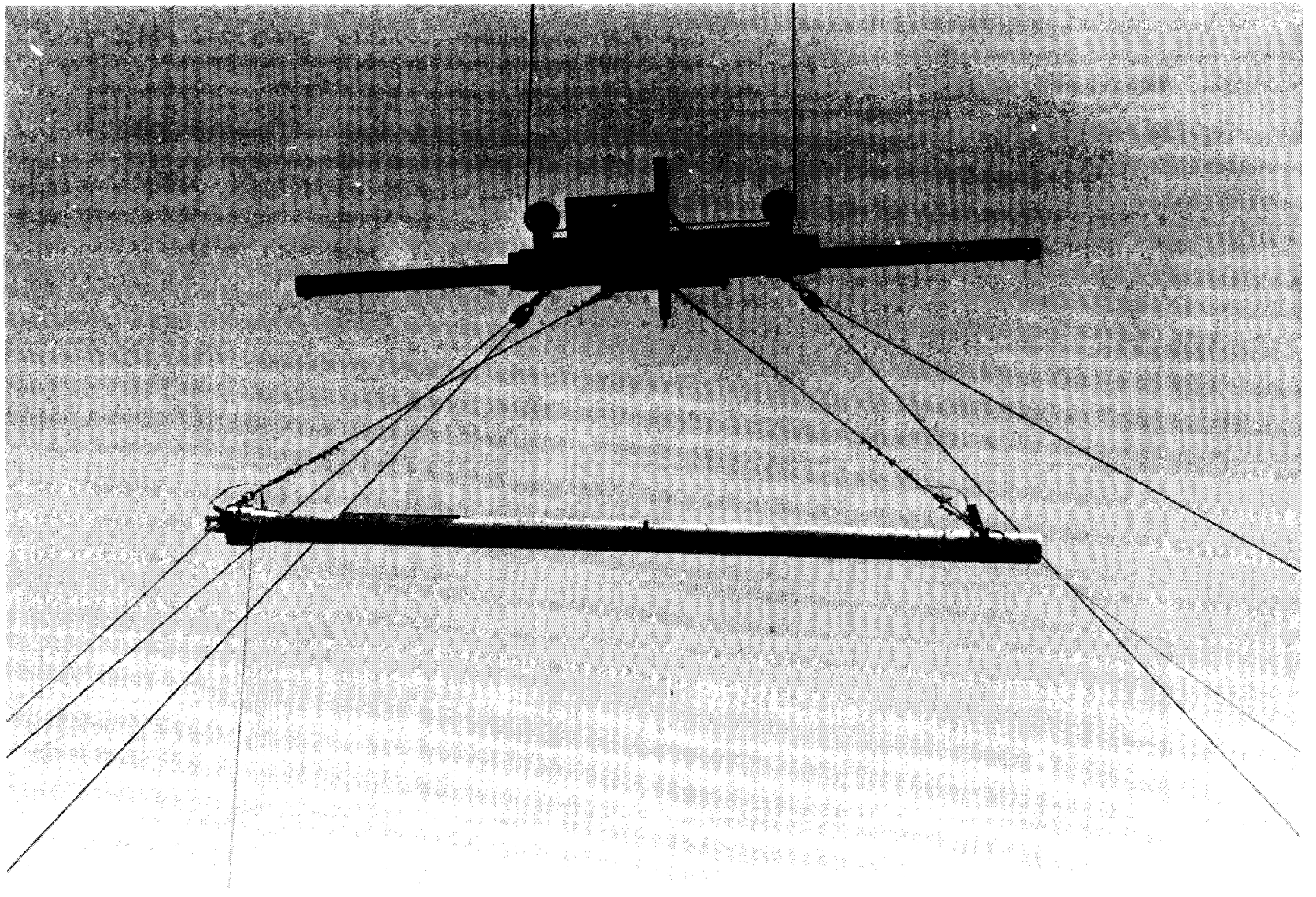

Figure 35. Prettest, 90-Degree Drop

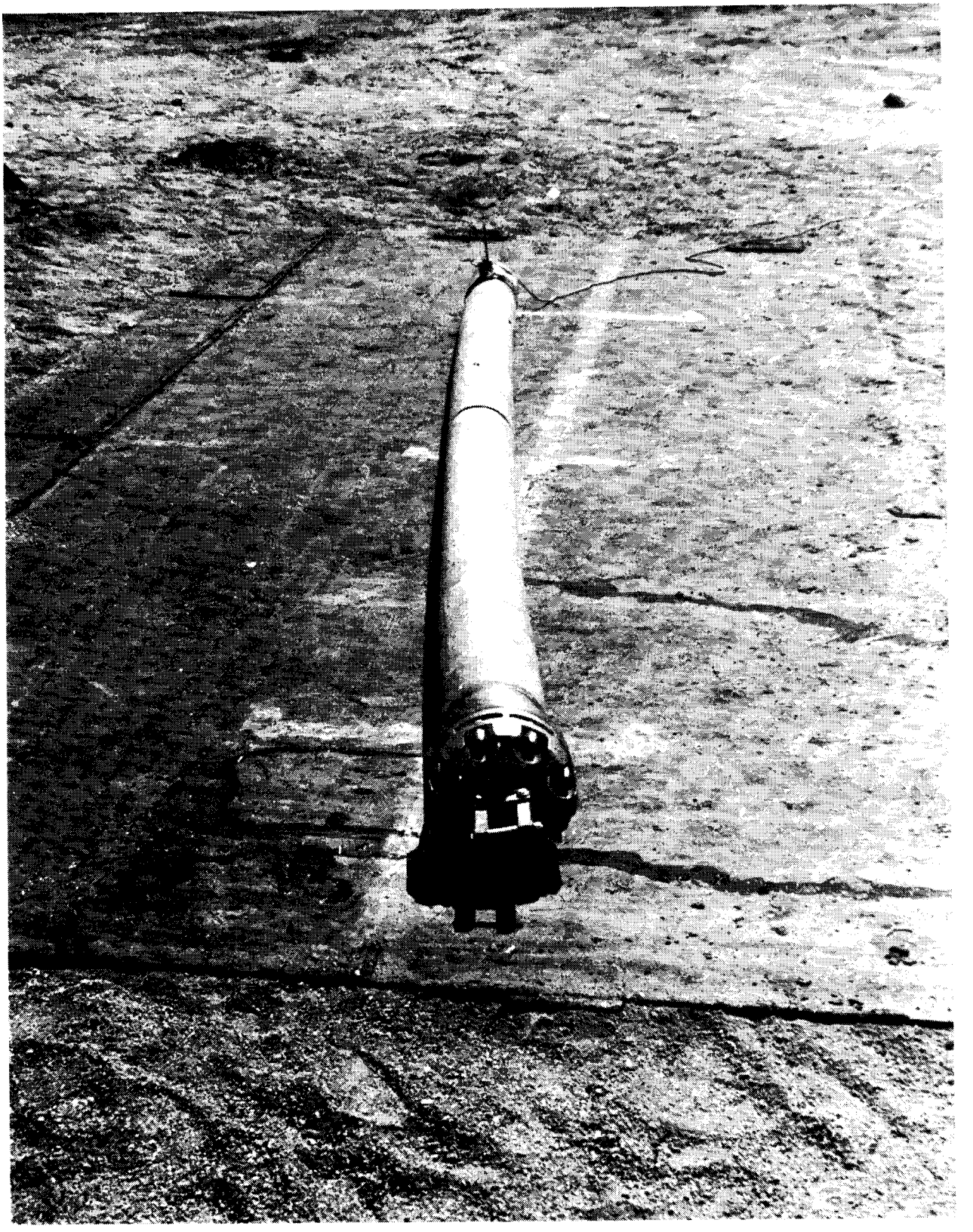

Figure 36. Posttest, 90-Degree Drop

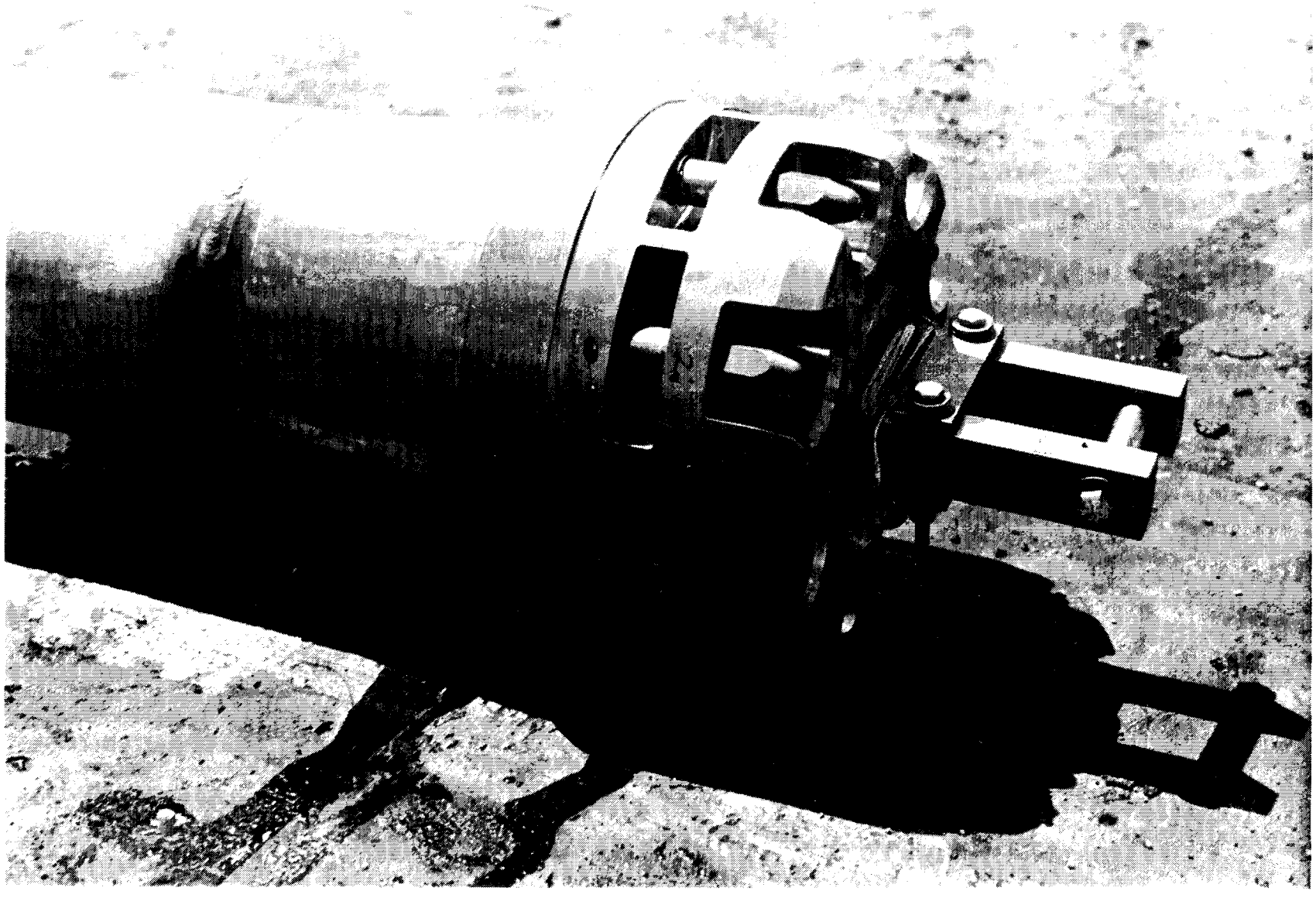

Figure 37. Posttest, 90-Degree Drop, Head

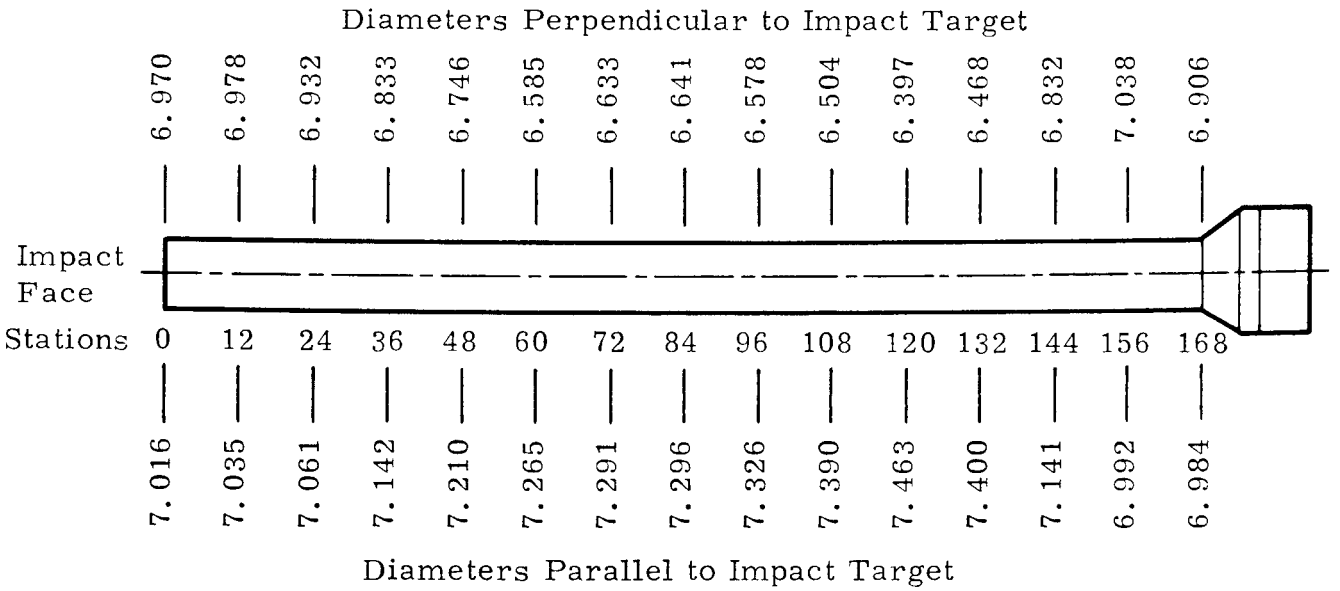

Figure 38. Body Deformation, 90-Degree Drop

The energy dissipated or converted through Modes 1 through 3 is then compared with the initial kinetic energy generated by the 9.1-m (30-ft) drop, again neglecting the influence of the steel, fuel-simulating pin.

As one would anticipate, the energy available is found to exceed that which is calculated to be dissipated. This discrepancy is due to neglect of other loss mechanisms which were not calculated, such as stress waves propagating into the target, pressure waves radiating away from the canister into the air, and residual kinetic energy of the fluid.

Each of the energy absorption mechanisms is first considered individually, and the sum of these energies will be compared later with that which is available from the drop.

5.4.2 Mode 1: Plastic Hoop-Straining of the Canister Wall

As shown in Figure 1, the canister has a nominal 0.6-cm (1/4-in.) wall, except near the ends. The residual circumferential strain is plotted as a function of axial distance from the impacting end in Figure 39. Note that circumferential strain values are calculated from diametral changes rather than determined from strain gages due to the few locations at which strain gages were placed. The plot is continued a total distance of 2.4 m (8 ft) from the impacting end, just slightly over half the overall length of the canister. Note that strains for greater distances were not plotted since they were small and within the accuracy of the measuring instruments. Except near the impacting end where measurements were made more frequently, strains were measured every 12 in. of axial length by determining diametral growth.

The energy absorbed is calculated using the general formula

$$\epsilon = \int_V \left[\int_0^{\epsilon_{max}} \sigma \, d\epsilon \right] dV, \tag{41}$$

where σ and ϵ denote, respectively, the circumferential stress and strain and V is the volume of material absorbing energy. The inner integral is the strain energy density at a point in the canister. This strain energy density is then integrated (summed) over the volume of the canister. The details of evaluation of Eq (41) for the energy absorbed by hoop straining are as follows. (Note that care must be taken to account for changing canister wall thickness (see Figure 2) as well as the nonlinear stress-strain curve for the material.)

Consider the quasi-static stress-strain curve shown in Figure 40 for 304 stainless steel. As shown in Figure 39, the circumferential residual strain varies as a function of distance from the impacting end. The approach taken is to effectively break the canister up into a number (11) of small regions of material over which the strain and wall thickness are approximately uniform. These regions are numbered I through XI in

Figure 39. The strain energy density of each such region is determined based upon the final strain measurement. By multiplying the strain energy density by the volume of the particular region and summing the results for all the regions of the canister, the total amount of elastic-plastic energy absorbed can be calculated.

As an illustration of the process, say that the residual hoop strain at one particular location from the end of the canister is 0.005 m/m (in./in.). That particular ring segment of the canister suffered a peak strain larger than 0.005 m/m (in./in.) before unloading to that value. Assuming that unloading occurs along a line with slope equal to the initial elastic slope, a line with that slope is constructed from the residual strain point A on Figure 40 (0, 0.005) to the maximum strain point B where the elastic unloading line intersects the stress-strain curve of the material. The coordinates of point B are (38,000, 0.008). Thus, the peak hoop strain reached at that particular location of the canister was 0.008 m/m (in./in.) at a stress of 38,000 psi (262 MPa). As indicated in Figure 40, the shaded area is the energy density associated with plastic deformations and the cross-hatched region is that which is recoverable elastic energy. The sum of the two areas represents the total energy density absorbed at that location in the canister.

To facilitate calculations, a cumulative energy density curve was constructed by numerical integration of Figure 40, as shown schematically in Figure 41. The resulting cumulative energy density curve so constructed is shown in Figure 42.

The procedure for calculating the total energy absorbed in the hoop deformation mode is now straightforward. First the average residual strain for a given region is determined for each of the 11 regions shown in Figure 39. Next, using Figure 40, the strain is converted from residual strain (generic point A) to peak strain (generic point B). The value of peak strain is then used in combination with Figure 42 to determine the strain energy density associated with the particular region. After multiplying by the volume of the region (taking due account of the axial length and possible varying thickness of the region), the strain energies for each of the 11 regions of Figure 39 are summed to give the total energy absorbed in the hoop deformation mode. Calculations are indicated in Table 17. The first column identifies the region, and the second and third columns denote, respectively, the residual strain values (based upon diametral change) on the two ends of the region. The last column gives the total strain energy for the region, calculated by multiplying the volume of stainless steel material and the associated energy density. The sum of values in the last column, 12641 J (9324 ft-lbs), represents the total energy absorbed in the hoop deformation mode.

Table 17. Energy Absorbed in Hoop Deformation Mode

Area	Strain-Left (in./in.)	Strain-Right (in./in.)	Average Residual Strain (in./in.)	Peak Strain (in./in.)	Energy Density (in.-lbf/in.^{3})	Length (in.)	Thickness (in.)	Strain Energy (in.-lb)
I	0.0	0.000761	0.000381	0.0025	37.0	2.0	1.089	1709
II	0.000761	0.000050	0.000406	0.0025	37.0	2.0	0.949	1489
III	0.000263	0.001956	0.00111	0.0035	68.0	2.0	0.389	1122
IV	0.001956	0.0188	0.0104	0.0135	448.0	6.0	0.250	14250
V	0.0188	0.0144	0.0166	0.020	725.0	2.0	0.250	7687
VI	0.0144	0.0079	0.0111	0.0137	456.0	16.0	0.250	38679
VII	0.0079	0.0042	0.0061	0.009	260.0	12.0	0.250	16540
VIII	0.0042	0.0027	0.00345	0.0062	153.0	12.0	0.250	9733
IX	0.0027	0.0032	0.00295	0.0057	140.0	12.0	0.250	8906
X	0.0032	0.0015	0.00235	0.0050	117.0	12.0	0.250	7443
XI	0.0015	0.0009	0.0012	0.0035	68.0	12.0	0.250	4325

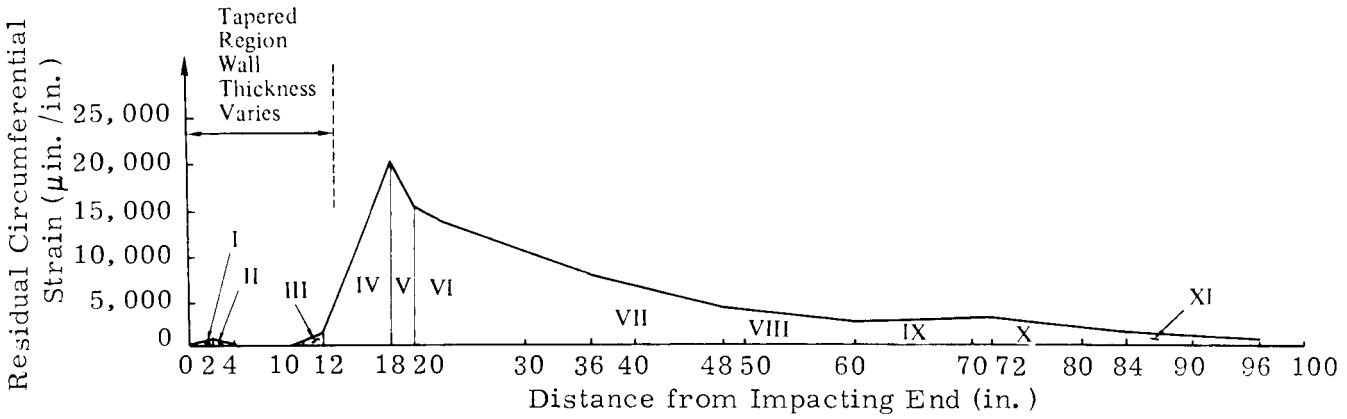

Figure 39. Residual Hoop Strain. As a function of distance from the impacting end.

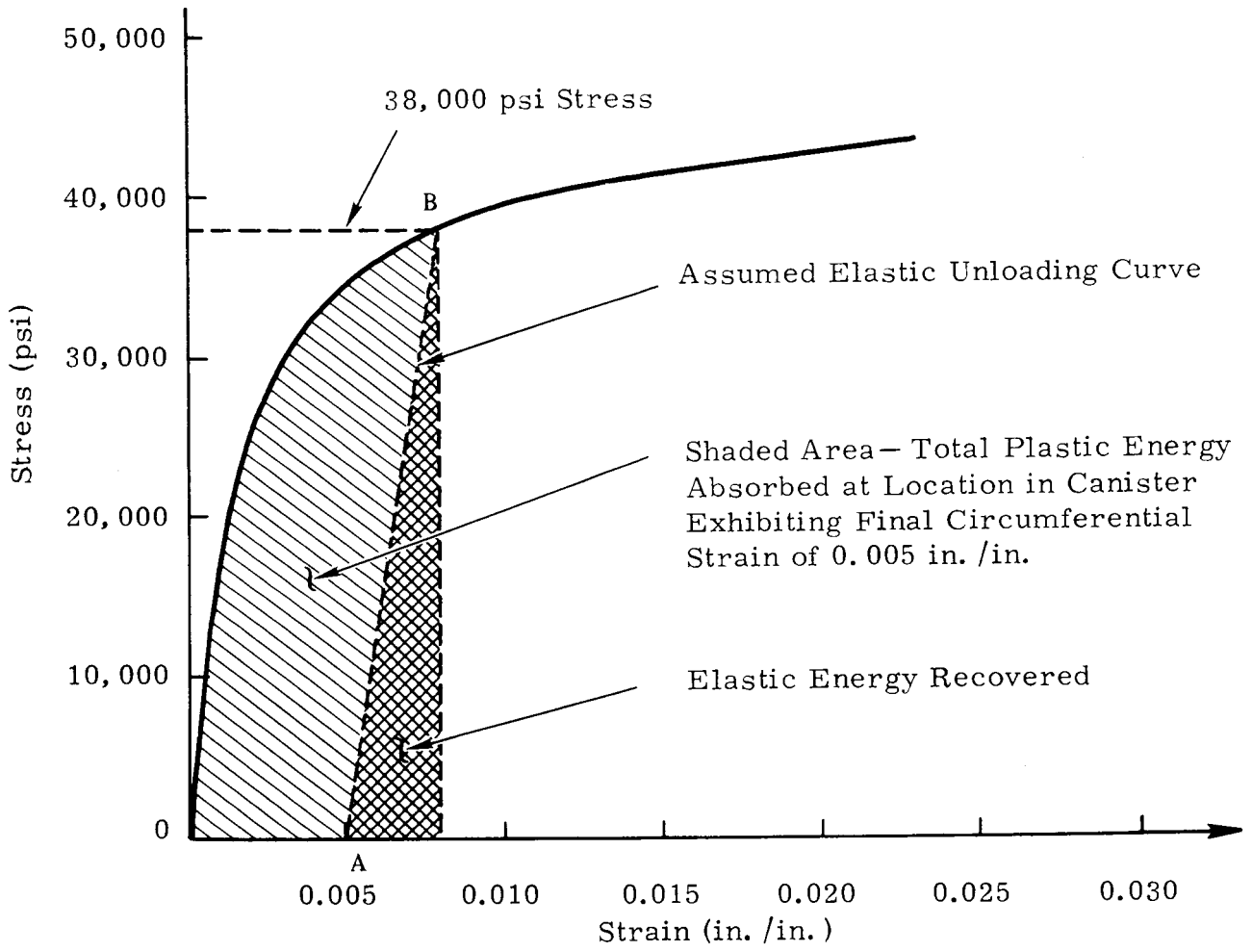

Figure 40. Stress-Strain Data for 304 Stainless at 21°C (70°F) (Quasi-static)

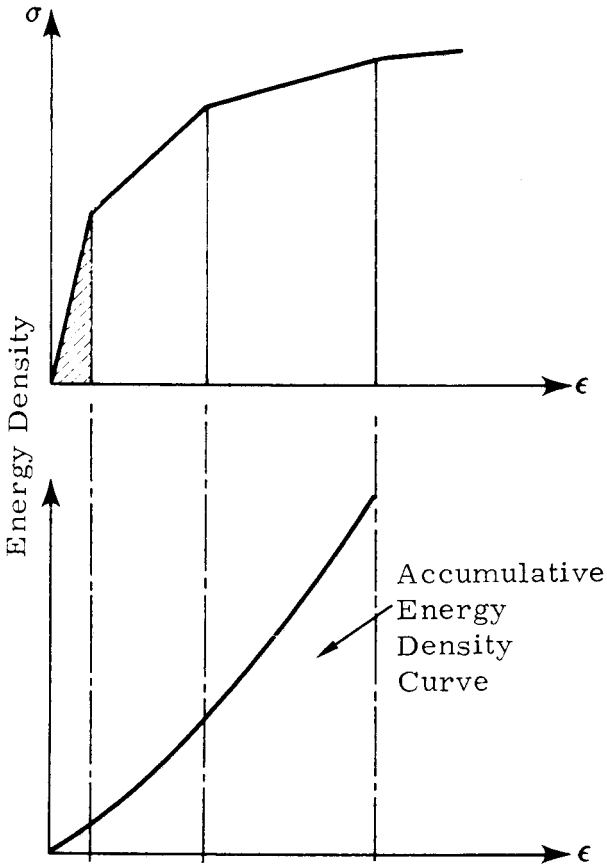

Figure 41. Construction of Cumulative Energy Curve

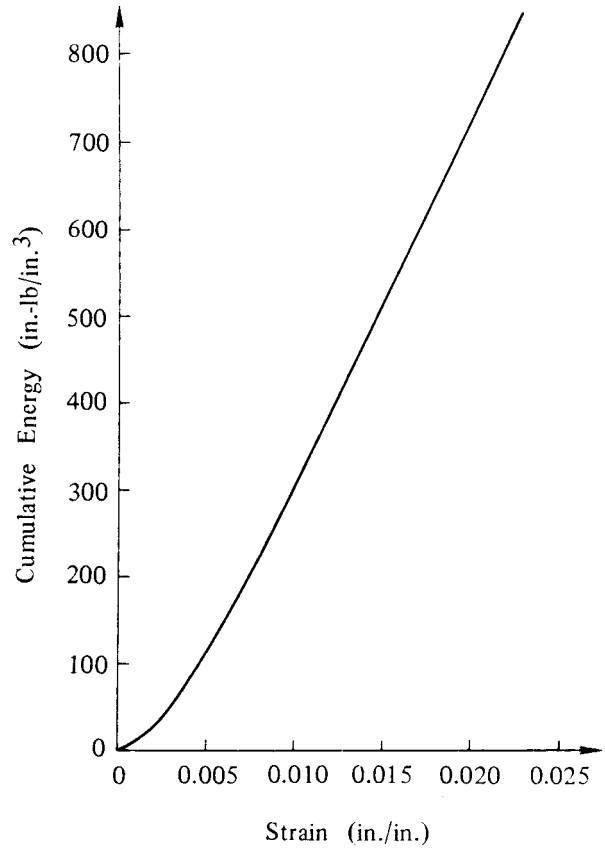

Figure 42. Cumulative Energy Density

5.4.3 Mode 2: Axial Plastic Crush-Up (Shortening) of the Canister

Posttest measurements indicated that the canister underwent a permanent axial shortening of 0.3 cm (0.125 in.). Because the actual strain distribution is unknown, assume that this axial shortening occurs in the region where the wall is 0.63 cm (0.25 in.) and, further, that the material is rigid-perfectly plastic. The energy absorbed plastically in the axial crush-up mode is

$$\text{Energy} = \int_0^{\delta} F dx = \sigma_y A\delta \qquad (42)$$

where δ is the maximum crush-up, σ_y is the yield stress and A is the cross-sectional area of the canister.

For

$$\begin{aligned} \sigma_y &= 276 \text{ MPa (40,000 psi)} \\ A &= 34.2 \text{ cm}^2 \text{ (5.30 sq in.)} \\ \delta &= 0.317 \text{ cm (0.125 in.)} \qquad (43) \\ \text{Energy} &= 2995 \text{ J (2209 ft-lb}_f\text{)} \end{aligned}$$

5.4.4 Mode 3: Rigid Body Rebound

Following direct target impact, the canister rebounded upward to a photographically recorded height of 0.693 m (27.3 in.). Thus, the energy associated with rebound is

$$\text{Energy} = Mgh = 1749 \text{ J (1290 ft-lbs)} \qquad (44)$$

5.4.5 Kinetic Energy Available at Impact

The mild steel pin (which simulates fuel) basically stops itself through plastic deformation without significant energy transfer to the canister. For simplicity, the energy associated with the pin is therefore not included in the energy balance.

Masses of remaining material are as follows:

Canister Assembly	=	178.2 kg (393 lb)
Liquid	=	75.3 kg (166 lb)
Handling Fixture	=	3.62 kg (8 lb)
TOTAL Mass (less pin)	=	257.2 kg (567 lb)

Kinetic energy at impact, neglecting air drag, is given by

$$KE = Mgh ,$$

where Mg is total weight and h is drop height. For Mg = 257.2 kg (567 lb_f) and h = 9.1 m (30 ft), total kinetic energy at the instant of impact is

$$KE = 23062 \text{ J } (17010 \text{ ft-lb}).$$

5.4.6 Overall Energy Balance and Conclusions

The overall energy balance is as follows:

Available Impact Kinetic Energy	=	23062 J	(17010 ft-lb)
−Rebound Energy	=	−1749 J	(1290 ft-lb)
−Energy Absorbed thru Axial Shortening	=	−2995 J	(2209 ft-lb)
−Energy Absorbed in Hoop Deformations	=	−12641 J	(9324 ft-lb)
Excess Energy	=	5677 J	(4187 ft-lb)

Approximately 24% of the original kinetic energy is unaccounted for. Other sinks for this energy not considered here include air drag, residual kinetic energy of the fluid, radiation of sound waves into the surrounding air, elastic deformations of portions of the canister (over half) not considered here, and stress waves propagated into the target.

Results obtained in this section suggest that equating of initial kinetic energy to the energy associated with some given deformation mode of an impacting structure will generally lead to conservative results, i.e., deformations which are overpredicted.

Although no analysis or verification tests have been performed, it is expected that energy absorption by plastic deformation will increase as the body temperature and, consequently, ductility increases.

6 Conclusions and Recommendations

6.1 Conclusions

A preliminary analysis of the 9.1-m (30-ft) normal impact situation revealed that hoop stresses in the initial canister design were excessive, particularly when superimposed with axial wall stresses, making rupture of the canister a likely possibility. Plastic buckling as a result of normal impact was also predicted to occur.

Two methods of surmounting these difficulties were suggested: use of a crushable, energy absorbing material or increase of the canister wall thickness near the impact end of the canister. The latter design modification was introduced into the initial canister design, and a series of 9.1-m (30-ft) drop tests was performed.

It was concluded that the modified design body structure is capable of surviving the regulatory impact test. The seal, however, requires additional development work for which time and funding are not available.

A simplified energy balance was performed after the end-on impact test in an attempt to account for the partitioning of initial kinetic energy into the various modes of canister deformation. Results indicated that 68% of the initial energy was absorbed by plastic deformation of the canister body. It is expected that the percentage will be higher when the canister is at operating temperature since the steel will then be more ductile.

6.2 Recommendations

1. Develop the structural model further to perform necessary correlations with test results and licensing calculations.
2. Run evaluation tests to find metal seals that can survive the impact test and remain leak-tight. To reduce expense this could be done with only the head portion of the canister. Significant head redesign may be necessary. Test velocity would be 20.7 m/s (68.0 ft/s) as measured in the 45-degree test. Tests would be done at both ambient and operating temperature.
3. Redesign the complete canister to incorporate seal test and analysis results.
4. Perform drop tests on a sodium-filled, complete canister at operating temperature.

7 References

[1] *Packaging of Radioactive Material for Transportation and Transportation of Radioactive Material Under Certain Conditions: Compatibility with IAEA Regulations,* proposed Rule, Federal Register, Vol 44, No. 161, August 17, 1979.

[2] *Leakage Test on Packages for Shipment of Radioactive Materials,* US Nuclear Regulatory Commission Regulatory Guide 7.4, June 1975.

[3] *American National Standard for Leakage Tests on Packages for Shipment of Radioactive Materials,* ANSI-N14.5-1977, October 1977.

[4] *Design Criteria for the Structural Analysis of Shipping Cask Containment Vessels,* Regulatory Guide 7.6, U.S. Nuclear Regulatory Commission, Revision 1, 1978.

[5] *Load Combinations for the Structural Analysis of Shipping Casks,* Regulatory Guide 7.8, U.S. Nuclear Regulatory Commission, May 1977.

[6] T. A. Duffey and D. E. Mitchell, "Containment of Explosions in Cylindrical Shells," *International Journal of Mechanical Sciences,* 1973.

[7] R. E. Berry, et al, *Accident Resistant Container Materials and Structures Evaluation,* SAND74-0010 (Albuquerque, NM: Sandia Laboratories, August 1975).

[8] T. K. Hill and W. W. Joseph, *Energy-Absorbing Characteristics of Materials,* SLA-74-0159 (Albuquerque, NM: Sandia Laboratories, May 1974).

[9] L. H. N. Lee, "Inelastic Buckling of Initially Imperfect Cylindrical Shells Subject to Axial Compression," *Journal of the Aerospace Sciences,* Vol 29, January 1962, p 87.

[10] S. C. Batterman, "Plastic Buckling of Axially Compressed Cylindrical Shells," *AIAA Journal,* Vol 3, February 1965, p 316.

[11] S. C. Batterman, "Tangent Modulus Theory for Cylindrical Shells: Buckling Under Increasing Load," *International Journal of Solids and Structures,* Vol 3, July 1967, p 500.

[12] S. C. Batterman, "Free-Edge Plastic Buckling of Axially Compressed Cylindrical Shells," *Journal of Applied Mechanics,* March 1968, p 73.

[13] A. L. Florence and J. N. Goodier, "Dynamic Plastic Buckling of Cylindrical Shells in Sustained Axial Compressive Flow," *Journal of Applied Mechanics,* March 1968, p 80.

[14] ASME Boiler and Pressure Vessel Code, Case N-47 (1592-10), Nuclear Components, American Society of Mechanical Engineers, New York, NY, July 1, 1977.

[15] R. J. Roark, *Formulas for Stress and Strain* (New York: McGraw-Hill, 1965), p 298.

APPENDIX

Mass Properties Report

MASS PROPERTIES REPORT

TEST UNIT DESCRIPTION Fuel Rod Canister T 57583

CLASSIFICATION: TEST UNIT UNC TEST DATA UNC

DATE AVAILABLE: 5-23-80 SPECIAL FIXTURES REQUIRED? YES NO AVAILABLE? YES NO

TARGE R- OR CASE NO. 8712.315 SHIP COMPLETED UNIT TO: _____

HAZARDS: NONE x EXPLOSIVES ___ TOXIC MATERIALS ___ (DESCRIBE BELOW)

INSTRUCTIONS, SOP'S, ETC.:

REQUESTED BY: D. Steinberg DIVISION 4552 PHONE 9181 DATE 5-23

CEPTED BY: [illegible] DIVISION 1137 SCHEDULED COMPLETION _____

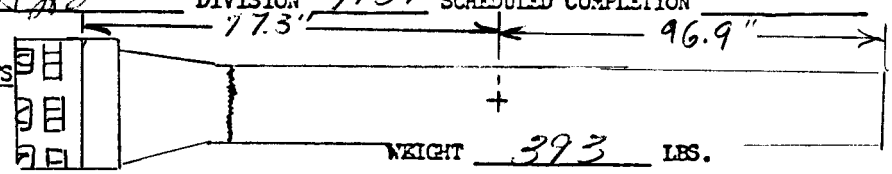

REQUESTED MEASUREMENTS

MEASUREMENT

___ WEIGHT — WEIGHT 393 LBS.

CENTER OF GRAVITY

___ X AXIS — X AXIS 77.3 IN. from point

___ Y AXIS — Y AXIS ___ IN.

___ Z AXIS — Z AXIS ___ IN.

MOMENTS OF INERTIA

___ IXX — IXX ___ LB-IN^2

___ IYY — IYY 4,515,410 LB-IN^2 327 SLUG ft^2

___ IZZ — IZZ ___ LB-IN^2

DYNAMIC IMBALANCE

C. G. OFFSETS: Y-BAR ___ IN.

Z-BAR ___ IN.

___ ___ PRODUCTS OF INERTIA: IXY ___ LB-IN^2

___ IXZ ___ LB-IN^2

___ ANGLES OF INCLINATION: EY ___ DEGREES

EZ ___ DEGREES

RESULTANT: EYZ ___ DEGREES

DATE: 5/30/80 REPORTED BY: [illegible] DIVISION 1137

Definition of Axes ☐ 1127 Convention (Below) ☐ Other (Specify on Dwg or Sketch)

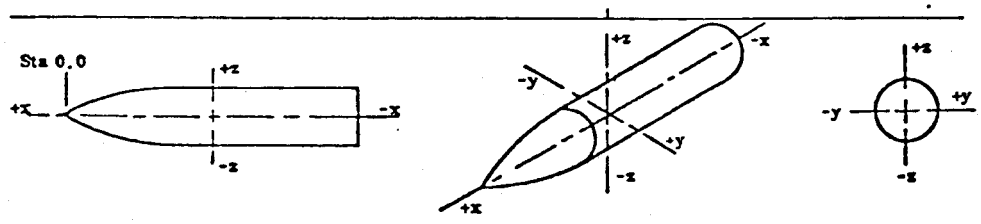

MASS PROPERTIES REPORT

TEST UNIT DESCRIPTION Fuel Rod Mockup

CLASSIFICATION: TEST UNIT UNC TEST DATA UNC

DATE AVAILABLE: 5-23-80 SPECIAL FIXTURES REQUIRED? YES NO AVAILABLE? YES NO

HARGE R- OR CASE NO. 8912.315 SHIP COMPLETED UNIT TO: _____

HAZARDS: NONE x EXPLOSIVES ___ TOXIC MATERIALS ___ (DESCRIBE BELOW)

INSTRUCTIONS, SOP'S, ETC.:

REQUESTED BY: D. STERNBERG DIVISION 4552 PHONE 9184 DATE 5-23

ACCEPTED BY: [illegible] DIVISION 1137 SCHEDULED COMPLETION _____

REQUESTED MEASUREMENTS

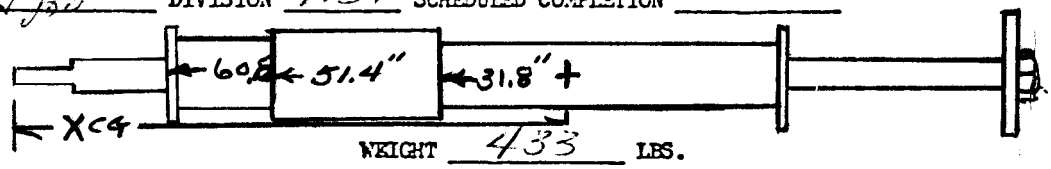

MEASUREMENT

___ WEIGHT — WEIGHT 433 LBS.

CENTER OF GRAVITY

___ X AXIS — X AXIS 74.7 IN. FROM END

___ Y AXIS — Y AXIS _____ IN.

___ Z AXIS — Z AXIS _____ IN.

MOMENTS OF INERTIA

___ IXX — IXX _____ LB-IN^2

___ IYY — IYY 730820 LB-IN^2 157.7 SLUG FT^2

___ IZZ — IZZ 43 / 125 LB-IN^2

DYNAMIC IMBALANCE

C. G. OFFSETS: Y-BAR _____ IN.

___ Z-BAR _____ IN.

___ PRODUCTS OF INERTIA: IXY _____ LB-IN^2

___ IXZ _____ LB-IN^2

___ ANGLES OF INCLINATION: EY _____ DEGREES

___ EZ _____ DEGREES

RESULTANT: EYZ _____ DEGREES

DATE: 5-30-80 REPORTED BY: [illegible] DIVISION 1137

Definition of Axes ☐ 1127 Convention (Below) ☐ Other (Specify on Dwg or Sketch)

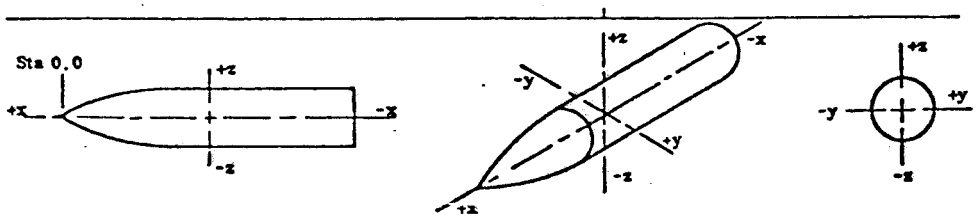

MASS PROPERTIES REPORT

TEST UNIT DESCRIPTION Fuel Rod Canister

CLASSIFICATION: TEST UNIT UNC TEST DATA UNC

DATE AVAILABLE: 5-23-80 SPECIAL FIXTURES REQUIRED? YES NO AVAILABLE? YES NO

HARGE R- OR CASE NO. 8912-315 SHIP COMPLETED UNIT TO: _____

HAZARDS: NONE X EXPLOSIVES ___ TOXIC MATERIALS ___ (DESCRIBE BELOW)

INSTRUCTIONS, SOP'S, ETC.:

REQUESTED BY: D. Steinberg DIVISION 4552 PHONE 9184 DATE 5-23

ACCEPTED BY: 1188 DIVISION 1137 SCHEDULED COMPLETION _____

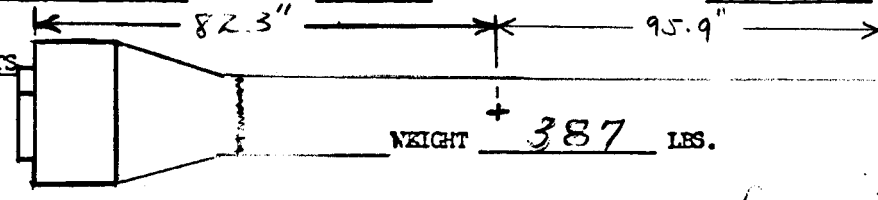

REQUESTED MEASUREMENTS

MEASUREMENT

___ WEIGHT — WEIGHT + 387 LBS.

CENTER OF GRAVITY

___ X AXIS — X AXIS 82.3 IN. FROM END

___ Y AXIS — Y AXIS _____ IN.

___ Z AXIS — Z AXIS _____ IN.

MOMENTS OF INERTIA

___ IXX — IXX _____ LB-IN^2

___ IYY — IYY 1,486,230 LB-IN^2 3248 SLUG FT^2

___ IZZ — IZZ _____ LB-IN^2

DYNAMIC IMBALANCE

C. G. OFFSETS: Y-BAR _____ IN.

Z-BAR _____ IN.

___ ___ PRODUCTS OF INERTIA: IXY _____ LB-IN^2

___ IXZ _____ LB-IN^2

___ ANGLES OF INCLINATION: EY _____ DEGREES

EZ _____ DEGREES

RESULTANT: EYZ _____ DEGREES

DATE: 5-30-80 REPORTED BY: A. G. Blackwood DIVISION 1137

Definition of Axes ☐ 1127 Convention (Below) ☐ Other (Specify on Dwg or Sketch)

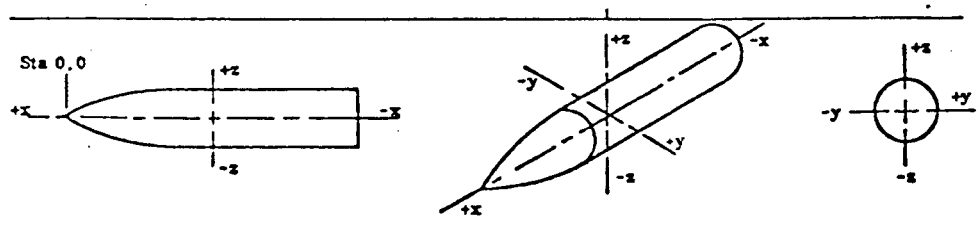

DISTRIBUTION:

TIC-4500-R69 UC-71 (154)

Allied-General Nuc Serv
PO Box 847
Barnwell, SC 29812
Attn: P. Highberger

Applied Science and Technology
16630 Sagewood Lane
Poway, CA
Attn: R. E. Nickell

Atomics International (2)
PO Box 309
Canoga Park, CA 91304
Attn: K. Foster
R. Crosgrove

Battelle Memorial Inst
Office of Nuclear Isolation
505 King Ave
Columbus, OH 43201
Attn: R. W. Peterson

Battelle Memorial Inst
505 King Ave
Columbus, OH 43201
Attn: K. D. Kok

Batelle Memorial Inst
Pacific Northwest Lab
PO Box 999
Richland, WA 99352
Attn: K. J. Schneider

The Boeing Co
PO Box 3707, MS 8A-68
Seattle, WA 98124
Attn: J. W. Baxter

Clinch River Breeder Reactor Project (5)
PO Box U
Oak Ridge, TN 37830
Attn: P. T. Becknell (2)
L. W. Caffey
E. A. Wright (2)

E. I. duPont de Nemours & Co.
Engineering Dept
Louviers Building
Wilmington, DE 19898
Attn: J. Cherney

General Atomic Co
PO Box 81608
San Diego, CA 92138
Attn: R. M. Burgoyne

General Electric Co
175 Curtner Ave
San Jose, CA 95125
Attn: C. Davis

Nuclear Assurance Corp
24 Executive Park West
Atlanta, GA 30329
Attn: C. Johnson

Nuclear Packaging, Inc
1733 South Fawcett
Tacoma, WA 98402
Attn: J. D. Simchuk

Oak Ridge National Lab (3)
PO Box X
Oak Ridge, TN 37830
Attn: S. A. Meacham
L. M. Petrie
L. B. Shappert

Ridihalgh, Eggers & Assoc
2122 Iuka Avenue
Columbus, OH 43201
Attn: J. L. Ridihalgh, President

Stearns-Roger, Inc
PO Box 5888
Denver, CO 80217
Attn: W. H. Brinkman

Transnuclear, Inc
One North Broadway
White Plains, NY 10601
Attn: L. Macklin

US Dept of Energy (9)
Washington, DC 20545
Attn: F. P. Falci (2)
R. F. Garrison
J. R. Hunter
J. R. Longenecker
D. K. Magnus
D. J. McGoff
G. Oertel
J. A. Sisler

DISTRIBUTION (cont):

US Dept of Energy (2)
Albuquerque Operations Office
Albuquerque, NM 87115
Attn: K. Carlson
R. Y. Lowrey

US Dept of Energy
Oak Ridge Operations Office
PO Box E
Oak Ridge, TN 37830
Attn: W. A. Pryor

US Dept of Energy
FFTF Project Office
PO Box 550
Richland, WA 99352
Attn: John Patterson

US Dept of Transportation
MTB (DMT-221)
Washington, DC 20590
Attn: R. Rawl

US Nuclear Regulatory Com (3)
Washington, DC 20555
Attn: W. R. Lahs
C. E. MacDonald
D. R. Hopkins

Westinghouse Electric Corp (5)
PO Box W
Oak Ridge, TN 37830
Attn: E. H. Petrie (2)
W. J. Purcell
J. E. Rutenber (2)

Westinghouse Hanford Co
W/A-98
PO Box 1970
Richland, WA 99352
Attn: J. D. Berger
P. R. Clements

1537 N. R. Keltner
1725 J. A. Andersen
4000 A. Narath
4400 A. W. Snyder
4700 E. H. Beckner
Attn: W. D. Weart, 4730
R. W. Lynch, 4760
G. E. Branvold, 4770
4780 R. M. Jefferson
Attn: TTC Master File
4781 R. E. Luna
4781 TTC Library (15)
4782 R. B. Pope (15)
4782 T. A. Duffey
4782 R. G. Eakes
4782 G. H. Lamoreaux
4782 W. B. Leisher
4782 J. M. Ortman
4782 R. T. Reese
4782 L. E. Romesberg
4782 A. A. Trujillo
4782 M. G. Vigil
4783 G. C. Allen
4783 S. H. Sutherland
5523 R. C. Reuter, Jr
5523 K. W. Gwinn
8214 M. A. Pound
3141 L. J. Erickson (5)
3151 W. L. Garner (3)